National Library
of Canada

Acquisitions and
Bibliographic Services Branch

395 Wellington Street
Ottawa, Ontario
K1A 0N4

Bibliothèque nationale
du Canada

Direction des acquisitions et
des services bibliographiques

395, rue Wellington
Ottawa (Ontario)
K1A 0N4

Your file Votre référence

Our file Notre référence

NOTICE

The quality of this microform is heavily dependent upon the quality of the original thesis submitted for microfilming. Every effort has been made to ensure the highest quality of reproduction possible.

If pages are missing, contact the university which granted the degree.

Some pages may have indistinct print especially if the original pages were typed with a poor typewriter ribbon or if the university sent us an inferior photocopy.

Reproduction in full or in part of this microform is governed by the Canadian Copyright Act, R.S.C. 1970, c. C-30, and subsequent amendments.

AVIS

La qualité de cette microforme dépend grandement de la qualité de la thèse soumise au microfilmage. Nous avons tout fait pour assurer une qualité supérieure de reproduction.

S'il manque des pages, veuillez communiquer avec l'université qui a conféré le grade.

La qualité d'impression de certaines pages peut laisser à désirer, surtout si les pages originales ont été dactylographiées à l'aide d'un ruban usé ou si l'université nous a fait parvenir une photocopie de qualité inférieure.

La reproduction, même partielle, de cette microforme est soumise à la Loi canadienne sur le droit d'auteur, SRC 1970, c. C-30, et ses amendements subséquents.

Canada

A Time-Accurate Finite Element Solution of the Navier-Stokes Equations

Mohamad Sleiman

A Thesis

in

The Department

of

Mechanical Engineering

Presented in Partial Fulfillment of the Requirements
for the Degree of Masters of Applied Science at
Concordia University
Montréal, Québec, Canada

March 1995

National Library
of Canada

Acquisitions and
Bibliographic Services Branch

395 Wellington Street
Ottawa, Ontario
K1A 0N4

Bibliothèque nationale
du Canada

Direction des acquisitions et
des services bibliographiques

395, rue Wellington
Ottawa (Ontario)
K1A 0N4

Your file Votre référence

Our file Notre référence

THE AUTHOR HAS GRANTED AN IRREVOCABLE NON-EXCLUSIVE LICENCE ALLOWING THE NATIONAL LIBRARY OF CANADA TO REPRODUCE, LOAN, DISTRIBUTE OR SELL COPIES OF HIS/HER THESIS BY ANY MEANS AND IN ANY FORM OR FORMAT, MAKING THIS THESIS AVAILABLE TO INTERESTED PERSONS.

L'AUTEUR A ACCORDE UNE LICENCE IRREVOCABLE ET NON EXCLUSIVE PERMETTANT A LA BIBLIOTHEQUE NATIONALE DU CANADA DE REPRODUIRE, PRETER, DISTRIBUER OU VENDRE DES COPIES DE SA THESE DE QUELQUE MANIERE ET SOUS QUELQUE FORME QUE CE SOIT POUR METTRE DES EXEMPLAIRES DE CETTE THESE A LA DISPOSITION DES PERSONNE INTERESSEES.

THE AUTHOR RETAINS OWNERSHIP OF THE COPYRIGHT IN HIS/HER THESIS. NEITHER THE THESIS NOR SUBSTANTIAL EXTRACTS FROM IT MAY BE PRINTED OR OTHERWISE REPRODUCED WITHOUT HIS/HER PERMISSION.

L'AUTEUR CONSERVE LA PROPRIETE DU DROIT D'AUTEUR QUI PROTEGE SA THESE. NI LA THESE NI DES EXTRAITS SUBSTANTIELS DE CELLE-CI NE DOIVENT ETRE IMPRIMES OU AUTREMENT REPRODUITS SANS SON AUTORISATION.

ISBN 0-612-01358-8

Canada

ABSTRACT

A Time-Accurate Finite Element Solution of the Navier-Stokes Equations

Mohamad Sleiman

A finite element formulation of the Reynolds-averaged Navier-Stokes equations (RANS) for three-dimensional unsteady, viscous, compressible, turbulent flow, written in conservation form, is presented. The equations are linearized using the Newton method. They are discretized in space using a Galerkin finite element approach and are integrated in time using the Gear scheme: a multi-level, implicit, unconditionally stable method, with an order of accuracy that can be controlled by using a number of preceding time levels at each time step. The resulting set of algebraic equations for continuity and momentum, at each time step, are solved in a fully-coupled manner by a preconditioned iterative solver. To reduce memory requirements, the $\kappa-\varepsilon$ two-equation turbulence model is solved in a segregated manner, by the same solver.

The solution of the unsteady viscous Burgers equation, a model equation for the Navier-Stokes system, is presented by both the Gear method and the more popular Crank-Nicolson method, and the results used as a justification for the selection of the Gear method.

The outcome of this Thesis has been embedded into a Concordia-Pratt & Whitney Canada code, *NS3D*. The unsteady capabilities of the code have been validated against two incompressible test cases: the laminar flow over a circular cylinder at Re=100 and the turbulent flow around a triangular flame holder at Re=45,000. The von Karman vortex street shedding, observed experimentally, is captured in both cases and its computed shedding frequency is shown to be within 5% of the measured ones.

Acknowledgments

I would first like to thank my supervisor, Professor W.G. Habashi, for his guidance and support throughout my graduate studies and for providing the opportunity, the environment and the resources to carry out this research. Special thanks go to my co-supervisor, Professor W.S. Ghaly, with whom, even while he still was at Pratt & Whitney Canada (P&WC), I have had many invaluable technical discussions concerning my Thesis.

I would like to acknowledge the graciousness of Pratt & Whitney Canada who allowed me, through its long term collaboration with Dr. Habashi, to carry out the bulk of my computations in the company, and hiring me even before completing my Thesis.

I would also like to personally thank the Natural Sciences and Engineering Research Council of Canada (NSERC) for their financial support of my graduate studies through scholarships.

This Thesis is dedicated to my parents, Hussein and Taghrid, and my wife, Dareen.

Table of Contents

List of Figures

List of Tables

Nomenclature

A	domain area
C_p, C_v	specific heat coefficients
C_l, C_d	lift and drag coefficients
D	diameter of the circular cylinder
Ec	Eckert number
E	total number of elements
e	element index
f	frequency of vortex shedding
H	height of the triangular shaped flame holder
H_o	stagnation enthalpy
K	Global influence matrix
k	element influence matrix
k	order of the Gear scheme
k	thermal conductivity
^oK	temperature in degrees Kelvin
L	reference length
L_2	L-2 residual norm
M	Mach number
n	outward normal to a domain boundary
$\vec{n}$	unit vector in normal direction at the domain boundary
N	finite element shape function
$O(\,)$	order of magnitude
p	pressure
Pr	Prandtl number

R	specific gas constant
R	residual of a discretized partial differential equation
R_g	gas constant
Re	Reynolds number
s	distance along boundaries of domain
S	solution domain surfaces
S	source terms in the turbulence equations
Sr	Strouhal number, fD/ V_∞
t	time
T	temperature
T	Period for shedding voticies
u, v, w	Cartesian velocity components
$\vec{V}$	velocity vector
V_∞	reference velocity
W	finite element weight function
x,y,z	Cartesian coordinates
∞	relates to reference quantities

Greek symbols

α_i	coefficients of the Gear scheme
γ	isentropic exponent
λ	pressure dissipation parameter, in continuity equation
κ	kinetic turbulent energy
ξ, η, ζ	non-dimensional coordinates of the parent element
Δ	change in a variable between iterations
∇	gradient

μ	viscosity, molecular, turbulent or artificial
ρ	density
τ	viscous stress tensor
ϕ	viscous dissipation function
Φ	general notation for a vector of unknowns
ϑ	domain volume

Subscripts

eff	effective value
i, j	nodal indices
n	component in the direction normal to the boundary
o	stagnation value
p	part of a discretized equation, related to the continuity equation
ref	reference value
t	time level
$turb$	related to turbulence
$\rho u, \rho v, \rho w$	contribution from the $\rho u, \rho v, \rho w$ terms to an equation
x, y, z	partial derivative in the x, y, and z-directions
∞	free-stream value

Superscripts

n	iteration number
$\rho u, \rho v, \rho w$	contribution from any term to the x, y and z-momentum equations

p	part of a discretized equation related to the continuity equation
t	transpose of a vector

1. Introduction

This Thesis extends the computational capabilities of the Concordia CFD Laboratory, in partnership with Pratt & Whitney Canada, to the analysis of unsteady flow phenomena.

Most fluid flow problems of current interest in Computational Fluid Dynamics (CFD) are three dimensional, viscous, turbulent and unsteady. The ensuing complexity of the governing nonlinear Navier-Stokes equations makes the solution of such flows quite challenging, with great demands on computer power and memory.

For situations of interest, depending on the type of applications, researchers continuously make appropriate assumptions to circumvent complexities and reduce the cost of solving these equations. In the absence of extremely large computational resources, the major assumption has been, and will continue to be in the foreseeable future, to eliminate the need to resolve the structure of turbulent flows in time-accurate detail. This simplification is provided by ensemble-averaging the Navier-Stokes equations to yield their Reynolds-Averaged Navier-Stokes (RANS) form. In this case, turbulence is accounted for by means of a Reynolds stress and a scalar flux tensor, with the Reynolds stress simulated by various techniques, ranging from algebraic models, to one- and two-equation models, Reynolds' stress models, etc. Furthermore, for high-speed external aerodynamics, researchers have assumed that, away from the boundary layers, one can neglect the viscous terms in the RANS, obtaining the Euler equations, with their further lower order approximation to potential irrotational and rotational flows. These simplifications have permitted them over the last few decades to numerically compute various flow problems of interest. Currently, a focus of research is the development of methodology and the application of the RANS to a wide range of problems of industrial interest.

The assumption of flow steadiness must be carefully assessed as one can argue that, strictly speaking, all fluid flows are unsteady by their nature. Unsteadiness can, in general, be due to two phenomena:

a. A time-dependent input at a boundary or the interaction of adjacent stationary and moving components. Such situations are encountered in turbomachines where sources of unsteadiness are present such as stator/rotor interaction, flutter and inlet distortion, blade wake interaction, vortex shedding, passage and tip vortices, etc. The unsteadiness due to the relative motion between stators and rotors has lately become the focus of intense computational research and is the motivation behind the work of this Thesis, considered a building block towards achieving an unsteady predictive capability for the interaction of stationary and moving components [1].

b. Inherent unsteadiness due to the instability of the flow itself (bifurcation), such as behind bluff and profiled bodies, at high Reynolds numbers. The flow around bluff bodies, such as circular, square, or triangular cylinders, is a good example of such unsteadiness. The flow past a circular cylinder is known to be symmetric, stable, and steady for Reynolds numbers of up to 40. For higher values of Reynolds numbers, however, the flow structure changes dramatically, with, two attached oscillating eddies of unequal kinetic energies form behind the cylinder. Then, the one having higher kinetic energy divides the other into an eddy remaining near the cylinder and another convecting downstream and shedding in the form of the well-known von Karman vortex street [2].

The focus of this research, therefore, is to develop a finite element code for the time-accurate solution of the unsteady compressible Navier-Stokes equations. These equations are discretized in space using a Galerkin finite element approach, linearized using a Newton method and integrated in time using the Gear scheme, a multi-level, implicit, unconditionally stable method, with an order of accuracy that can be controlled by the use of a number of time levels at each time step. The resulting sets of linear equations, at a given time step, are solved by preconditioned iterative solvers.

This time integration scheme has been embedded into a Concordia-Pratt & Whitney 3D, turbulent, steady Navier-Stokes code, *NS3D* [3]. The time-accurate implementation has been validated, for the purpose of this Thesis, against two 2D test cases: that of a laminar flow over a circular cylinder and of a turbulent flow around a triangular flame holder. The von Karman vortex street shedding, observed experimentally, is captured in both cases and its computed shedding frequency is shown to be within 5% of the measured ones.

1.1 Review of Previous Work

The time-dependent numerical solutions of complex fluid flow problems have become more affordable with the advent of powerful computer resources [4]. The numerical solution of the unsteady Navier-Stokes (N-S) equations requires both space discretization and time integration. Space discretization can be performed by finite difference methods (FDM), finite element methods (FEM), or finite volume methods (FVM). FDM can be used for structured meshes while FEM and FVM can be applied to structured as well as unstructured meshes. It is not the aim of this Thesis to assess the merits of each one of these methods. In this work, however, the Galerkin finite element method (GFEM) is used for the space discretization.

In this section, a brief review of time integration schemes for the N-S equations is presented. For time discretization, a choice can be made between explicit multi-step schemes and implicit multi-level schemes. Explicit multi-step schemes such as the Runga-Kutta (R-K) methods [5], and implicit time integration schemes such as the θ-family of methods [6] are widely used in the solution of the N-S equations.

The solution of the unsteady N-S equations using explicit methods has been reported in numerous studies. Jordan and Fromm [7] applied the ADI method to solve the vorticity-stream function formulation of the unsteady N-S equations. Braza et al. [8] used a second-order finite volume method to analyze the pressure and velocity fields of the unsteady wake behind a circular cylinder. An explicit R-K time integration scheme has been introduced by Jameson [5]. Based on Jameson's work, Chima et al. [9]

developed a code to study flow phenomena in turbomachinery components. San-Yih Lin et al. [10] developed an explicit R-K finite element method for the solutions of Euler and N-S equations and investigated the accuracy and convergence of the method for the unsteady flow over a NACA 0012 in pitching motion.

Aside from the explicit methods described above, many authors have chosen to apply implicit schemes to solve the unsteady N-S equations. Bristeau et al. [11] presented a finite difference scheme for space discretization of the compressible N-S equations and implemented the Gear scheme of second-order accuracy for time discretization. Launder and Kota [12] investigated the turbulent unsteady flow around a square cylinder using the finite volume method for space dicretization and the θ-family of methods for time integration. Gresho et al. [13] developed a finite element code to study vortex shedding phenomena. They formulated a time integration scheme by a combination of two second-order time integration techniques, namely the implicit trapezoid rule and the explicit Adams-Bashforth formula. Von de Vosse et al. [14] studied the flow behind a circular cylinder using the penalty finite element method and analyzed the performance of the implicit-Euler and C-N time integration methods as well as their stability and convergence properties. Li et al. [2] developed a finite element velocity-pressure based method to simulate the vortex shedding behind one and two circular cylinders. They carried out a performance evaluation for the implicit-Euler and C-N methods and obtained a relationship between θ and Δt.

1.2 Brief Overview of Thesis

The Thesis is divided into six chapters. In Chapter 2, various methods of time approximations are presented and commented on. The solution of the viscous Burgers equation, a model equation for the Navier-Stokes system, is presented by both the Gear method and the Theta-family of methods, and the results used as a justification for the selection of the Gear method.

Chapter 3 presents the governing equations of the present work, namely the Reynolds-Averaged Navier-Stokes equations, the energy equation, and the κ-ε two-equation turbulence model. The chapter details the space and time discretization, the linearization and the boundary conditions of the various equations.

Chapter 4 highlights the solution strategy and analyzes the details of the overall outer and inner iterative procedures, involving marching in time and the solution at each time step of a set of nonlinear equations by a Newton approach. The linearization step yields a set of algebraic equations that are solved by a preconditioned iterative method. The chapter also describes the use of the unsteady formulation, in a time-marching algorithm, for the solution of steady-state problems.

Chapter 5 presents the results of code validation on two well-documented inherently unsteady flows over bluff bodies.

Chapter 6 draws conclusions from this work and describes possible natural extensions of this work.

2. Time Integration Methods

In this chapter, various methods of time approximation for partial differential equations of unsteady flows are presented. The time integration of the Burgers equation, a model equation for the Navier-Stokes system, is carried out using the Gear scheme and the Crank-Nicolson method. A discussion of the results of both methods clarifies the reason for choosing the Gear scheme.

Upon space discretization and linearization of the governing equations (details in following Chapters), the Navier-stokes equations, for all points in the computational domain, can be represented by the following set of ordinary differential equations in time:

$$M\dot{U} + KU = F \qquad 0 \le t \le T \qquad (2.1)$$

where

U Global vector of nodal point values of the variable $U(x,y,z,t)$

$\dot{U}$ First derivative of U with respect to time

M Mass matrix

K Coefficient matrix representing the convective and viscous terms

F Source vector, generally a function of U and t

t Time

T Time span within which the vector U is computed

Equation (2.1) is written in semi-discrete form, i.e. it is a continuous ordinary differential equation in time, discretized in space. There are essentially two approaches for the time discretization:

a. A finite element time integration, and
b. A finite difference time integration.

The second approach is the more convenient one in the current work because of its lesser demands on computer time and memory. In such approximations, the time span *[0, T]* (*T* could be any time level or the steady state) can be thought of as divided into a number of discrete time intervals between t_o, t_1, t_2, ...t_{a-1}, t_a. The different classes of time approximation, are:

1- Theta, θ, family.
    a- Euler-forward (explicit, single-level, single-step method)
    b- Crank-Nicolson (implicit, single-level, single-step method)
    c- Euler-backward (implicit, single-level, single-step method)
    d- Galerkin (implicit, single-level, single-step method),
2- Modified Euler (explicit, single-level, two-step method),
3- Runge-Kutta (explicit, single-level, multi-step method),
4- Adams-Bashforth (explicit, multi-level, single-step method),
5- Gear (implicit, multi-level, single-step method).

The θ–family is a single-level, single-step method in which the solution between two successive time levels t_{a-1} and t_a is assumed to vary linearly [2]. Consequently, at a time $t_r = t_{a-1}\text{-}\theta\Delta t$, located between times t_{a-1} and t_a, one can write:

$$U(t_r) = U_r = \theta\, U_t + (1 - \theta)U_{t-\Delta t} = \theta\, U_a + (1 - \theta)U_{a-1} \qquad 0 \leq \theta \leq 1 \quad (2.2)$$

where $$\theta = \frac{t - t_r}{\Delta t} \qquad [t_{a-1},\, t_a] \quad (2.3)$$

therefore, $$\frac{\partial U}{\partial t} = \frac{\partial U}{\partial \theta}\frac{\partial \theta}{\partial t} = (U_a - U_{a-1})\frac{1}{\Delta t} \quad (2.4)$$

To illustrate the differences between an explicit and an implicit scheme, the θ–family is applied to the general model equation (2.1), as follows:

Within the time interval $[t_{a-1},\, t_a]$, a linear variation of vectors F and KU is assumed, hence one can write

$$F_r = \theta F_a + (1\text{-}\theta)F_{a-1} \qquad 0 \leq \theta \leq 1$$

and $$(KU)_r = \theta(KU)_a + (1\text{-}\theta)(KU)_{a-1} \qquad 0 \leq \theta \leq 1 \quad (2.5)$$

Substituting equations (2.2-2.5) into equation (2.1) yields:

$$\frac{1}{\Delta t}M(U_a - U_{a-1}) + \theta(KU)_a + (1\text{-}\theta)(KU)_{a-1} = \theta F_a + (1\text{-}\theta)F_{a-1} \quad (2.6)$$

a- Setting $\theta = 0$ in equation (2.6) gives:

$$U_a = U_{a-1} + \Delta t\, M^{-1}[F_{a-1} - (KU)_{a-1}] \quad (2.7)$$

Equation (2.7) can be used to determine the solution U_a at time level t_a, using information from the previous time level t_{a-2}. The scheme of (2.7) is the Euler-forward method and is an explicit method since both the F and KU vectors are known from the previous time level. In addition, it is first-order accurate in time, conditionally stable, but has a stringent stability restriction on the time step size. This explicit scheme, however, requires minimum computer storage since a matrix solution is not required.

b- Setting $\theta = 1/2$ in equation (2.6) gives the Crank-Nicolson, or implicit trapezoidal scheme:

$$U_a = U_{a-1} + \Delta t\, M^{-1}[F_r - (KU)_r] \tag{2.8}$$

The solution U_a is computed using information from the previous time level t_{a-1}, and can be thought of as a centered scheme in time around a half-time step. The scheme of (2.8) is implicit since the vectors F and KU are also a function of the unknown solution U_a. The scheme is unconditionally stable and second-order accurate in time. Although it has no restriction on the time step size for stability, it suffers, as any other implicit scheme, from temporal oscillations in the solution if the time step is excessively large. Because of its improved accuracy and stability, the Crank-Nicolson scheme is widely used in the solution of the unsteady Navier-Stokes equations.

c- Setting $\theta = 1$ in equation (2.6) gives:

$$U_a = U_{a-1} + \Delta t\, M^{-1}[F_a - (KU)_a] \tag{2.9}$$

The solution U_a at time level t_a is computed using information from the previous time level t_{a-2}. Scheme (2.9) is an implicit one and is often called the Euler-backward scheme. In this formulation, the vectors F and KU are a function of the unknown solution U_a at the new time level. The scheme is first-order accurate in time, conditionally stable, and widely used in the solution of the Navier-Stokes equations because of its large values of time step sizes. It is also commonly used as a matrix preconditioner to augment the diagonal dominance, and hence stability, of time-marching iterative approaches to steady-state problems.

d- Finally, the unconditionally stable Galerkin method, is obtained by setting $\theta = 2/3$ in equation (2.6).

2- Modified Euler or Predictor-Corrector method (explicit, single-level, two-step method)

The time integration methods outlined above are single-step methods, i.e., the solution at time level t_a is obtained by evaluating the first order derivative once, the penalty being that they are only first order accurate. Higher time accuracy can be obtained by using multi-step methods (methods which require at least two derivative function evaluation per time level) or multi-level methods (methods which use solutions from two previous time levels or more), or a combination of both. In this context, the modified Euler method is a two-step method in which an explicit Euler step is first used to predict a solution at the new time step, and a trapezoidal integration rule similar to Crank-Nicolson, but fully explicit, is used to correct that solution. This method is therefore numerically explicit but yields second-order accuracy in time [15].

3- Runge-Kutta (explicit, single-level, multi-step method).

When higher accuracy is desirable, multi-step methods such as the Runge-Kutta approach, can be used. The basic idea of the method is to assume that the change in the solution $\Delta U_a = (U_a - U_{a-1})$ between time levels t_a, t_{a-1} is the weighted sum of a number of changes Δ evaluated at intermediate time locations within the time interval $[t_a, t_{a-1}]$. The number of these changes Δ is equal to the order of accuracy of the chosen Runge-Kutta method.

For the fourth-order Runge-Kutta method, for example, the total change in the solution between the current and the previous time levels ΔU_a can be written as:

$$\Delta U_a = U_a - U_{a-1} = b_1 \Delta U_1 + b_2 \Delta U_2 + b_3 \Delta U_3 + b_4 \Delta U_4 \tag{2.10}$$

The parameters b_i, the time locations t_i, the solution U_i at which the changes $\Delta U_i(t_i, U_i)$ are evaluated, are chosen such that equation (2.10) and a Taylor series expansions for the solution U_{a-1} are made identical through the specified or desired order of the Runge-Kutta method [15].

4- Adams-Bashforth (explicit, multi-level, single-step method).

The θ-family of methods is a single-level, single-step, method since the solution at time level t_a is obtained by using information from one time level only, t_{a-1}. The Modified Euler method, on the other hand, is a single-level two-step method that requires the evaluation of two derivatives. Higher-order methods with fewer derivative evaluations can, however, be developed by using solutions at different time levels.

The fourth-order Adams-Bashforth method is a widely used multi-level single-step approach that is obtained by fitting a third-order Newton backward difference polynomial to base time level t_{a-1} and integrating from that base time level to the next one t_a. This time integration method is explicit, conditionally stable, and has a fourth-order accuracy [15].

5- Gear (implicit, multi-level, single-step method).

The implicit Euler method is unconditionally stable, with first-order accuracy, while the Crank-Nicolson method improves this to second-order accuracy. Higher-order implicit methods are often desirable. Gear (1971) devised a series of implicit time integration schemes having large stability limits. The method is often referred to as the k-level method, with k being the order of accuracy. The method is of the backward differentiation type and has a variable order of accuracy in time that can be controlled by the number of time levels used [15]. For example, a first order Gear scheme (k=1), identical to the Euler-backward scheme, requires information from one time level, to solve for the current one.

The time term in equation (2.1) is approximated using the kth order Gear scheme as follows:

$$\left(\frac{\partial U}{\partial t}\right)^t = \frac{1}{\Delta t}\left(\alpha_0 U^t + \sum_{i=1}^{k} \alpha_i U^{t-i\Delta t}\right) = \frac{1}{\Delta t}\left(\alpha_0 U_a + \sum_{i=1}^{k} \alpha_i U_{a-i}\right) \tag{2.11}$$

where $\alpha_i (i = 0, 1, 2, ..., k)$ and k are the coefficients and the required order of time accuracy of the Gear scheme, respectively. Table 2.1 presents the values of the coefficients α_i associated with their corresponding Gear order k.

k	α_0	α_1	α_2	α_3	α_4
1	1	-1			
2	3/2	-4/2	1/2		
3	11/6	-18/6	9/6	-2/6	
4	25/12	-48/12	36/12	-16/12	3/12

Table 2.1 Coefficients for the increasing order of Gear finite difference approximations.

Equation (2.1) is time discretized using a Gear scheme of kth order accuracy in time as follows:

$$U_a = - \sum_{i=1}^{k} \frac{\alpha_i}{\alpha_0} U_{a-i} + \frac{\Delta t}{\alpha_0} M^{-1}[F - KU]_a \tag{2.12}$$

As can be seen from (2.12), the method requires an iterative procedure at every time step, even for a linear equation. A perceived disadvantage may also be that it requires multi-initial solutions at different time levels. However, one can make all initial solutions identical at the beginning of a computation. An alternative, say for a second-order Gear scheme (k=2), where two initial solutions are required, U_{a-2} and U_{a-1}, with U_{a-2} given, is to obtain U_{a-1} by a first-order Gear scheme (k=1), using an appropriately small first time step. The global accuracy of the second-order Gear scheme can be maintained by ensuring, through a smaller initial time step, that the accuracy of the first-order Gear step is the same as the larger step taken with the second-order Gear scheme.

A great advantage of this scheme in the solution of the unsteady Navier-Stokes equations is the large time step allowable, and the choice of order of accuracy, in an otherwise general code.

In conclusion, for fluid flow problems with rapid transient behavior, small time steps may be required for accuracy and stability, and explicit methods may then be appropriate to generate solutions. However, for problems with relative low transient behavior, implicit schemes allow the use of much larger time steps.

2.1 Analogy between the Burgers and Navier-Stokes Equations

In solving the Navier-Stokes equations one should carry out a detailed analysis of the discretization technique in order to assess its ability to simulate the equations. A simpler analog equation for nonlinear fluid mechanics would be quite useful. This model equation should have terms that closely duplicate the behavior of the essential terms, i.e. it should have a convective, a diffusive, and a time-dependent term.

The Burgers equation is a simple nonlinear equation which meets these requirements. It is a time-dependent parabolic equation, with convection and diffusion, which has served well as a model for the Navier-Stokes system. It has exact analytical solutions for certain initial and boundary conditions, useful when comparing time integration schemes and space discretization schemes.

2.2 A Finite Element Formulation of the Burgers Equation

The proposed Newton-Galerkin finite element method is applied to the Burgers equation, the purpose being to use this test problem to aid in the development of a general method for time dependent, viscous flows. The 1-D time dependent Burgers equation can be written as

$$\underbrace{\frac{\partial u}{\partial t}}_{\text{Unsteady term}} + \underbrace{u\frac{\partial u}{\partial x}}_{\text{Convection term}} - \underbrace{\mu\frac{\partial^2 u}{\partial x^2}}_{\text{Diffusion term}} = \underbrace{s(x,t)}_{\text{Source term}} \tag{2.13}$$

Equation (2.13) requires one initial condition and two boundary conditions. The general form of such conditions is as follows:

initial condition:

$$u(x,t{=}0) = u_o(x) \tag{2.14}$$

boundary conditions:

$$\begin{aligned} u(x{=}\Gamma_1,t) &= u_{\Gamma_1}(t) \\ \frac{\partial u}{\partial x}(x{=}\Gamma_2,t) &= u_{\Gamma_2}(t) \end{aligned} \tag{2.15}$$

To discretize equation (2.13), the Galerkin method is applied. The variable u is approximated in space as:

$$u(x,t) = \sum_{j=1}^{2} N_j(x)\; u_j(t) \tag{2.16}$$

where $u_i(t)$ are the time dependent nodal unknowns, and $N_i(x)$ (Figure 2.1) are the interpolation functions, $N_i(x)$, chosen here to vary linearly over the 1-D element, can be written as:

$$N_1(x) = \frac{x - x_1}{x_2 - x_1}$$

$$N_2(x) = \frac{x_2 - x}{x_2 - x_1} \tag{2.17}$$

The Galerkin integral formulation of equation (2.13) in the domain, Γ, is:

$$\int_{\Gamma_e} \left\{ \frac{\partial u}{\partial t} + u \frac{\partial u}{\partial x} - \mu \frac{\partial^2 u}{\partial x^2} - s(x,t) \right\} W \, d\Gamma = 0 \tag{2.18}$$

After integration by parts, the weak-Galerkin form of equation (2.18) is:

$$\int_{\Gamma_e} \left\{ \left[\frac{\partial u}{\partial t} + u \frac{\partial u}{\partial x} - s(x,t) \right] W + \mu \frac{\partial u}{\partial x} \frac{\partial W}{\partial x} \right\} d\Gamma - \left[\mu \, W \frac{\partial u}{\partial x} \right]_{\Gamma_e} = 0 \tag{2.19}$$

Introducing the Gear time discretization:

$$\left(\frac{\partial u}{\partial t} \right)^t = \frac{1}{\Delta t} \left(\alpha_o u^t + \sum_{i=1}^{k} \alpha_i u_i^{t-i\Delta t} \right) \tag{2.20}$$

Substituting equation (2.20) into equation (2.19) gives:

$$\int_{\Gamma_e} \left\{ \frac{1}{\Delta t}\left[\alpha_o u^{\,t} + \sum_{i=1}^{k} \alpha_i u_i^{\,t-i\Delta t}\right] W + \left[u\frac{\partial u}{\partial x} - s(x,t)\right]^t W + \mu\left(\frac{\partial u}{\partial x}\right)^t W_x \right\} d\Gamma \\ - \mu W\left[\frac{\partial u}{\partial x}\right]^t_{\Gamma_e} = 0 \tag{2.21}$$

Using the Newton linearization:

$$u^{n+1} = u^n + \Delta u \tag{2.22}$$

into equation (2.21) gives:

$$\int_{\Gamma_e} \left\{ \frac{\alpha_o}{\Delta t}\left[\Delta u^{\,t}\right] W + \left[u^n \Delta u_x + u_x^n \Delta u\right]^t W + \mu\left[\Delta u_x\right]^t W_x \right\} d\Gamma \\ - \mu W\left[\Delta u_x\right]^t_{\Gamma_e} = - R_u^n \tag{2.23}$$

where R_u^n is the residual of equation (2.23), given by:

$$R_u^n = \int_{\Gamma_e} \left\{ \frac{1}{\Delta t}\left[\alpha_o u^{\,t,n} + \sum_{i=1}^{k} \alpha_i u_i^{\,t-i\Delta t}\right] W + \left[u\frac{\partial u}{\partial x} - s(x,t)\right]^{t,n} W \\ + \mu\left[\frac{\partial u}{\partial x}\right]^{t,n} W_x \right\} d\Gamma - \mu W\left[\frac{\partial u}{\partial x}\right]^{t,n}_{\Gamma_e} \tag{2.24}$$

Substituting equation (2.16) into equation (2.23) gives:

$$\sum_{e=1}^{E} \left[\left\{ \sum_{j=1}^{2} m_{i,j} + k_{i,j}^1 + k_{i,j}^2 + k_{i,j}^3 \right\} \Delta u_j \right] = - R_u^n \tag{2.25}$$

where, $m_{i,j}$ and $k_{i,j}$ are the element influence matrices, given by:

$$m_{i,j} = \int_{\Gamma_e} \left[\frac{\alpha_o}{\Delta t} N_j W_i \right] d\Gamma \qquad k^1_{i,j} = \int_{\Gamma_e} \left[u^n \frac{\partial N_j}{\partial x} W_i \right] d\Gamma$$

$$k^2_{i,j} = \int_{\Gamma_e} \left[u^n_x N_j W_i \right] d\Gamma \qquad k^3_{i,j} = \int_{\Gamma_e} \left[\mu \frac{\partial N_j}{\partial x} \frac{\partial W_i}{\partial x} \right] d\Gamma$$

Because 1-D linear elements are used, the matrices $m_{i,j}$ and $k_{i,j}$ can be integrated analytically to give:

$$m_{i,j} = \frac{L^e}{6\Delta t} \begin{bmatrix} 2 & 1 \\ 1 & 2 \end{bmatrix} \qquad k^1_{i,j} = \frac{1}{6} \begin{bmatrix} -\left(2u^n_1 + u^n_2\right) & \left(2u^n_1 + u^n_2\right) \\ -\left(u^n_1 + 2u^n_2\right) & \left(u^n_1 + 2u^n_2\right) \end{bmatrix}$$

$$k^2_{i,j} = \frac{1}{6} \begin{bmatrix} 2(u^n_2 - u^n_1) & (u^n_2 - u^n_1) \\ (u^n_2 - u^n_1) & 2(u^n_2 - u^n_1) \end{bmatrix} \qquad k^3_{i,j} = \frac{\mu}{L^e} \begin{bmatrix} 1 & -1 \\ -1 & 1 \end{bmatrix}$$

where $L^e = x_2 - x_1$ is the length of the element.

In order to evaluate the proposed time integration scheme, the following procedure was carried out:

Step 1: Choose a test function $u(x,t)$ satisfying the Burgers equation (2.13), here:

$$u(x,t) = e^{ax+bt} \sin(cx+dt) \tag{2.26}$$

where a, b, c, and d are constant coefficients through which one can control the solution. Coefficient *a* produces an exponentially decaying or growing solution in space, *b* produces an exponentially decaying or growing solution in time, *c* controls the spatial periodicity of the solution, and, finally, *d* alters the frequency of oscillation of the solution. Therefore, through these coefficients, one could make the solution:

- A weak or strong exponential or sinusoidal function in space only;
- A weak or strong exponential or sinusoidal function in time only;
- Combinations of the above.

Knowing the function *u(x,t)*, all terms in equation (2.13) can be exactly evaluated as follows:

$$\frac{\partial u}{\partial t} = e^{(ax+bt)}\left[b\,sin(cx+dt) + d\,cos(cx+dt)\right] \tag{2.27}$$

$$\frac{\partial u}{\partial x} = e^{(ax+bt)}\left[a\,sin(cx+dt) + c\,cos(cx+dt)\right] \tag{2.28}$$

$$\frac{\partial^2 u}{\partial x^2} = e^{(ax+bt)}\left[(a^2-c^2)\,sin(cx+dt) + 2ac\,cos(cx+dt)\right] \tag{2.29}$$

Step 2: Evaluate the source term *s(x,t)* by substituting equations (2.27-2.29) into equation (2.13).

$$\begin{aligned} s(x,t) = e^{(ax+bt)} \Big\{ & \left[b\,sin(cx+dt) + d\,cos(cx+dt)\right] \\ & + e^{(ax+bt)}\,sin(cx+dt)\left[a\,sin(cx+dt) + c\,cos(cx+dt)\right] \\ & - \mu\left[(a^2-c^2)\,sin(cx+dt) + 2ac\,cos(cx+dt)\right]\Big\} \end{aligned} \tag{2.30}$$

Step 3: Evaluate the initial and boundary conditions by substituting equation (2.14) into equation (2.27), and equation (2.15) into equation (2.28). The resulting conditions are:

initial condition:

$$u(x,t{=}0) = u_o(x) = e^{ax}\, sin(cx) \tag{2.31}$$

boundary conditions:

$$u(x{=}\Gamma_1,t) = u_{\Gamma_1}(t) = e^{(a\Gamma_1+bt)}\, sin(c\Gamma_1+dt)$$

$$\frac{\partial u}{\partial x}(x{=}\Gamma_2,t) = u_{\Gamma_2}(t) = e^{(a\Gamma_2+bt)}\left[a\, sin(c\Gamma_2+dt) + c\, cos(c\Gamma_2+dt)\right] \tag{2.32}$$

With this, one can numerically solve for *u(x,t)* from Equation (2.13), given the specified source term *s(x,t)* and the initial and the boundary conditions of equations (2.30, 2.31, 2.32).

2.3 Evaluation of Performance of the Gear Method

In this section a performance evaluation of the Gear method is carried out, versus the θ-family of methods, in particular Crank-Nicolson. The test function considered is a sine wave traveling in the positive *x*-direction, given by:

$$u(x,t) = sin(2\pi(x-t)) \qquad x[0,1] \quad t[0,2] \tag{2.33}$$

Equation (2.33) is chosen because it is representative of the time history of a fluid particle that is being convected downstream, as vortices are shed behind a circular cylinder. The coefficients *a, b, c,* and *d* of equation (2.26) are, in this case:

$$a=0, b=0, c=2\pi, \text{ and } d=-2\pi \tag{2.34}$$

The equation is solved by both the Gear method (k=1,2,3,4) and the Crank-Nicolson method for time step sizes of Δt=0.01, 0.02, 0.04, 0.08 and values of μ=0.1, 0.01, and 0.001. Note that μ in the Burgers equation is analogous to 1/**Re** in the Navier-Stokes equations. The computations are carried out using the parameters given in table 2.2.

Integration method	Gear	Crank-Nicolson
Time step size Δt	0.01, 0.02, 0.04, 0.08	0.01, 0.02, 0.04, 0.08
Order of Gear method, k	1, 2, 3, 4	inherently 2

Table 2.2 Parameters used for the evaluation of the Gear method.

The domain of computation extends 1 unit in the x-direction and contains 20 grid points i.e. Δx=0.05. The time-dependent computations start at time t=0 and end at t=2, covering 2 complete cycles. The initial condition is obtained by setting $t=0$, $a=0$, $b=0$, $c=2\pi$, and $d=-2\pi$ in equation (2.31).

At each time step, the Burgers equation is solved via Newton method, with the time varying boundary conditions obtained from equation (2.32). It is interesting to note that only 3-4 Newton iterations are sufficient to reduce the residual of equation (2.24) to machine accuracy for both methods.

The exact and numerical solutions (Figures 2.2, 2.4, 2.6, 2.8), and the error (Figures 2.3, 2.5, 2.7, 2.9), defined as the absolute difference between the numerical solution and the exact solution, are presented at the point x=0.5, for μ=0.1, Δx=0.05, k=1,2,3,4, θ=0.5 and Δt=0.01, 0.02, 0.04, and 0.08. The numerical solutions given in figure (2.2), are in good agreement with the exact solution due to the small time step used, Δt=0.01. It is clear from figure (2.3) that the error associated with the first-order Gear method (k=1) is lower than all the other methods used, and that the error associated with the higher-order Gear methods (k=2,3,4) is almost identical to the one obtained by the Crank-Nicolson method. For Δt=0.02, figure (2.4) shows pronounced phase and amplitude distortions for the first-order Gear method. Such distortions are expected due to the sinusoidal behavior of the truncation error terms in the finite difference equation. The error associated with these numerical solutions is shown in figure (2.5). For the first-order Gear method the error increases from 0.04 to 0.08 when the time step size increases from 0.01 to 0.02, at time t=1, as shown in figures (2.3) and (2.5). Similar remarks can be made from figures (2.6-2.9) showing the numerical solutions obtained with higher values of time step sizes. It is shown that for all methods the error increases as the time step size increases, while it is also clearly shown that for all values of the time step size the error decreases as the order of accuracy of the Gear method increases. Figure (2.9), for instance, presents the error in the numerical solutions for Δt=0.08, showing the fourth-order Gear method giving the smallest error and the first-order Gear method the largest. The error of the Crank-Nicolson method is smaller than that of the first-order Gear method, but larger than that of the fourth-order one.

The performance of the second-order Gear method is evaluated for a time step size of Δt=0.08 and μ=0.1, 0.01, 0.001. As shown in figure (2.10), the amplitude and phase distortions in the numerical solution become more pronounced with decreasing values of the dissipation coefficient μ. As expected, the maximum error in the solution occurs when the lowest value μ=0.001 is used, (see figure (2.11)). This discrepancy in the solution is due to two main reasons:

1- Nonlinearity of equation (2.13),
2- Matrix conditioning.

When very small values of μ are used, the degree of nonlinearity in the Burgers equation (2.13) becomes more pronounced and therefore more Newton iterations per time step are required to converge. It can be shown that the condition number of the global coefficient matrix becomes poor when very small values of μ are used.

To assess the stability limits of the Gear method for high values of Δt , the following test function is considered:

$$u(x,t) = e^{-t} sin(2\pi x) \qquad x[0,1] \quad t[0,20] \tag{2.35}$$

The coefficients a, b, c, and d of equation (2.26) are, in this case:

$$a=0, b=-1, c=2\pi, \text{ and } d=0 \tag{2.36}$$

The domain of computation extends 1 unit in the x-direction and contains 20 grid points i.e. Δx=0.05. The time-dependent computations start at time t=0 and end at t=20. The initial condition is obtained by setting $t=0$, $a=0$, $b=-1$, $c=2\pi$, and $d=0$ in equation (2.31).

Numerical solutions are obtained by the second-order Gear method (k=2) and the Crank-Nicolson method for μ=0.1 at two time step sizes Δt=0.5, 3.0.

Figures (2.12, 2.13) present both the exact and numerical solutions for the time steps, Δt=0.5 and 3.0, at the point x=0.8, for μ=0.1, Δx=0.05, k=2 and θ=0.5. For Δt=0.5, as shown in figure (2.12), both the second-order Gear method and the Crank-Nicolson method provide stable solutions that are in good agreement with the exact solution. For Δt=3.0, as shown in figure (2.13), the second-order Gear method gives a stable solution while the Crank-Nicolson method produces an oscillating one.

The present analysis has shown that the Gear method (a) provides a wide range of accuracy (truncation error O(Δt)-O(Δt^4)), (b) requires only one derivative function per time step to be evaluated, offering inexpensive computing cost, and (c) provides stable solutions for high values of time step sizes. Because of its good features: implicit, stable, accurate, easy to implement into our steady code, the Gear method was therefore chosen to be implemented into the Navier-Stokes code developed between the Concordia CFD Lab. and Pratt & Whitney Canada.

3. Governing Equations and Finite Element Discretization

This chapter describes the space discretization, Newton linearization, time integration, and boundary conditions of the governing equations in the present work. Although the constant total enthalpy condition is applied in all the validation test cases, the formulation of the full energy equation is presented in this chapter for the sake of completeness.

3.1 Non-dimensionalization

Using the following non-dimensionalization,

$$x^* = \frac{x}{L} \; ; \; t^* = \frac{tV_\infty}{L} \; ; \; V = \frac{V}{V_\infty} \; ; \; p^* = \frac{p}{\rho_\infty} \; ; \; \rho^* = \frac{\rho}{\rho_\infty V_\infty^2} \; ; \; T^* = \frac{R_g T}{V_\infty^2} \qquad (3.1)$$

the time-averaged form of the Navier-Stokes equations for three-dimensional unsteady, viscous, compressible, turbulent flow, in terms of the conservative variables, $\left(\rho\vec{V}, p\right)$, are:

Continuity equation:

$$\frac{\partial \rho}{\partial t} + \nabla \bullet \left(\rho \vec{V}\right) = 0 \qquad (3.2)$$

Momentum equation:

$$\frac{\partial\left(\rho\vec{V}\right)}{\partial t} + \rho\left(\vec{V}\bullet\nabla\right)\vec{V} + \vec{V}\left(\nabla\bullet\rho\vec{V}\right) = -\nabla p$$
$$+ \frac{1}{\mathbf{Re}}\left[-\frac{2}{3}\nabla\left(\mu_{eff}\nabla\bullet\vec{V}\right) + \nabla\times\mu_{eff}\left(\nabla\times\vec{V}\right) + 2\left(\nabla\bullet\mu_{eff}\nabla\right)\vec{V}\right] \qquad (3.3)$$

where **Re** is the Reynolds number and μ_{eff} the effective viscosity. External body forces are neglected.

The energy equation under the assumption of a variable property perfect gas, and in the absence of heat sources and radiation heat transfer, can be written as [16]:

$$\rho C_p \frac{DT_o}{Dt} - \frac{1}{\mathbf{Pr}\ \mathbf{Re}} \nabla \bullet \left[k_{eff} \nabla \left(T_o - \frac{\vec{V}^2}{2C_p} \right) \right] = \mathbf{Ec} \frac{\partial p}{\partial t} + \frac{\mathbf{Ec}}{\mathbf{Re}} \nabla \bullet (\vec{V} \tau_{ij}) \tag{3.4}$$

where ρ is the density, C_p the specific heat coefficient at constant pressure, k_{eff} the effective thermal conductivity; τ_{ij} the viscous stress tensor and **Re**, **Pr** and **Ec** the Reynolds, Prandtl, and Eckert numbers, respectively.

The energy equation can be conveniently simplified, as in the present work, under the assumption of constant total enthalpy along streamlines as:

$$H_o = \frac{\gamma}{\gamma - 1} \frac{p}{\rho} + \frac{1}{2} \vec{V} \bullet \vec{V} \tag{3.5}$$

In particular for turbomachines, in the absence of variable power input or heat transfer at walls, this simplified form is quite adequate.

Under the ideal gas assumption the non-dimensional pressure, density, and temperature are related through the equation of state, as follows:

$$\frac{p}{\rho} = T \tag{3.6}$$

3.2 Effective Viscosity Calculation

For laminar flows, viscosity changes only with temperature and the empirical Sutherland's law is used for an effective viscosity calculation [17]:

$$\frac{\mu_{eff}}{\mu_\infty} = \left(\frac{T}{T_\infty}\right)^{1.5}\left(\frac{T_\infty + 110°K}{T + 110°K}\right) \tag{3.7}$$

3.3 Turbulent Thermal Conductivity

The effective thermal conductivity k_{eff} is calculated from:

$$k_{eff} = k + k_{turb} \tag{3.8}$$

where the subscript $turb$ denotes incremental values introduced by turbulence.

Following Reynolds' postulate, the turbulent momentum and heat fluxes are assumed equivalent, since both fluxes are due to the same mechanism of time-averaged convection. The turbulent thermal conductivity k_{turb} is thus calculated as follows:

$$\frac{k_{turb}}{k_{ref}} = \frac{\mathbf{Pr}}{\mathbf{Pr}_{turb}}\frac{\mu_{turb}}{\mu_{ref}} \tag{3.9}$$

and $\mathbf{Pr}_{turb}$ is given as:

$$\mathbf{Pr}_{turb}^{-1} = 416\,\mathbf{Pr}\left[\frac{1}{15} - \frac{6}{\pi^4}\sum_{m=1}^{\infty}\frac{1}{m^4}\,exp\left(\frac{-0.0024\,\pi^2 m^2}{\mathbf{Pr}}\right)\right] \tag{3.10}$$

This formula for $\mathbf{Pr}_{turb}$ is derived from a theory that takes into account the heat transfer by molecular conduction during turbulent travels of a typical eddy [18,19].

For turbulent flows, there are a number of turbulence models that can be used, ranging from algebraic models, to one-equation and two-equation models. It is not one of the aims of this Thesis to determine the most appropriate turbulence model and the one used was the κ-ε model [20], already implemented in the steady code. The equations governing the two variables of the turbulence model: κ, the kinetic energy of turbulence and ε, the dissipation energy, are:

κ- equation:

$$\rho\frac{\partial\kappa}{\partial t} + \rho\left(\vec{V}\bullet\nabla\right)\kappa - \frac{1}{\mathbf{Re}}\nabla\bullet\left(\frac{\mu_{turb}}{\sigma_\kappa}\nabla\kappa\right) + \rho\varepsilon - \mu_{turb}S = 0 \qquad (3.11)$$

ε- equation:

$$\rho\frac{\partial\varepsilon}{\partial t} + \rho\left(\vec{V}\bullet\nabla\right)\varepsilon - \frac{1}{\mathbf{Re}}\nabla\bullet\left(\frac{\mu_{turb}}{\sigma_\varepsilon}\nabla\varepsilon\right) + C_2\rho\frac{\varepsilon^2}{\kappa} - C_1C_\mu\rho\kappa S = 0 \qquad (3.12)$$

where

$$S = \frac{1}{2}\left[\nabla\vec{V} + \nabla\vec{V}^{t}\right]^2 \; ; \; \mu_{turb} = \frac{C_\mu\kappa^2}{\varepsilon} \qquad (3.13)$$

and the chosen constants for the model are:

$$C_1 = 1.44\,,\; C_2 = 1.92\,,\; C_\mu = 0.09 \;;\; \sigma_\kappa = 1.0\,,\; \sigma_\varepsilon = 1.3 \qquad (3.14)$$

and

$$\mu_{eff} = \mu + \mu_{turb} \qquad (3.15)$$

One should immediately notice the similarity between the κ-ε equations and the momentum equations. In addition, if only the 3 leftmost terms are compared, then equations (3.11) and (3.12) are identical, but with different source terms.

3.4 Solution Regularization Procedure

In the solution of the Navier-Stokes equations, it is known that odd-even decoupling or checkerboarding would occur unless unequal order interpolations of velocity and pressure are used in finite element methods or staggered grids are used in finite differences. To overcome this decoupling in a simpler manner, it is suggested to add a pressure dissipation term, $\lambda \nabla^2 p$, to the right-hand-side of the continuity equation, where λ is a small controllable parameter. The continuity equation (3.2) can then be rewritten as [3]:

$$\frac{\partial \rho}{\partial t} + \nabla \bullet \left(\rho \vec{V} \right) = \lambda \nabla^2 p \qquad (3.16)$$

The pressure dissipation term, necessary for stabilization, produces a first order error in mass conservation. To refine this to second order accuracy, equation (3.16) can then be rewritten as [21]:

$$\frac{\partial \rho}{\partial t} + \nabla \bullet \left(\rho \vec{V} \right) = \lambda \nabla \bullet \left[\nabla p - \nabla \hat{p} \right] \qquad (3.17)$$

where the balancing term $\nabla \hat{p}$ is calculated by extrapolating ∇p from the Gauss points to the corner nodes, followed by averaging over neighboring elements. In fact, this approach of subtracting two second order dissipation terms on a uniform grid is equivalent to using a fourth order one.

With such regularization, it is then permissible to interpolate all variables $\phi = (u,\ v,\ w, p,\ T)$ by equal order shape functions. In this thesis, hexahedral elements are used and a trilinear interpolation function in each, in terms of local element coordinates $(\xi,\ \eta,\ \zeta)$, as follows:

$$\phi = \sum_{j=1}^{8} N_j \phi_j \tag{3.18}$$

where $$N_j(\xi, \eta, \zeta) = \frac{1}{8}(1 + \xi\xi_j)(1 + \eta\eta_j)(1 + \zeta\zeta_j); \quad j=1,\ldots, 8 \tag{3.19}$$

3.5 Weak-Galerkin Finite Element Method

The discretized form of the governing equations is obtained by minimizing, in a weighted average sense, the residuals of the system of equations (3.2-3.6, 3.11-3.12) over the solution domain. This is done by multiplying each equation by a weight function, *W*, and integrating over the domain. In the Galerkin method, in particular, the weight functions, *W*, are chosen to be identical to the shape functions, *N*. The weak form is then obtained by integrating by parts the weighted residual form of the system of equations.

3.5.1 Continuity Equation

The continuity equation (3.17) is multiplied by a weight function, *W,* and integrated over the volume as follows:

$$\int_{\vartheta}\left\{\frac{\partial\rho}{\partial t} + \nabla\bullet\left(\rho\vec{V}\right) - \lambda\nabla\bullet\left[\nabla p - \nabla\hat{p}\right]\right\}W\,d\vartheta = 0 \tag{3.20}$$

After integration by parts, the weak-Galerkin form of equation (3.20) can be written as:

$$\begin{aligned}&\int_{\vartheta}\frac{\partial\rho}{\partial t}W\,d\vartheta + \int_{S}\left(\rho\vec{V}\right)\bullet\vec{n}\,W\,dS - \int_{\vartheta}\left(\rho\vec{V}\right)\bullet\nabla W\,d\vartheta\\ &- \lambda\int_{S}\left[\nabla p - \nabla\hat{p}\right]\bullet\vec{n}\,W\,dS + \lambda\int_{\vartheta}\left[\nabla p - \nabla\hat{p}\right]\bullet\nabla W\,d\vartheta = 0\end{aligned} \tag{3.21}$$

After grouping similar terms, equation (3.21) can be rewritten as:

$$\begin{aligned}&\int_{\vartheta}\left\{\frac{\partial\rho}{\partial t}W - \left[\left(\rho\vec{V}\right) - \lambda\left(\nabla p - \nabla\hat{p}\right)\right]\bullet\nabla W\right\}d\vartheta\\ &\quad + \int_{S}\left[\rho\vec{V} - \lambda\left(\nabla p - \nabla\hat{p}\right)\right]\bullet\vec{n}\,W\,dS\end{aligned} \tag{3.22}$$

whose scalar form is:

$$\int_{\vartheta}\left\{\frac{\partial\rho}{\partial t}W - \left[\rho u - \lambda\left(p_x - \hat{p}_x\right)\right]W_x - \left[\rho v - \lambda\left(p_y - \hat{p}_y\right)\right]W_y\right.$$

$$- \left[\rho w - \lambda(p_z - \hat{p}_z)\right] W_z \Big\} \, d\vartheta$$

$$+ \int_S \Big\{ \left[\rho u - \lambda(p_x - \hat{p}_x)\right] n_x + \left[\rho v - \lambda(p_y - \hat{p}_y)\right] n_y$$

$$+ \left[\rho w - \lambda(p_z - \hat{p}_z)\right] n_z \Big\} W dS = 0 \qquad (3.23)$$

3.5.2 Momentum Equations

The x-momentum equation in Cartesian coordinates reads:

$$\frac{\partial(\rho u)}{\partial t} + \frac{\partial(\rho u^2)}{\partial x} + \frac{\partial(\rho v u)}{\partial y} + \frac{\partial(\rho w u)}{\partial z} + \frac{\partial p}{\partial x}$$

$$- \left[\frac{2}{3} \frac{\mu_{eff}}{\mathbf{Re}} (2u_x - v_y - w_z)\right]_x - \left[\frac{\mu_{eff}}{\mathbf{Re}} (v_x + u_y)\right]_y$$

$$- \left[\frac{\mu_{eff}}{\mathbf{Re}} (w_x + u_z)\right]_z = 0 \qquad (3.24)$$

Equation (3.24) is multiplied by a weight function, W, and integrated over the volume as follows:

$$\int_\vartheta \left\{ \frac{\partial(\rho u)}{\partial t} + \frac{\partial(\rho u^2)}{\partial x} + \frac{\partial(\rho v u)}{\partial y} + \frac{\partial(\rho w u)}{\partial z} + \frac{\partial p}{\partial x} \right.$$

$$- \left[\frac{2}{3} \frac{\mu_{eff}}{\mathbf{Re}} (2u_x - v_y - w_z)\right]_x - \left[\frac{\mu_{eff}}{\mathbf{Re}} (v_x + u_y)\right]_y$$

$$\left. - \left[\frac{\mu_{eff}}{\mathbf{Re}} (w_x + u_z)\right]_z \right\} W d\vartheta = 0 \qquad (3.25)$$

After integration by parts, the weak-Galerkin form of equation (3.25) can be written as:

$$\begin{aligned}
&\int_{\vartheta}\Big\{\frac{\partial(\rho u)}{\partial t}W - \Big[p + \rho u^2 - \frac{2}{3}\frac{\mu_{eff}}{\mathbf{Re}}(2u_x - v_y - w_z)\Big]W_x - \Big[\rho vu - \frac{\mu_{eff}}{\mathbf{Re}}(v_x + u_y)\Big]W_y \\
&\qquad - \Big[\rho wu - \frac{\mu_{eff}}{\mathbf{Re}}(w_x + u_z)\Big]W_z\Big\}\,d\vartheta \\
&+\int_S \Big\{\Big[p + \rho u^2 + \frac{2}{3}\frac{\mu_{eff}}{\mathbf{Re}}(v_y + w_z) - \frac{1}{3}\frac{\mu_{eff}}{\mathbf{Re}}u_x\Big]n_x + \Big[\rho vu - \frac{\mu_{eff}}{\mathbf{Re}}v_x\Big]n_y \\
&\qquad + \Big[\rho wu - \frac{\mu_{eff}}{\mathbf{Re}}w_x\Big]n_z - \frac{\mu_{eff}}{\mathbf{Re}}u_n\Big\}W\,dS = 0
\end{aligned} \tag{3.26}$$

Similarly for the *y*-momentum equation in Cartesian coordinates:

$$\begin{aligned}
&\frac{\partial(\rho v)}{\partial t} + \frac{\partial(\rho v^2)}{\partial y} + \frac{\partial(\rho u v)}{\partial x} + \frac{\partial(\rho w v)}{\partial z} + \frac{\partial p}{\partial y} \\
&- \Big[\frac{\mu_{eff}}{\mathbf{Re}}(u_y + v_x)\Big]_x - \Big[\frac{2}{3}\frac{\mu_{eff}}{\mathbf{Re}}(2v_y - u_x - w_z)\Big]_y \\
&- \Big[\frac{\mu_{eff}}{\mathbf{Re}}(w_y + v_z)\Big]_z = 0
\end{aligned} \tag{3.27}$$

The weak-Galerkin form of equation (3.27) can be written as:

$$\begin{aligned}
&\int_{\vartheta}\Big\{\frac{\partial(\rho v)}{\partial t}W - \Big[\rho uv - \frac{\mu_{eff}}{\mathbf{Re}}(v_x + u_y)\Big]W_x - \Big[p + \rho v^2 - \frac{2}{3}\frac{\mu_{eff}}{\mathbf{Re}}(2v_y - u_x - w_z)\Big]W_y \\
&\qquad - \Big[\rho wv - \frac{\mu_{eff}}{\mathbf{Re}}(w_y + v_z)\Big]W_z\Big\}\,d\vartheta \\
&+\int_S \Big\{\Big[\rho uv - \frac{\mu_{eff}}{\mathbf{Re}}u_y\Big]n_x + \Big[p + \rho v^2 + \frac{2}{3}\frac{\mu_{eff}}{\mathbf{Re}}(u_x + w_z) - \frac{1}{3}\frac{\mu_{eff}}{\mathbf{Re}}v_y\Big]n_y \\
&\qquad + \Big[\rho wv - \frac{\mu_{eff}}{\mathbf{Re}}w_y\Big]n_z - \frac{\mu_{eff}}{\mathbf{Re}}v_n\Big\}W\,dS = 0
\end{aligned} \tag{3.28}$$

While for the z-momentum equation in Cartesian coordinates:

$$\frac{\partial(\rho w)}{\partial t} + \frac{\partial(\rho w^2)}{\partial z} + \frac{\partial(\rho u w)}{\partial x} + \frac{\partial(\rho v w)}{\partial y} + \frac{\partial p}{\partial z}$$
$$- \left[\frac{\mu_{eff}}{\mathbf{Re}} (u_z + w_x)\right]_x - \left[\frac{\mu_{eff}}{\mathbf{Re}} (v_z + w_y)\right]_y$$
$$- \left[\frac{2}{3}\frac{\mu_{eff}}{\mathbf{Re}} (2w_z - u_x - v_y)\right]_z = 0 \tag{3.29}$$

The weak-Galerkin form of equation (3.29) can be written as:

$$\int_{\vartheta} \left\{ \frac{\partial(\rho w)}{\partial t} W - \left[\rho u w - \frac{\mu_{eff}}{\mathbf{Re}} (u_z + w_x)\right] W_x - \left[\rho v w - \frac{\mu_{eff}}{\mathbf{Re}} (v_z + w_y)\right] W_y \right.$$
$$\left. - \left[p + \rho w^2 - \frac{2}{3}\frac{\mu_{eff}}{\mathbf{Re}} (2w_z - u_x - v_z)\right] W_z \right\} d\vartheta$$
$$+ \int_S \left\{ \left[\rho u w - \frac{\mu_{eff}}{\mathbf{Re}} u_z\right] n_x + \left[p + \rho w^2 + \frac{2}{3}\frac{\mu_{eff}}{\mathbf{Re}} (u_x + v_y) - \frac{1}{3}\frac{\mu_{eff}}{\mathbf{Re}} w_z\right] n_z \right.$$
$$\left. + \left[\rho v w - \frac{\mu_{eff}}{\mathbf{Re}} v_z\right] n_y - \frac{\mu_{eff}}{\mathbf{Re}} w_n \right\} W dS = 0 \tag{3.30}$$

3.5.3 Energy Equation

The energy equation (3.4) is multiplied by a weight function, W, and integrated over the volume as follows:

$$\int_{\vartheta} \left\{ \rho C_p \frac{DT_o}{Dt} - \frac{1}{\mathbf{Pr}\ \mathbf{Re}} \nabla \bullet \left[k_{eff} \nabla \left(T_o - \frac{\vec{V}^2}{2C_p} \right) \right] - \mathbf{Ec} \frac{\partial p}{\partial t} - \frac{\mathbf{Ec}}{\mathbf{Re}} \nabla \bullet (\vec{V} \tau_{ij}) \right\} W d\vartheta = 0 \tag{3.31}$$

After integration by parts, the weak-Galerkin form of equation (3.31) can be written as:

$$\int_{\vartheta} \left\{ \left[\rho C_p \left(\frac{\partial T_o}{\partial t} + \vec{V} \bullet \nabla T_o \right) - \mathbf{Ec} \frac{\partial p}{\partial t} \right] W + \left[\frac{k_{eff}}{\mathbf{Pr\ Re}} \nabla \left(T_o - \frac{\vec{V}^2}{2C_p} \right) + \frac{\mathbf{Ec}}{\mathbf{Re}} \vec{V} \tau_{ij} \right] \bullet \nabla W \right\} d\vartheta$$

$$- \int_S \left\{ \left[\frac{k_{eff}}{\mathbf{Pr\ Re}} \nabla T + \frac{\mathbf{Ec}}{\mathbf{Re}} \vec{V} \tau_{ij} \right] \bullet \vec{n} \right\} W dS = 0 \qquad (3.32)$$

The viscous dissipation term $\nabla \bullet V \tau_{ij}$ in equation (3.32) may be explicitly written as:

$$\frac{\partial}{\partial x}(u\tau_{xx} + v\tau_{xy} + w\tau_{xz}) + \frac{\partial}{\partial y}(u\tau_{yx} + v\tau_{yy} + w\tau_{yz}) + \frac{\partial}{\partial z}(u\tau_{zx} + v\tau_{zy} + w\tau_{zz})$$

where, for example: $$\tau_{xx} = \frac{2}{3}\mu(2u_x - v_y - w_z) \qquad (3.33)$$

Now, if

$$\begin{aligned} \Phi_1 &= u\tau_{xx} + v\tau_{xy} + w\tau_{xz} \\ \Phi_2 &= u\tau_{yx} + v\tau_{yy} + w\tau_{yz} \\ \Phi_3 &= u\tau_{xx} + v\tau_{zy} + w\tau_{zz} \end{aligned} \qquad (3.34)$$

then equation (3.32) can then be rewritten as follows:

$$\int_{\vartheta} \left\{ \rho C_p \frac{\partial T_o}{\partial t} W + C_p [\rho u T_{ox} + \rho v T_{oy} + \rho w T_{oz}] W \right.$$

$$\left. + \frac{k_{eff}}{\mathbf{Pr\ Re}} [T_{ox} W_x + T_{oy} W_y + T_{oy} W_z] \right\} d\vartheta$$

$$+ \int_S \left[\frac{k_{eff}}{\mathbf{Pr\ Re}} T_n \right] W dS = RHS \qquad (3.35)$$

where

$$RHS = \int_{\vartheta} \left\{ \mathbf{Ec} \frac{\partial p}{\partial t} W + \frac{k_{eff}}{\mathbf{Pr}\ \mathbf{Re}} \left[\left(\frac{\vec{V}^2}{2C_p} \right)_x W_x + \left(\frac{\vec{V}^2}{2C_p} \right)_y W_y + \left(\frac{\vec{V}^2}{2C_p} \right)_z W_z \right] \right.$$

$$\frac{\mathbf{Ec}}{\mathbf{Re}} \int_{s} \left[\Phi_1 n_x + \Phi_2 n_y + \Phi_3 n_z \right] W dS \tag{3.36}$$

3.5.4 Turbulence Equations

The κ-equation (3.11) is multiplied by a weight function, *W*, and integrated over the volume as follows:

$$\int_{\vartheta} \left\{ \rho \frac{\partial \kappa}{\partial t} + \rho \left(\vec{V} \bullet \nabla \right) \kappa - \frac{1}{\mathbf{Re}} \nabla \bullet \left(\frac{\mu_{turb}}{\sigma_\kappa} \nabla \kappa \right) + \rho \varepsilon - \mu_{turb} S \right\} W d\vartheta = 0 \tag{3.37}$$

After integration by parts, its weak-Galerkin form is:

$$\int_{\vartheta} \left\{ \left[\rho \frac{\partial \kappa}{\partial t} + \rho \left(\vec{V} \bullet \nabla \right) \kappa + \rho \varepsilon - \mu_{turb} S \right] W + \frac{1}{\mathbf{Re}} \frac{\mu_{turb}}{\sigma_\kappa} \nabla \kappa \bullet \nabla W \right\} d\vartheta$$

$$- \frac{1}{\mathbf{Re}} \int_{S} \left[\frac{\mu_{turb}}{\sigma_\kappa} \nabla \kappa \bullet \vec{n} \right] W dS = 0 \tag{3.38}$$

The scalar form of equation (3.38) can be written as:

$$\int_{\vartheta} \left\{ \left[\rho \frac{\partial \kappa}{\partial t} + \rho u \kappa_x + \rho v \kappa_y + \rho w \kappa_z + \rho \varepsilon - \mu_{turb} S \right] W \right.$$

$$+ \frac{1}{\mathbf{Re}}\left[\frac{\mu_{turb}}{\sigma_{\kappa}}\left(\kappa_x W_x + \kappa_y W_y + \kappa_z W_z\right)\right]\Bigg\} d\vartheta$$

$$- \frac{1}{\mathbf{Re}}\int_S \left[\frac{\mu_{turb}}{\sigma_{\kappa}}\,\kappa_n\right] W dS = 0 \qquad (3.39)$$

Similarly, the ε-equation (3.12) is multiplied by a weight function, *W*, and integrated over the volume as follows:

$$\int_{\vartheta}\left\{\rho\frac{\partial\varepsilon}{\partial t} + \rho\left(\vec{V}\bullet\nabla\right)\varepsilon - \frac{1}{\mathbf{Re}}\nabla\bullet\left(\frac{\mu_{turb}}{\sigma_{\varepsilon}}\nabla\varepsilon\right) + C_2\rho\frac{\varepsilon^2}{\kappa} - C_1C_{\mu}\rho\kappa S\right\} W d\vartheta = 0 \qquad (3.40)$$

After integration by parts, its weak-Galerkin is:

$$\int_{\vartheta}\left\{\left[\rho\frac{\partial\varepsilon}{\partial t} + \rho\left(\vec{V}\bullet\nabla\right)\varepsilon + C_2\rho\left(\frac{\varepsilon^2}{\kappa}\right) - C_1C_{\mu}\rho\kappa S\right] W + \frac{1}{\mathbf{Re}}\frac{\mu_{turb}}{\sigma_{\varepsilon}}\nabla\varepsilon\bullet\nabla W\right\} d\vartheta$$

$$- \frac{1}{\mathbf{Re}}\int_S \left[\frac{\mu_{turb}}{\sigma_{\varepsilon}}\nabla\varepsilon\bullet\vec{n}\right] W dS = 0 \qquad (3.41)$$

The scalar form of equation (3.41) can be written as follows:

$$\int_{\vartheta}\Bigg\{\left[\rho\frac{\partial\varepsilon}{\partial t} + \rho u\varepsilon_x + \rho v\varepsilon_y + \rho w\varepsilon_z + C_2\rho\left(\frac{\varepsilon^2}{\kappa}\right) - C_1C_{\mu}\rho\kappa S\right] W$$

$$+ \frac{1}{\mathbf{Re}}\left[\frac{\mu_{turb}}{\sigma_{\varepsilon}}\left(\varepsilon_x W_x + \varepsilon_y W_y + \varepsilon_z W_z\right)\right]\Bigg\} d\vartheta$$

$$- \frac{1}{\mathbf{Re}}\int_S \left[\frac{\mu_{turb}}{\sigma_{\varepsilon}}\,\varepsilon_n\right] W dS = 0 \qquad (3.42)$$

3.5.5 Finite Element Discretization

The geometrical discretization is based on a trilinear hexahedral (8-nodes) elements:

$$x=\sum_{j=1}^{8} N_j(\xi,\eta,\zeta)\,x_j \qquad y=\sum_{j=1}^{8} N_j(\xi,\eta,\zeta)\,y_j \qquad z=\sum_{j=1}^{8} N_j(\xi,\eta,\zeta)\,z_j \tag{3.43}$$

A typical trilinear hexahedral (8-nodes) element is shown in figure (3.1).

The regularization provided by the added pressure dissipation term to the continuity equation permits all variables, $\phi=(u,\ v,\ w,\ p,\ T,\ \kappa,\ \varepsilon)$, to be interpolated by the same interpolant. Here, a trilinear shape function is used in terms of local non-dimensional undistorted element coordinates $(\xi,\ \eta,\ \zeta)$ as:

$$\phi=\sum_{j=1}^{8} N_j\phi_j \tag{3.18}$$

where $$N_j(\xi,\ \eta,\ \zeta)=\frac{1}{8}(1+\xi\xi_j)(1+\eta\eta_j)(1+\zeta\zeta_j); \quad j=1,\ldots,8 \tag{3.19}$$

In the Galerkin weighted residual method, the weight functions, W_j, are chosen to be identical to their corresponding interpolation functions N_j. This implies that:

$$W_j(\xi,\eta,\ \zeta)=N_j(\xi,\ \eta,\ \zeta) \tag{3.44}$$

3.6 Time Discretization

The time derivatives in the governing equations are discretized by an unconditionally stable multi-level Gear implicit scheme. This method has a variable order of time accuracy, controlled by the number of time levels used. For example, a first order Gear scheme (identical to the Euler-backward scheme), requires information from one time level, to solve at the current one. The time derivative of a general variable ϕ is expressed as follows:

$$\left(\frac{\partial \phi}{\partial t}\right)^t = \frac{1}{\Delta t}\left(\alpha_o \phi^{\,t} + \sum_{i=1}^{k} \alpha_i \phi^{\,t-i\Delta t}\right) \tag{3.45}$$

where $\alpha_i\,(i = 0, 1, 2, \ldots, k)$ and k are the coefficients and the required order of time accuracy of the Gear scheme, respectively.

3.6.1 Continuity Equation

The weak-Galerkin form of the continuity equation (3.23) is time discretized using a Gear scheme of kth order accuracy in time as follows:

$$\begin{aligned}
&\int_{\vartheta} \left\{ \frac{1}{\Delta t}\left[\alpha_o \rho^{\,t} + \sum_{i=1}^{k} \alpha_i \rho^{\,t-i\Delta t}\right] W - \left[\rho u - \lambda(p_x - \hat{p}_x)\right]^t W_x \right. \\
&\quad \left. - \left[\rho v - \lambda(p_y - \hat{p}_y)\right]^t W_y - \left[\rho w - \lambda(p_z - \hat{p}_z)\right]^t W_z \right\} d\vartheta \\
&\quad + \int_S \left\{ \left[\rho u - \lambda(p_x - \hat{p}_x)\right]^t n_x + \left[\rho v - \lambda(p_y - \hat{p}_y)\right]^t n_y \right. \\
&\qquad \left. + \left[\rho w - \lambda(p_z - \hat{p}_z)\right]^t n_z \right\} W dS = 0
\end{aligned} \tag{3.46}$$

3.6.2 Momentum Equations

The weak-Galerkin form of the x-momentum equation (3.26) is time discretized using a Gear scheme of kth order accuracy in time as follows:

$$
\begin{aligned}
\int_{\vartheta} & \left\{ \frac{1}{\Delta t} \left[\alpha_0 (\rho u)^t + \sum_{i=1}^{k} \alpha_i (\rho u)^{t-i\Delta t} \right] W - \left[p + \rho u^2 - \frac{2}{3} \frac{\mu_{eff}}{\mathbf{Re}} (2u_x - v_y - w_z) \right]^t W_x \right. \\
& \left. - \left[\rho v u - \frac{\mu_{eff}}{\mathbf{Re}} (v_x + u_y) \right]^t W_y - \left[\rho w u - \frac{\mu_{eff}}{\mathbf{Re}} (w_x + u_z) \right]^t W_z \right\} d\vartheta \\
+ \int_{S} & \left\{ \left[p + \rho u^2 + \frac{2}{3} \frac{\mu_{eff}}{\mathbf{Re}} (v_y + w_z) - \frac{1}{3} \frac{\mu_{eff}}{\mathbf{Re}} u_x \right]^t n_x + \left[\rho v u - \frac{\mu_{eff}}{\mathbf{Re}} v_x \right]^t n_y \right. \\
& \left. + \left[\rho w u - \frac{\mu_{eff}}{\mathbf{Re}} w_x \right]^t n_z - \left[\frac{\mu_{eff}}{\mathbf{Re}} u_h \right]^t \right\} W dS = 0 \qquad (3.47)
\end{aligned}
$$

while for the y-momentum, equation (3.28):

$$
\begin{aligned}
\int_{\vartheta} & \left\{ \frac{1}{\Delta t} \left[\alpha_0 (\rho v)^t + \sum_{i=1}^{k} \alpha_i (\rho v)^{t-i\Delta t} \right] W - \left[p + \rho v^2 - \frac{2}{3} \frac{\mu_{eff}}{\mathbf{Re}} (2v_y - u_x - w_z) \right]^t W_y \right. \\
& \left. - \left[\rho u v - \frac{\mu_{eff}}{\mathbf{Re}} (v_x + u_y) \right]^t W_x - \left[\rho w v - \frac{\mu_{eff}}{\mathbf{Re}} (w_y + v_z) \right]^t W_z \right\} d\vartheta \\
+ \int_{S} & \left\{ \left[\rho u v - \frac{\mu_{eff}}{\mathbf{Re}} u_y \right]^t n_x + \left[p + \rho v^2 + \frac{2}{3} \frac{\mu_{eff}}{\mathbf{Re}} (u_x + w_z) - \frac{1}{3} \frac{\mu_{eff}}{Re} v_y \right]^t n_y \right. \\
& \left. + \left[\rho w v - \frac{\mu_{eff}}{\mathbf{Re}} w_y \right]^t n_z - \left[\frac{\mu_{eff}}{\mathbf{Re}} v_h \right]^t \right\} W dS = 0 \qquad (3.48)
\end{aligned}
$$

and the z-momentum, equation (3.30):

$$
\begin{aligned}
\int_{\vartheta} & \left\{ \frac{1}{\Delta t} \left[\alpha_0 (\rho w)^t + \sum_{i=1}^{k} \alpha_i (\rho w)^{t-i\Delta t} \right] W - \left[p + \rho w^2 - \frac{2}{3} \frac{\mu_{eff}}{\mathbf{Re}} (2w_z - u_x - v_y) \right]^t W_z \right\} \\
& - \left[\rho u w - \frac{\mu_{eff}}{\mathbf{Re}} (u_z + w_x) \right]^t W_x - \left[\rho v w - \frac{\mu_{eff}}{\mathbf{Re}} (v_z + w_y) \right]^t W_y \; d\vartheta
\end{aligned}
$$

$$+ \int_S \left\{ \left[\rho u w - \frac{\mu_{eff}}{\mathbf{Re}} \, u_z \right]^t n_x + \left[p + \rho w^2 + \frac{2}{3} \frac{\mu_{eff}}{\mathbf{Re}} (u_x + v_y) - \frac{1}{3} \frac{\mu_{eff}}{\mathbf{Re}} \, w_z \right]^t n_z \right.$$

$$\left. + \left[\rho v w - \frac{\mu_{eff}}{\mathbf{Re}} \, v_z \right]^t n_y - \left[\frac{\mu_{eff}}{\mathbf{Re}} \, w_n \right]^t W \right\} dS = 0 \qquad (3.49)$$

3.6.3 Energy Equation

The weak-Galerkin form of the energy equation (3.35) is time discretized using a Gear scheme of kth order accuracy in time as follows:

$$\int_\vartheta \left\{ (\rho C_p)^t \frac{1}{\Delta t} \left[\alpha_o T_o^t + \sum_{i=1}^{k} \alpha_i T_o^{t-i\Delta t} \right] W + \left[C_p (\rho u T_{ox} + \rho v T_{oy} + \rho w T_{oz}) \right]^t W \right.$$

$$\left. + \left[\frac{k_{eff}}{\mathbf{Pr} \ \mathbf{Re}} (T_{ox} W_x + T_{oy} W_y + T_{oy} W_z) \right]^t \right\} d\vartheta + \int_S \left[\frac{k_{eff}}{\mathbf{Pr} \ \mathbf{Re}} T_n \right]^t W dS = RHS^t \qquad (3.50)$$

where

$$RHS^t = \int_\vartheta \left\{ \frac{\mathbf{Ec}}{\Delta t} \left[\alpha_o p^t + \sum_{i=1}^{k} \alpha_i p^{t-i\Delta t} \right] W - \frac{\mathbf{Ec}}{\mathbf{Re}} \left[\Phi_1 W_x + \Phi_2 W_y + \Phi_3 W_z \right]^t \right.$$

$$\left. + \frac{k_{eff}^t}{\mathbf{Pr} \ \mathbf{Re}} \left[\left(\frac{\vec{V}^2}{2C_p} \right)_x W_x + \left(\frac{\vec{V}^2}{2C_p} \right)_y W_y + \left(\frac{\vec{V}^2}{2C_p} \right)_z W_z \right]^t \right\} d\vartheta$$

$$+ \frac{\mathbf{Ec}}{\mathbf{Re}} \int_S \left[\Phi_1 n_x + \Phi_2 n_y + \Phi_3 n_z \right]^t W dS \qquad (3.51)$$

3.6.4 Turbulence Equations

The weak-Galerkin form of the κ-equation (3.39) is time discretized using Gear scheme of kth order accuracy in time as follows:

$$\begin{aligned}\int_{\vartheta} \Bigg\{ & \frac{\rho^{t}}{\Delta t}\left[\alpha_0 \kappa^{t} + \sum_{i=1}^{k} \alpha_i \kappa^{t-i\Delta t}\right] W + \left[\rho u \kappa_x + \rho v \kappa_y + \rho w \kappa_z\right]^{t} W \\ & + \left[\rho \varepsilon - \mu_{turb} S\right]^{t} W + \frac{1}{\mathrm{Re}}\left[\frac{\mu_{turb}}{\sigma_\kappa}\left(\kappa_x W_x + \kappa_y W_y + \kappa_z W_z\right)\right]^{t} \Bigg\} d\vartheta \\ & - \frac{1}{\mathrm{Re}} \int_{S} \left[\frac{\mu_{turb}}{\sigma_\kappa}\left(\kappa_x n_x + \kappa_y n_y + \kappa_z n_z\right)\right]^{t} W dS = 0 \end{aligned} \tag{3.52}$$

The weak-Galerkin form of the ε-equation (3.42) is time discretized using Gear scheme of kth order accuracy in time as follows:

$$\begin{aligned}\int_{\vartheta} \Bigg\{ & \frac{\rho^{t}}{\Delta t}\left[\alpha_0 \varepsilon^{t} + \sum_{i=1}^{k} \alpha_i \varepsilon^{t-i\Delta t}\right] W + \left[\rho u \varepsilon_x + \rho v \varepsilon_y + \rho w \varepsilon_z\right]^{t} W \\ & + \left[C_2 \rho \frac{\varepsilon^2}{\kappa} - C_1 C_\mu \rho \kappa S\right]^{t} W + \frac{1}{\mathrm{Re}}\left[\frac{\mu_{turb}}{\sigma_\varepsilon}\left(\varepsilon_x W_x + \varepsilon_y W_y + \varepsilon_z W_z\right)\right]^{t} \Bigg\} d\vartheta \\ & - \frac{1}{\mathrm{Re}} \int_{S} \left[\frac{\mu_{turb}}{\sigma_\varepsilon}\left(\varepsilon_x n_x + \varepsilon_y n_y + \varepsilon_z n_z\right)\right]^{t} W dS = 0 \end{aligned} \tag{3.53}$$

3.7 Newton Linearization

The system of equations (3.2-3.6, 3.11-3.12) must be linearized before a numerical solution is attempted. Here, the equations are linearized via Newton method by setting for any general variable:

$$\Delta\phi = \phi^{n+1} - \phi^{n} \tag{3.54}$$

and obtaining the Jacobian matrix.

3.7.1 Continuity Equation

After introducing the Newton method and neglecting second order terms, the continuity equation (3.46) can be written as follows:

$$\begin{aligned}
&\int_{\vartheta} \left\{ \frac{\alpha_o}{\Delta t} \left[\Delta\left(\frac{P}{T}\right) \right]^t W - \left[\Delta(\rho u) - \lambda \Delta p_x \right]^t W_x - \left[\Delta(\rho v) - \lambda \Delta p_y \right]^t W_y \right. \\
&\qquad \left. - \left[\Delta(\rho w) - \lambda \Delta p_z \right]^t W_z \right\} d\vartheta \\
&\quad + \int_S \left\{ \left[\Delta(\rho u) - \lambda \Delta p_x \right]^t n_x + \left[\Delta(\rho v) - \lambda \Delta p_y \right]^t n_y \right. \\
&\qquad \left. + \left[\Delta(\rho w) - \lambda \Delta p_z \right]^t n_z \right\} W dS = - R_p^n
\end{aligned} \tag{3.55}$$

where R_p^n is the residual of the discretized continuity equation at Newton step n of the time level t, and is given by:

$$\begin{aligned}
R_p^n = \int_{\vartheta} &\left\{ \frac{1}{\Delta t} \left[\alpha_o \left(\frac{P}{T}\right)^{t,n} + \sum_{i=1}^{k} \alpha_i \left(\frac{P}{T}\right)^{t-i\Delta t} \right] W - \left[\rho u - \lambda(p_x - \hat{p}_x) \right]^{t,n} W_x \right. \\
&\left. - \left[\rho v - \lambda(p_y - \hat{p}_y) \right]^{t,n} W_y - \left[\rho w - \lambda(p_z - \hat{p}_z) \right]^{t,n} W_z \right\} d\vartheta
\end{aligned}$$

$$+\int_S \Big\{\left[\rho u - \lambda(p_x - \hat{p}_x)\right]^{t,n} n_x + \left[\rho v - \lambda(p_y - \hat{p}_y)\right]^{t,n} n_y + \left[\rho w - \lambda(p_z - \hat{p}_z)\right]^{t,n} n_z\Big\} W dS \tag{3.56}$$

Substituting the shape and weight functions into equation (3.55), the following delta form of the continuity equation is assembled, over all elements E, in terms of the cell-vertex unknowns of pressure and velocity:

$$\sum_{e=1}^{E}\left[\left\{\sum_{j=1}^{8}\left[k_{i,j}^{\rho u}\right]_P \Delta(\rho u)_j + \left[k_{i,j}^{\rho v}\right]_P \Delta(\rho v)_j + \left[k_{i,j}^{\rho w}\right]_P \Delta(\rho w)_j + \left[k_{i,j}^{P}\right]_P \Delta(p)_j\right\}\right] = - R_P^n \tag{3.57}$$

where $k_{i,j}$ are the element influence matrices from the continuity equation:

$$\left[k_{i,j}^{P}\right]_P = \int_{\vartheta}\left[\frac{\alpha_0}{\Delta t}\frac{1}{T_j} N_j W_i + \lambda\left(\frac{\partial W_i}{\partial x}\frac{\partial N_j}{\partial x} + \frac{\partial W_i}{\partial y}\frac{\partial N_j}{\partial y} + \frac{\partial W_i}{\partial z}\frac{\partial N_j}{\partial z}\right)\right] d\vartheta$$

$$\left[k_{i,j}^{\rho u}\right]_P = - \int_{\vartheta}\left[\frac{\partial W_i}{\partial x} N_j\right] d\vartheta$$

$$\left[k_{i,j}^{\rho v}\right]_P = - \int_{\vartheta}\left[\frac{\partial W_i}{\partial y} N_j\right] d\vartheta$$

$$\left[k_{i,j}^{\rho w}\right]_P = - \int_{\vartheta}\left[\frac{\partial W_i}{\partial z} N_j\right] d\vartheta$$

3.7.2 Momentum Equations

After introducing the Newton method and neglecting second order terms, the x-momentum equation (3.47) can be written as follows:

$$
\begin{aligned}
\int_{\vartheta} \Bigg\{ & \frac{\alpha_0}{\Delta t}\left[\Delta(\rho u)^t\right] W - \left[\Delta p + 2u^n \Delta(\rho u) - \frac{2}{3}\frac{\mu_{eff}}{\mathbf{Re}}(2\Delta u_x - \Delta v_y - \Delta w_z)\right]^t W_x \\
& - \left[u^n \Delta(\rho v) + v^n \Delta(\rho u) - \frac{\mu_{eff}}{\mathbf{Re}}(\Delta v_x + \Delta u_y)\right]^t W_y \\
& - \left[u^n \Delta(\rho w) + w^n \Delta(\rho u) - \frac{\mu_{eff}}{\mathbf{Re}}(\Delta w_x + \Delta u_z)\right]^t W_z \Bigg\} d\vartheta \\
+ \int_S \Bigg\{ & \left[\Delta p + 2u^n \Delta(\rho u) + \frac{2}{3}\frac{\mu_{eff}}{\mathbf{Re}}(\Delta v_y + \Delta w_z) - \frac{1}{3}\frac{\mu_{eff}}{Re}\Delta u_x\right]^t n_x \\
& + \left[u^n \Delta(\rho v) + v^n \Delta(\rho u) - \frac{\mu_{eff}}{\mathbf{Re}}\Delta v_x\right]^t n_y \\
& + \left[u^n \Delta(\rho w) + w^n \Delta(\rho u) - \frac{\mu_{eff}}{\mathbf{Re}}\Delta w_x\right]^t n_z \\
& + \left[\Delta(\rho w) - \lambda \Delta p_z\right]^t n_z \Bigg\} W dS = - R^n_{\rho u}
\end{aligned}
\tag{3.58}
$$

where $R^n_{\rho u}$ is the residual of the x-momentum equation and is given by:

$$
\begin{aligned}
R^n_{\rho u} = \int_{\vartheta} \Bigg\{ & \frac{1}{\Delta t}\left[\alpha_o(\rho u)^{t,n} + \sum_{i=1}^{k} \alpha_i (\rho u)^{t-i\Delta t}\right] W - \left[\rho v u - \frac{\mu_{eff}}{\mathbf{Re}}(v_x + u_y)\right]^{t,n} W_y \\
& - \left[p + \rho u^2 - \frac{2}{3}\frac{\mu_{eff}}{\mathbf{Re}}(2u_x - v_y - w_z)\right]^{t,n} W_x - \left[\rho w u - \frac{\mu_{eff}}{\mathbf{Re}}(w_x + u_z)\right]^{t,n} W_z \Bigg\} d\vartheta \\
+ \int_S \Bigg\{ & \left[p + \rho u^2 + \frac{2}{3}\frac{\mu_{eff}}{\mathbf{Re}}(v_y + w_z) - \frac{1}{3}\frac{\mu_{eff}}{\mathbf{Re}} u_x\right]^{t,n} n_x + \left[\rho v u - \frac{\mu_{eff}}{\mathbf{Re}} v_x\right]^{t,n} n_y \\
& + \left[\rho w u - \frac{\mu_{eff}}{\mathbf{Re}} w_x\right]^{t,n} n_z - \left[\frac{\mu_{eff}}{\mathbf{Re}} u_n\right]^{t,n} \Bigg\} W dS
\end{aligned}
\tag{3.59}
$$

Assembling the delta form of the *x*-momentum equation over the elements, in terms of the cell-vertex unknowns of pressure and velocity components, one obtains:

$$\sum_{e=1}^{E}\left[\left\{\sum_{j=1}^{8}\left[k_{i,j}^{\rho u}\right]_{\rho u}\Delta(\rho u)_j + \left[k_{i,j}^{\rho v}\right]_{\rho u}\Delta(\rho v)_j + \left[k_{i,j}^{\rho w}\right]_{\rho u}\Delta(\rho w)_j + \left[k_{i,j}^{P}\right]_{\rho u}\Delta(p)_j\right\}\right] = -R_{\rho u}^{n} \tag{3.60}$$

where $k_{i,j}$ are the element influence matrices from the *x*-momentum equation:

$$\left[k_{i,j}^{\rho u}\right]_{\rho u} = \int_{\vartheta}\left[\frac{\alpha_o}{\Delta t}(W_i N_j) - N_j\left(2u^n\frac{\partial W_i}{\partial x} + v^n\frac{\partial W_i}{\partial y} + w^n\frac{\partial W_i}{\partial z}\right)\right.$$
$$\left. + \frac{\mu_{eff}}{\mathbf{Re}\rho_j}\left(\frac{4}{3}\frac{\partial W_i}{\partial x}\frac{\partial N_j}{\partial x} + \frac{\partial W_i}{\partial y}\frac{\partial N_j}{\partial y} + \frac{\partial W_i}{\partial z}\frac{\partial N_j}{\partial z}\right)\right] d\vartheta$$

$$\left[k_{i,j}^{\rho v}\right]_{\rho u} = -\int_{\vartheta}\left[N_j\, u^n\frac{\partial W_i}{\partial y} + \frac{\mu_{eff}}{\mathbf{Re}\rho_j}\left(\frac{2}{3}\frac{\partial W_i}{\partial x}\frac{\partial N_j}{\partial y} - \frac{\partial W_i}{\partial y}\frac{\partial N_j}{\partial x}\right)\right] d\vartheta$$

$$\left[k_{i,j}^{\rho w}\right]_{\rho u} = -\int_{\vartheta}\left[N_j\, u^n\frac{\partial W_i}{\partial z} + \frac{\mu_{eff}}{\mathbf{Re}\rho_j}\left(\frac{2}{3}\frac{\partial W_i}{\partial x}\frac{\partial N_j}{\partial z} - \frac{\partial W_i}{\partial z}\frac{\partial N_j}{\partial x}\right)\right] d\vartheta$$

$$\left[k_{i,j}^{P}\right]_{\rho u} = -\int_{\vartheta}\left[N_j\frac{\partial W_i}{\partial x}\right] d\vartheta$$

After introducing the Newton method and neglecting second order terms, the y-momentum equation (3.48) can be written as follows:

$$
\begin{aligned}
\int_{\vartheta} \Bigg\{ & \frac{\alpha_0}{\Delta t}\left[\Delta(\rho v)^t\right] W - \left[u^n \Delta(\rho v) + v^n \Delta(\rho u) - \frac{\mu_{eff}}{\mathbf{Re}} (\Delta v_x + \Delta u_y)\right]^t W_x \\
& - \left[\Delta p + 2 v^n \Delta(\rho v) - \frac{2}{3}\frac{\mu_{eff}}{\mathbf{Re}} (2\Delta v_y - \Delta u_x - \Delta w_z)\right]^t W_y \\
& - \left[v^n \Delta(\rho w) + w^n \Delta(\rho v) - \frac{\mu_{eff}}{\mathbf{Re}} (\Delta w_y + \Delta v_z)\right]^t W_z \Bigg\} d\vartheta \\
+ \int_S \Bigg\{ & + \left[\Delta p + 2 v^n \Delta(\rho v) + \frac{2}{3}\frac{\mu_{eff}}{\mathbf{Re}} (\Delta u_x + \Delta w_z) - \frac{1}{3}\frac{\mu_{eff}}{\mathbf{Re}} \Delta v_y\right]^t n_y \\
& + \left[u^n \Delta(\rho v) \div v^n \Delta(\rho u) - \frac{\mu_{eff}}{\mathbf{Re}} \Delta u_y\right]^t n_x \\
& + \left[v^n \Delta(\rho w) + w^n \Delta(\rho v) - \frac{\mu_{eff}}{\mathbf{Re}} \Delta w_y\right]^t n_z \\
& \frac{\mu_{eff}}{\mathbf{Re}}\left[\Delta v_x n_x + \Delta v_y n_y + \Delta v_z n_z\right]^t \Bigg\} W dS = - R_{\rho v}^n
\end{aligned}
\tag{3.61}
$$

where $R_{\rho v}^n$ is the residual of the y-momentum equation at Newton iteration n of time level t and is given by:

$$
\begin{aligned}
R_{\rho v}^n = \int_{\vartheta} \Bigg\{ & \frac{1}{\Delta t}\left[\alpha_0(\rho v)^{t,n} + \sum_{i=1}^{k} \alpha_i(\rho v)^{t-i\Delta t}\right] W - \left[\rho u v - \frac{\mu_{eff}}{\mathbf{Re}}(v_x + u_y)\right]^{t,n} W_x \\
& - \left[p + \rho v^2 - \frac{2}{3}\frac{\mu_{eff}}{\mathbf{Re}} (2v_y - u_x - w_z)\right]^{t,n} W_y - \left[\rho w v - \frac{\mu_{eff}}{\mathbf{Re}} (w_y + v_z)\right]^{t,n} W_z \Bigg\} d\vartheta \\
+ \int_S \Bigg\{ & \left[\rho u v - \frac{\mu_{eff}}{\mathbf{Re}} u_y\right]^{t,n} n_x + \left[p + \rho v^2 + \frac{2}{3}\frac{\mu_{eff}}{\mathbf{Re}} (u_x + w_z) - \frac{1}{3}\frac{\mu_{eff}}{Re} v_y\right]^{t,n} n_y \\
& + \left[\rho w v - \frac{\mu_{eff}}{\mathbf{Re}} w_y\right]^{t,n} n_z - \left[\frac{\mu_{eff}}{\mathbf{Re}} v_n\right]^{t,n} \Bigg\} W dS
\end{aligned}
\tag{3.62}
$$

and the delta form of the *y*-momentum equation is:

$$\sum_{e=1}^{E}\left[\sum_{j=1}^{8}\left\{\left[k_{ij}^{\rho u}\right]_{\rho v}\Delta(\rho u)_j + \left[k_{ij}^{\rho v}\right]_{\rho v}\Delta(\rho v)_j + \left[k_{ij}^{\rho w}\right]_{\rho v}\Delta(\rho w)_j + \left[k_{ij}^{p}\right]_{\rho v}\Delta(p)_j\right\}\right] = -R^n_{\rho v_i} \quad (3.63)$$

where $k_{i,j}$ are the element influence matrices from the *y*-momentum equation:

$$\left[k_{ij}^{\rho u}\right]_{\rho v} = -\int_{\vartheta}\left[N_j\, v^n\frac{\partial W_j}{\partial x} + \frac{\mu_{eff}}{\mathbf{Re}\,\rho_j}\left(\frac{2}{3}\frac{\partial W_i}{\partial y}\frac{\partial N_j}{\partial x} - \frac{\partial W_i}{\partial x}\frac{\partial N_j}{\partial y}\right)\right]d\vartheta$$

$$\left[k_{ij}^{\rho v}\right]_{\rho v} = \int_{\vartheta}\left[\frac{\alpha_o}{\Delta t}(W_i N_j) - N_j\left(u^n\frac{\partial W_i}{\partial x} + 2v^n\frac{\partial W_i}{\partial y} + w^n\frac{\partial W_i}{\partial z}\right)\right.$$
$$\left. + \frac{\mu_{eff}}{\mathbf{Re}\rho_j}\left(\frac{\partial W_i}{\partial x}\frac{\partial N_j}{\partial x} + \frac{4}{3}\frac{\partial W_i}{\partial y}\frac{\partial N_j}{\partial y} + \frac{\partial W_i}{\partial z}\frac{\partial N_j}{\partial z}\right)\right]d\vartheta$$

$$\left[k_{ij}^{\rho w}\right]_{\rho v} = -\int_{\vartheta}\left[N_j\, v^n\frac{\partial W_i}{\partial z} + \frac{\mu_{eff}}{\mathbf{Re}\,\rho_j}\left(\frac{2}{3}\frac{\partial W_i}{\partial y}\frac{\partial N_j}{\partial z} - \frac{\partial W_i}{\partial z}\frac{\partial N_j}{\partial y}\right)\right]d\vartheta$$

$$\left[k_{ij}^{p}\right]_{\rho v} = -\int_{\vartheta}\left[N_j\frac{\partial W_i}{\partial y}\right]d\vartheta$$

After introducing Newton method and neglecting second order terms, the *z*-momentum equation (3.49) can be written as follows:

$$\int_{\vartheta}\left\{\frac{\alpha_o}{\Delta t}\left[\Delta(\rho w)^t\right]W - \left[u^n\Delta(\rho w) + w^n\Delta(\rho u) - \frac{\mu_{eff}}{\mathbf{Re}}(\Delta u_z + \Delta w_x)\right]^t W_x\right.$$
$$- \left[v^n\Delta(\rho w) + w^n\Delta(\rho v) - \frac{\mu_{eff}}{\mathbf{Re}}(\Delta v_z + \Delta w_y)\right]^t W_y$$

$$
\begin{aligned}
&- \left[\Delta p + 2w^n \Delta(\rho w) - \frac{2}{3}\frac{\mu_{eff}}{\mathbf{Re}}\left(2\Delta w_z - \Delta u_x - \Delta v_y\right)\right]^t W_z \Bigg\} d\vartheta \\
&+ \int_S \Bigg\{ \left[\Delta p + 2w^n \Delta(\rho w) + \frac{2}{3}\frac{\mu_{eff}}{\mathbf{Re}}\left(\Delta u_x + \Delta v_y\right) - \frac{1}{3}\frac{\mu_{eff}}{\mathbf{Re}} \Delta w_z\right]^t n_z \\
&\qquad + \left[u^n \Delta(\rho w) + w^n \Delta(\rho u) - \frac{\mu_{eff}}{\mathbf{Re}} \Delta u_z\right]^t n_x \\
&\qquad + \left[v^n \Delta(\rho w) + w^n \Delta(\rho v) - \frac{\mu_{eff}}{\mathbf{Re}} \Delta v_z\right]^t n_y \\
&- \frac{\mu_{eff}}{\mathbf{Re}}\left[\Delta w_x n_x + \Delta w_y n_y + \Delta w_z n_z\right]^t \Bigg\} W dS = - R^n_{\rho w} \qquad (3.64)
\end{aligned}
$$

where $R^n_{\rho w}$ is the residual of the *z*-momentum equation at Newton iteration n of time level t and is given by:

$$
\begin{aligned}
R_{\rho w} = &\int_\vartheta \Bigg\{ \left[\alpha_o (\rho w)^{t,n} + \sum_{i=1}^{k} \alpha_i (\rho w)^{t-i\Delta t}\right] W - \left[\rho u w - \frac{\mu_{eff}}{\mathbf{Re}}\left(u_z + w_x\right)\right]^{t,n} W_x \\
&- \left[\rho v w - \frac{\mu_{eff}}{\mathbf{Re}}\left(v_z + w_y\right)\right]^{t,n} W_y - \left[p + \rho w^2 - \frac{2}{3}\frac{\mu_{eff}}{\mathbf{Re}}\left(2w_z - u_x - v_y\right)\right]^{t,n} W_z \Bigg\} d\vartheta \\
&+ \int_S \Bigg\{ \left[\rho u w - \frac{\mu_{eff}}{\mathbf{Re}} u_z\right]^{t,n} n_x + \left[p + \rho w^2 + \frac{2}{3}\frac{\mu_{eff}}{\mathbf{Re}}\left(u_x + v_y\right) - \frac{1}{3}\frac{\mu_{eff}}{\mathbf{Re}} w_z\right]^{t,n} n_z \\
&\qquad + \left[\rho v w - \frac{\mu_{eff}}{\mathbf{Re}} v_z\right]^{t,n} n_y - \left[\frac{\mu_{eff}}{\mathbf{Re}} w_n\right]^{t,n} \Bigg\} W dS \qquad (3.65)
\end{aligned}
$$

and the delta form of the *z*-momentum equation is:

$$
\sum_{e=1}^{E}\left[\sum_{j=1}^{8}\left\{\left[k_{ij}^{\rho u}\right]_{\rho w}\Delta(\rho u)_j + \left[k_{ij}^{\rho v}\right]_{\rho w}\Delta(\rho v)_j + \left[k_{ij}^{\rho w}\right]_{\rho w}\Delta(\rho w)_j + \left[k_{ij}^{p}\right]_{\rho w}\Delta(p)_j\right\}\right] = - R^n_{\rho w} \qquad (3.66)
$$

where k_{ij} are the element influence matrices from the z-momentum equation:

$$\left[K_{ij}^{\rho u}\right]_{\rho w} = - \int_{\vartheta}\left[N_j\, w^n \frac{\partial W_i}{\partial x} + \frac{\mu_{eff}}{\mathbf{Re}\rho_j}\left(\frac{2}{3}\frac{\partial W_i}{\partial z}\frac{\partial N_j}{\partial x} - \frac{\partial W_i}{\partial x}\frac{\partial N_j}{\partial z}\right)\right] d\vartheta$$

$$\left[K_{ij}^{\rho v}\right]_{\rho w} = - \int_{\vartheta}\left[N_j\, w^n \frac{\partial W_i}{\partial y} + \frac{\mu_{eff}}{\mathbf{Re}\rho_j}\left(\frac{2}{3}\frac{\partial W_i}{\partial z}\frac{\partial N_j}{\partial y} - \frac{\partial W_i}{\partial y}\frac{\partial N_j}{\partial z}\right)\right] d\vartheta$$

$$\left[K_{ij}^{\rho w}\right]_{\rho w} = \int_{\vartheta}\left[\frac{\alpha_o}{\Delta t}(W_i N_j) - N_j\left(u^n \frac{\partial W_i}{\partial x} + v^n \frac{\partial W_i}{\partial y} + 2w^n \frac{\partial W_i}{\partial z}\right)\right.$$
$$\left. + \frac{\mu_{eff}}{\mathbf{Re}\rho_j}\left(\frac{\partial W_i}{\partial x}\frac{\partial N_j}{\partial x} + \frac{\partial W_i}{\partial y}\frac{\partial N_j}{\partial y} + \frac{4}{3}\frac{\partial W_i}{\partial z}\frac{\partial N_j}{\partial z}\right)\right] d\vartheta$$

$$\left[K_{ij}^{p}\right]_{\rho w} = - \int_{\vartheta}\left[N_j \frac{\partial W_i}{\partial z}\right] d\vartheta$$

3.7.3 Energy Equation

After introducing Newton method and neglecting second order terms, the energy equation (3.56) can be written as:

$$\int_{\vartheta}\left\{\frac{\alpha_o}{\Delta t}(\rho C_p)^t \Delta T_o^t W + \left[C_p\left(\rho u \Delta T_{ox} + \rho v \Delta T_{oy} + \rho w \Delta T_{oz}\right)\right]^t W\right.$$
$$\left. + \left[\frac{k_{eff}}{\mathbf{Pr\ Re}}\left(\Delta T_{ox} W_x + \Delta T_{oy} W_y + \Delta T_{oy} W_z\right)\right]^t\right\} d\vartheta$$
$$+ \int_S \left[\frac{k_{eff}}{\mathbf{Pr\ Re}}\Delta T_n\right]^t W dS = - R_{T_o} \qquad (3.67)$$

where R_{T_o} is the residual of the discretized energy equation at time level t and is given by:

$$R_{T_0} = \int_{\vartheta} \left\{ (\rho C_p)^t \frac{1}{\Delta t} \left[\alpha_o T_o^t + \sum_{i=1}^{k} \alpha_i T_o^{t-i\Delta t} \right] W + \left[C_p (\rho u T_{ox} + \rho v T_{oy} + \rho w T_{oz}) \right]^{t,n} W \right.$$

$$\left. + \left[\frac{k_{eff}}{\mathbf{Pr}\ \mathbf{Re}} (T_{ox} W_x + T_{oy} W_y + T_{oy} W_z) \right]^{t,n} \right\} d\vartheta$$

$$+ \int_S \left[\frac{k_{eff}}{\mathbf{Pr}\ \mathbf{Re}} T_n \right]^{t,n} W dS - RHS^t \tag{3.68}$$

After substituting the shape and weight functions into equation (3.73), the following delta form of the energy equation is assembled, over the elements, in terms of the cell-vertex unknowns for the total temperature, T_o :

$$\sum_{e=1}^{E} \left[\left\{ \sum_{j=1}^{8} \left[k_{i,j}^{T_o} \right]_{T_o} (\Delta T_o)_j \right\} \right] = - R_{T_o} \tag{3.69}$$

where $k_{i,j}$ are the element influence matrices from the energy equation:

$$\left[k_{i,j}^{T_o} \right]_{T_o} = \int_{\vartheta} \left\{ \frac{\alpha_o}{\Delta t} \rho C_p N_j W_i + C_p \left(\rho u \frac{\partial N_i}{\partial x} + \rho v \frac{\partial N_i}{\partial y} + \rho w \frac{\partial N_i}{\partial z} \right) W_i \right.$$

$$\left. + \frac{k_{eff}}{\mathbf{Pr}\ \mathbf{Re}} \left(\frac{\partial N_i}{\partial x} \frac{\partial W_i}{\partial x} + \frac{\partial N_i}{\partial y} \frac{\partial W_i}{\partial y} + \frac{\partial N_i}{\partial z} \frac{\partial W_i}{\partial z} \right) \right\} d\vartheta \tag{3.70}$$

3.7.4 Turbulence Equations

After introducing Newton linearization and neglecting second order terms, the κ-equation (3.52) can be written as follows:

$$\int_{\vartheta}\left\{\frac{\alpha_o}{\Delta t}\rho^t\Delta\kappa^t W + \left[\rho u\Delta\kappa_x + \rho v\Delta\kappa_y + \rho w\Delta\kappa_z\right]^t W + \frac{1}{\mathbf{Re}}\left[\frac{\mu^n_{turb}}{\sigma_\kappa}\left(\Delta\kappa_x W_x + \Delta\kappa_y W_y + \Delta\kappa_z W_z\right)\right]^t\right\} d\vartheta - \frac{1}{\mathbf{Re}}\int_S\left[\frac{\mu^n_{turb}}{\sigma_\kappa}\left(\Delta\kappa_x n_x + \Delta\kappa_y n_y + \Delta\kappa_z n_z\right)\right]^t W dS = -R^n_\kappa \qquad (3.71)$$

where R^n_κ is the residual of the discretized κ-equation at Newton iteration n of time level t and is given by:

$$R^n_\kappa = \int_{\vartheta}\left\{\frac{\rho^t}{\Delta t}\left[\alpha_o\kappa^{t,n} + \sum_{i=1}^{k}\alpha_i\kappa^{t-i\Delta t}\right]W + \left[\rho u\kappa_x + \rho v\kappa_y + \rho w\kappa_z\right]^{t,n}W + \left[\rho\varepsilon - \mu_{tur}S\right]^{t,n}W + \frac{1}{\mathbf{Re}}\left[\frac{\mu_{turb}}{\sigma_\kappa}\left(\kappa_x W_x + \kappa_y W_y + \kappa_z W_z\right)\right]^{t,n}\right\} d\vartheta - \frac{1}{\mathbf{Re}}\int_S\left[\frac{\mu_{turb}}{\sigma_\kappa}\left(\kappa_x n_x + \kappa_y n_y + \kappa_z n_z\right)\right]^{t,n} W dS \qquad (3.72)$$

After substituting the shape and weight functions into equation (3.71), the Δ form of the κ-equation is assembled, over the elements, in terms of the cell-vertex unknown κ as follows:

$$\sum_{e=1}^{E}\left[\left\{\sum_{j=1}^{8}\left[k^{\kappa}_{i,j}\right]_{\kappa}\Delta\kappa_j\right\}\right] = -R^n_\kappa \qquad (3.73)$$

where $k_{i,j}$ are the elemental influence matrices of the κ -equation:

$$\left[k_{i,j}^{\kappa}\right]_{\kappa} = \int_{\vartheta} \left\{ \frac{\alpha_o}{\Delta t} \rho N_j W_i + \left[\rho u \frac{\partial N_j}{\partial x} + \rho v \frac{\partial N_j}{\partial y} + \rho w \frac{\partial N_j}{\partial z} \right] W_i \right.$$

$$\left. + \frac{1}{\mathbf{Re}} \frac{\mu_{turb}^{n}}{\sigma_\kappa} \left[\frac{\partial W_i}{\partial x} \frac{\partial N_j}{\partial x} + \frac{\partial W_i}{\partial y} \frac{\partial N_j}{\partial y} + \frac{\partial W_i}{\partial z} \frac{\partial N_j}{\partial z} \right] \right\} d\vartheta \tag{3.74}$$

After introducing the Newton method and neglecting second order terms, equation (3.53) can be written as follows:

$$\int_{\vartheta} \left\{ \frac{\alpha_o}{\Delta t} \rho^{t} \Delta\varepsilon^{t} W + \left[\rho u \Delta\varepsilon_x + \rho v \Delta\varepsilon_y + \rho w \Delta\varepsilon_z \right]^{t} W \right.$$

$$\left. + \frac{1}{\mathbf{Re}} \left[\frac{\mu_{turb}^{n}}{\sigma_\varepsilon} \left(\Delta\varepsilon_x W_x + \Delta\varepsilon_y W_y + \Delta\varepsilon_z W_z \right) \right]^{t} \right\} d\vartheta$$

$$- \frac{1}{\mathbf{Re}} \int_{S} \left[\frac{\mu_{turb}^{n}}{\sigma_\varepsilon} \left(\Delta\varepsilon_x n_x + \Delta\varepsilon_y n_y + \Delta\varepsilon_z n_z \right) \right]^{t} W dS = - R_{\kappa}^{n} \tag{3.75}$$

where R_{ε}^{n} is the residual of the discretized ε-equation at Newton iteration n of time level t and is given by:

$$R_{\varepsilon}^{n} = \int_{\vartheta} \left\{ \frac{\rho^{\,t}}{\Delta t} \left[\alpha_o \varepsilon^{t,n} + \sum_{i=1}^{k} \alpha_i \varepsilon^{t-i\Delta t} \right] W + \left[\rho u \varepsilon_x + \rho v \varepsilon_y + \rho w \varepsilon_z \right]^{t,n} W \right.$$

$$\left. + \left[C_2 \rho \left(\frac{\varepsilon^2}{\kappa} \right) - C_1 C_\mu \rho \kappa S \right]^{t,n} W + \frac{1}{\mathbf{Re}} \left[\frac{\mu_{turb}}{\sigma_\varepsilon} \left(\varepsilon_x W_x + \varepsilon_y W_y + \varepsilon_z W_z \right) \right]^{t,n} \right\} d\vartheta$$

$$- \frac{1}{\mathbf{Re}} \int_{S} \left[\frac{\mu_{turb}}{\sigma_\varepsilon} \left(\varepsilon_x n_x + \varepsilon_y n_y + \varepsilon_z n_z \right) \right]^{t,n} W dS \tag{3.76}$$

After substituting the shape and weight functions into equation (3.75), the delta form of the ε-equation is assembled, over the elements, in terms of the cell-vertex unknowns ε as follows:

$$\sum_{e=1}^{E}\left[\left\{\sum_{j=1}^{8}\left[k_{i,j}^{\varepsilon}\right]_{\varepsilon}\Delta\varepsilon_j\right\}\right] = -\,R_{\varepsilon}^{n} \tag{3.77}$$

where $k_{i,j}$ are the elemental influence matrices of the ε-equation:

$$\left[k_{i,j}^{\varepsilon}\right]_{\varepsilon} = \int_{\vartheta}\left\{\frac{\alpha_o}{\Delta t}\rho N_j W_i + \left[\rho u\frac{\partial N_j}{\partial x} + \rho v\frac{\partial N_j}{\partial y} + \rho w\frac{\partial N_j}{\partial z}\right]W_i \right.$$
$$\left. + \frac{1}{\mathbf{Re}}\frac{\mu_{turb}^{n}}{\sigma_{\varepsilon}}\left[\frac{\partial W_i}{\partial x}\frac{\partial N_j}{\partial x} + \frac{\partial W_i}{\partial y}\frac{\partial N_j}{\partial y} + \frac{\partial W_i}{\partial z}\frac{\partial N_j}{\partial z}\right]\right\}d\vartheta$$

3.8 Initial and Boundary Conditions

This section details the boundary conditions setup in the code. It must be recalled that the code is a general 3-D one and that to run it in a 2-D mode certain assumptions are made. First, a slice is taken of a full 3-D grid (*x,y,z*) and the following general conditions are assumed, in order to solve for a 2-D flow in the *x-y* plane :

a- Symmetry conditions exist between the two limiting x-y planes;

b- On these planes the velocity in the *z* direction is forced to be zero, with only two velocity components left to solve for.

These two conditions, taken together, insure a 2-D solution from a 3-D code.

The number of initial solutions needed to perform a time accurate calculation depends on the order of accuracy demanded, e.g. a second order Gear scheme would require two previous time levels to be known.

To obtain a viscous initial solution for time accurate flow calculations, a steady-state calculation is carried out using a first order Gear scheme until the residuals of the governing equations are reduced by three orders of magnitude.

3.8.1 Continuity Equation

The boundary surface integrals in the continuity equation (3.22) are:

$$I_p = \int_S \left[\rho\vec{V} - \lambda\left(\nabla p - \nabla\hat{p}\right)\right]\bullet\vec{n}\,W\,dS \qquad (3.78)$$

Due to the use of small λ, its contribution to the contour integral is neglected.

a- Inlet Boundary Condition:

The surface integrals in equation (3.78) are computed using a specified inlet mass flux $\rho\vec{V}$, after neglecting the pressure dissipation term due to the small value of λ.

b- Exit Boundary Condition:

Static pressure is specified at all exit points as a Dirichlet boundary condition. In this case, no surface integrals need to be evaluated.

c- Wall Boundary Condition:

The no-penetration condition is imposed at walls, i.e. $\rho\vec{V}\bullet\vec{n}=0$, and the surface integral of equation (3.78) drops out naturally.

d- Symmetry Boundary Condition:

Normal mass flux is set to zero by neglecting the boundary surface integral in equation (3.78).

3.8.2 Momentum Equations

The boundary surface integrals in the *x*-, *y*-, and *z*-momentum equations (3.26, 3.28, 3.30) are:

$$I_{\rho u}=\int_S\left\{\left[p+\rho u^2+\frac{2}{3}\frac{\mu_{eff}}{\mathbf{Re}}(v_y+w_z)-\frac{1}{3}\frac{\mu_{eff}}{\mathbf{Re}}u_x\right]n_x+\left[\rho vu-\frac{\mu_{eff}}{\mathbf{Re}}v_x\right]n_y\right.$$
$$\left.+\left[\rho wu-\frac{\mu_{eff}}{\mathbf{Re}}w_x\right]n_z-\frac{\mu_{eff}}{\mathbf{Re}}u_n\right\}WdS \qquad (3.79)$$

$$I_{\rho v}=\int_S\left\{\left[\rho uv-\frac{\mu_{eff}}{\mathbf{Re}}u_y\right]n_x+\left[p+\rho v^2+\frac{2}{3}\frac{\mu_{eff}}{\mathbf{Re}}(u_x+w_z)-\frac{1}{3}\frac{\mu_{eff}}{\mathbf{Re}}v_y\right]n_y\right.$$
$$\left.+\left[\rho wv-\frac{\mu_{eff}}{\mathbf{Re}}w_y\right]n_z-\frac{\mu_{eff}}{\mathbf{Re}}v_n\right\}WdS \qquad (3.80)$$

$$I_{\rho w}=\int_S\left\{\left[\rho uw-\frac{\mu_{eff}}{\mathbf{Re}}u_z\right]n_x+\left[p+\rho w^2+\frac{2}{3}\frac{\mu_{eff}}{\mathbf{Re}}(u_x+v_y)-\frac{1}{3}\frac{\mu_{eff}}{\mathbf{Re}}w_z\right]n_z\right.$$
$$\left.+\left[\rho vw-\frac{\mu_{eff}}{\mathbf{Re}}v_z\right]n_y-\frac{\mu_{eff}}{\mathbf{Re}}w_n\right\}WdS \qquad (3.81)$$

a- Inlet Boundary Condition:

A specified inlet mass flux $\rho\vec{V}$, is imposed. The inlet value of the velocity $\vec{V}$ is iteratively updated using the fixed value of inlet mass flux and the changing value of the inlet density, as $\rho^n = \left(\frac{P}{T}\right)^n$.

b- Exit Boundary Condition:

Two types are considered:

1- Normal derivatives are neglected when calculating the surface integrals in equations (3.79-3.81), meaning that streamlines are uniform.

2- A stress-free boundary condition is imposed, by retaining only the convective terms when calculating the surface integrals in equations (3.79-3.82).

c- Wall Boundary Condition:

The no-slip and no-penetration conditions are imposed as Dirichlet boundary conditions on the velocity $\vec{V}$, and hence no surface integrals in equations (3.79-3.82) need be evaluated.

d- Symmetry Boundary Condition:

Normal derivatives of velocity components are set to zero when calculating the surface integrals in equations (3.79-3.82).

3.8.3 Energy Equation

The boundary surface integrals in the energy equation (3.32) are:

$$I_{T_o} = - \int_S \left\{ \left[\frac{k_{eff}}{\mathbf{Pr\ Re}} \nabla T + \frac{\mathbf{Ec}}{\mathbf{Re}} \vec{V} \tau_{ij} \right] \bullet \vec{n} \right\} W dS \tag{3.83}$$

a- Inlet Boundary Condition:

The total temperature, T_o, is imposed as a Dirichlet condition and hence no surface integrals need be evaluated.

b- Exit Boundary Condition:

The surface integrals in equation (3.83) are evaluated after neglecting the normal derivative of static temperature (natural boundary condition).

c- Wall Boundary Conditions:

Two types are considered:

1- The wall static and total temperatures are identical. With this, the total temperature is imposed as a Dirichlet condition and no surface integrals need be evaluated.

2- The surface integrals in equation (3.83) are evaluated after neglecting the normal derivative of static temperature (natural boundary condition).

c- Symmetry Boundary Condition:

This condition is implemented by simply neglecting the normal derivative of static temperature, when evaluating the boundary surface integrals in equation (3.83).

3.8.4 Turbulence Equations

The boundary surface integral of the κ -equation (3.38) is:

$$I_\kappa = -\frac{1}{\mathrm{Re}}\int_S \left[\frac{\mu_{turb}}{\sigma_\kappa}\nabla\kappa \bullet \vec{n}\right] W dS \tag{3.84}$$

a- Inlet Boundary Condition:

The turbulent kinetic energy is imposed as a Dirichlet condition and hence no boundary surface integrals need be evaluated.

b- Exit Boundary Condition

The normal derivative of the turbulent kinetic energy is set to zero as a natural boundary condition and hence the surface integral of equation (3.84) drops out naturally.

c- Wall Boundary Condition:

This condition is set by using the standard wall functions. This approach relates the velocity components as well as κ and ε to the friction velocity u^+, which is obtained from the log-law of the wall.

d- Symmetry Boundary Condition:

This condition is implemented by simply neglecting the normal derivative of κ when evaluating the boundary surface integrals in equation (3.84).

The boundary surface integral in the ε-equation (3.41) is:

$$I_\varepsilon = -\frac{1}{\mathbf{Re}}\int_S \left[\frac{\mu_{turb}}{\sigma_\varepsilon}\nabla\varepsilon\bullet\vec{n}\right] W dS \qquad (3.85)$$

a- Inlet Boundary Condition:

The value of ε is specified as a Dirichlet boundary condition and hence no surface integrals need be evaluated.

b- Exit Boundary Condition:

The normal derivative of ε is set to zero as a natural boundary condition and hence the surface integral of equation (3.85) drops out naturally.

c- Wall Boundary Condition:

This condition is set by using the standard wall functions. This approach relates the velocity components, as well as κ and ε, to the friction velocity u^+, which is obtained from the log-law of the wall.

d- Symmetry Boundary Condition:

This condition is implemented by simply neglecting the normal derivative of ε when evaluating the boundary surface integrals in equation (3.85).

4. Solution Strategy for the Discretized Equations

In the previous chapter, it was shown how the nonlinear governing equations are linearized by the Newton method and the time derivatives discretized by the Gear scheme, a multi-level implicit, hence unconditionally stable method, with controllable accuracy. A second order Gear scheme, assuming two preceding time levels to be available, will be used throughout.

This chapter discusses the solution procedure and details the schemes used to iterate for time advance and for the spatial nonlinearity. In addition, two separate approaches are shown for the time-accurate solution of unsteady flows and for the time marching solution of steady flows [22]. Stabilization details through an artificial viscosity scheme are described. Robustness of the numerical scheme is ensured through the coupling of continuity and momentum equations. Finally, modeling aspects of the near-wall behavior of the turbulence equation, as implemented in the *NS3D* code, are briefly presented because of its novel idea of a wall finite element to represent the logarithmic law of the wall [23,24].

It has been previously demonstrated that the following systems of equations must be solved at each time iteration:

a. a coupled system for the continuity and momentum equations,
b. the algebraic energy equation, as implemented here, or the complete energy equation.
c. two equations describing the (κ-ε) turbulence model.

4.1 The Navier-Stokes Equation System

Upon space discretization and Newton linearization, the following delta form of the continuity and momentum equations is assembled, over the elements, in terms of the cell-vertex unknowns of pressure and velocity components:

$$
\begin{aligned}
&\sum_{e=1}^{E}\left[\left\{\sum_{j=1}^{8}\left[k_{i,j}^{\rho u}\right]_{p}\Delta(\rho u)_j+\left[k_{i,j}^{\rho v}\right]_{p}\Delta(\rho v)_j+\left[k_{i,j}^{\rho w}\right]_{p}\Delta(\rho w)_j+\left[k_{i,j}^{p}\right]_{p}\Delta(p)_j\right\}\right]=-R_p^n\\
&\sum_{e=1}^{E}\left[\left\{\sum_{j=1}^{8}\left[k_{i,j}^{\rho u}\right]_{\rho u}\Delta(\rho u)_j+\left[k_{i,j}^{\rho v}\right]_{\rho u}\Delta(\rho v)_j+\left[k_{i,j}^{\rho w}\right]_{\rho u}\Delta(\rho w)_j+\left[k_{i,j}^{p}\right]_{\rho u}\Delta(p)_j\right\}\right]=-R_{\rho u}^n\\
&\sum_{e=1}^{E}\left[\sum_{j=1}^{8}\left\{\left[k_{i,j}^{\rho u}\right]_{\rho v}\Delta(\rho u)_j+\left[k_{i,j}^{\rho v}\right]_{\rho v}\Delta(\rho v)_j+\left[k_{i,j}^{\rho w}\right]_{\rho v}\Delta(\rho w)_j+\left[k_{i,j}^{p}\right]_{\rho v}\Delta(p)_j\right\}\right]=-R_{\rho v}^n\\
&\sum_{e=1}^{E}\left[\sum_{j=1}^{8}\left\{\left[k_{i,j}^{\rho u}\right]_{\rho w}\Delta(\rho u)_j+\left[k_{i,j}^{\rho v}\right]_{\rho w}\Delta(\rho v)_j+\left[k_{i,j}^{\rho w}\right]_{\rho w}\Delta(\rho w)_j+\left[k_{i,j}^{p}\right]_{\rho w}\Delta(p)_j\right\}\right]=-R_{\rho w}^n
\end{aligned}
\tag{4.1}
$$

This system of equations (4.1) can be symbolically represented as:

$$
\begin{bmatrix}
\left[K^{\rho\vec{V}}\right]_{\vec{V}} & \left[K^{p}\right]_{\rho\vec{V}}\\
\left[K^{\rho\vec{V}}\right]_{p} & \left[K^{p}\right]_{p}
\end{bmatrix}
\begin{Bmatrix}
\Delta(\rho\vec{V})\\
\Delta p
\end{Bmatrix}
=-\begin{Bmatrix}
R_{\rho\vec{V}}\\
R_p
\end{Bmatrix}
\tag{4.2}
$$

4.2 The Energy Equation

To reduce overall memory requirements, the energy equation is solved for the total temperature in a segregated way. The discretized form of the energy equation (2.69) in term of the total temperature was derived in chapter 3 and has the following form:

$$\sum_{e=1}^{E}\left[\left\{\sum_{j=1}^{8}\left[k_{i,j}^{T_o}\right]_{T_o}\left(\Delta T_o\right)_j\right\}\right] = - R_{T_o} \tag{4.3}$$

where $k_{i,j}^{T_o}$ is the element influence matrix, given by:

$$\begin{aligned}\left[k_{i,j}^{T_o}\right]_{T_o} = \int_{\vartheta}\Bigg\{&\frac{\alpha_o}{\Delta t}\rho C_p N_j W_i + C_p\left(\rho u\frac{\partial N_i}{\partial x} + \rho v\frac{\partial N_i}{\partial y} + \rho w\frac{\partial N_i}{\partial z}\right)W_i \\ &+ \frac{k_{eff}}{\mathbf{Pr}\ \mathbf{Re}}\left(\frac{\partial N_i}{\partial x}\frac{\partial W_i}{\partial x} + \frac{\partial N_i}{\partial y}\frac{\partial W_i}{\partial y} + \frac{\partial N_i}{\partial z}\frac{\partial W_i}{\partial z}\right)\Bigg\}\, d\vartheta\end{aligned} \tag{4.4}$$

and R_{T_o} is the residual equation (2.68) , given by:

$$\begin{aligned}R_{T_o} = \int_{\vartheta}\Bigg\{&(\rho C_p)^t\frac{1}{\Delta t}\left[\alpha_o T_o^t + \sum_{i=1}^{k}\alpha_i T_o^{t-i\Delta t}\right]W + \left[C_p(\rho u T_{ox} + \rho v T_{oy} + \rho w T_{oz})\right]^{t,n}W \\ &+ \left[\frac{k_{eff}}{\mathbf{Pr}\ \mathbf{Re}}\left(T_{ox}W_x + T_{oy}W_y + T_{oy}W_z\right)\right]^{t,n}\Bigg\}\, d\vartheta \\ &+ \int_S\left[\frac{k_{eff}}{\mathbf{Pr}\ \mathbf{Re}}T_n\right]^{t,n} W dS - RHS^t\end{aligned} \tag{4.5}$$

Equation (4.3) is linear and hence simple to solve. This fact can be illustrated be examining the terms in equation (4.4). In order to construct the coefficient matrix of the energy equation, the density, velocity, and effective conductivity must be known throughout the flow field from the previous iteration, but the total temperature does not enter in the construction of the matrix $k_{i,j}^{T_o}$. Hence, one Newton iteration is sufficient to reduce the residual of the energy equation by five orders of magnitude.

The total temperature field obtained via equation (4.3), along with the velocity field from the Navier-Stokes iteration, are used to update the static temperature field.

4.3 The Turbulence Equations System

The discretized form of the (κ,ε) two-equation model, (2.73, 2.79) was derived in the previous chapter and is given by:

$$\sum_{e=1}^{E}\left[\left\{\sum_{j=1}^{8}\left[k_{i,j}^{\kappa}\right]_{\kappa}\Delta\kappa_j\right\}\right] = -\ R_{\kappa}^{n} \tag{4.6}$$

$$\sum_{e=1}^{E}\left[\left\{\sum_{j=1}^{8}\left[k_{i,j}^{\varepsilon}\right]_{\varepsilon}\Delta\varepsilon_j\right\}\right] = -\ R_{\varepsilon}^{n} \tag{4.7}$$

To reduce the computing cost of solving equations (4.6, 4.7), the Jacobian matrices $\left[k_{i,j}^{\kappa}\right]_{\kappa}$ and $\left[k_{i,j}^{\varepsilon}\right]_{\varepsilon}$ are made identical by considering only the essential, and similar, terms between the κ- and ε-equations (2.11, 2.12). Equations (4.6, 4.7) yield therefore identical influence matrices but are solved in a sequential manner. Equation (4.6) is solved first to update κ, followed by solving equation (4.7) to update ε, using the updated value of κ and the turbulent viscosity, μ_{turb}.

The strategy is for the turbulent parameters to be updated and the Navier-Stokes equations solved for a few Newton iterations, usually five, and the sequence repeated. At each turbulence update, the (κ,ε) equations are not solved to complete convergence; their residual is only reduced by an order of magnitude. At, or near, convergence of the governing equations, the (κ,ε) equations are, however, completely converged.

While a low-Reynolds number (κ,ε) model could be used near walls, it would require an additional resolution of 10 to 20 grid points in boundary layers. This would be quite demanding in terms of solution time and memory, making a Navier-Stokes code a less practical design tool. An alternative is using the wall function approach to exclude the high-gradient computational region near walls from the solution by imposing, at the first point off the wall, a slip velocity derived from the shear stress at the wall and respecting a certain behavior between that point and the wall. In the present work this slip velocity is given by:

$$\begin{aligned} u^+ &= y^+ && 6 > y^+ > 0 \\ u^+ &= \{y^+ * (20 - y^+) + (\tfrac{1}{s}\, ln y^+ + C)^*(y^+ - 20)\}/14 && 20 > y^+ > 6 \\ u^+ &= \tfrac{1}{s}\, ln\, y^+ + C && y^+ > 20 \end{aligned} \tag{4.8a}$$

where:

$$\begin{gathered} s = 0.4184\,;\, C = 5.1 \\ u^+ = u\,/u_\tau\,;\, y^+ = \rho\, y\, u_\tau / \mu\,;\;\; u_\tau = \sqrt{\tau_{wall}/\rho \mathrm{R}\,\mathbf{e}} \end{gathered} \tag{4.8b}$$

For the boundary conditions imposed on (κ,ε) the production and dissipation of turbulent energy at the wall are assumed to be equal. The turbulent shear stress at the wall, τ_{wall}, is obtained from the wall function assumption, equation (4.8), and is used to compute new values for (κ,ε).

While the wall-function approach reduces the number of grid points in the near-wall region, by avoiding the solution of the governing equations in this high gradient region, it proves to be a source of inaccuracy for three-dimensional and separated flows. In the 3-D code used, *NS3D*, an alternative approach, similar to [23,24], that is considerably more accurate than wall functions, yet far cheaper than implementing a low-Reynolds number turbulence model, is used. A special wall element, illustrated in figure (4.1), incorporates into its shape function the partially logarithmic behavior of the velocity vector in the direction normal to the wall, equation (4.8), while remaining linear in the other two directions. For elements adjacent to a wall, the velocity shape function in the normal direction to the face of the element lying on the wall is therefore modified to reflect the presumed flow behavior in this region, characterized by a viscous sublayer, a transition layer and a logarithmic outer layer, equation (4.8). For example, for the element shown in figure (4.1), assuming the bottom face to lie on a wall, $F_2(\eta)$ of nodes related to the opposite face, are re-expressed as $F_2\left(y^+/\, y^+_{edge}\right)$ to reflect a triple deck behavior [23,24].

As for the turbulent viscosity in the near-wall region it is interpolated as follows: a linear behavior starting at the edge of the near-wall region, where y^+ is assumed to be less than 300, to $y^+=30$, and a quadratic variation between $y^+=30$ and the wall i.e. $y^+=0$.

It must be appreciated that the velocity shape functions in this special near-wall element cannot be integrated accurately using a two-point Gauss quadrature as in the rest of the flow field. Through numerical experimentation, it was determined that nine Gauss points, in the direction normal to the wall, are sufficient to adequately integrate the logarithmic behavior.

4.4 Global Iterative Scheme: Outer Newton Iteration

It is seen that upon advancing to a given time, the Newton linearization leads to the solution of a series of systems of linear equations for (u,v,w,p), T, (κ, ε). This is denoted as the outer iteration. To solve the linear systems at each Newton iteration, a direct or iterative solver can be used. Since an iterative solver is used here, this solution step is denoted as the inner iteration, to distinguish it from the outer iteration for nonlinearity.

It is worthwhile to note that efficient direct and iterative methods have been developed at the Concordia CFD Lab-CERCA and P&WC and have been continuously incorporated in P&WC's *NS3D*. *NS3D* uses iterative solvers based on the Preconditioned Conjugate Gradient Squared method (PCGS) or the Generalized Minimum Residual Method (GMRES). The necessary preconditioning for these two iterative approaches is obtained through an incomplete factorization process [25,26,27,28].

To stabilize the convergence of the momentum equations at high Reynolds number, a strategy of a centered scheme with artificial viscosity or an upwinding scheme is always needed. Here, this extra artificial diffusion is introduced through a centered scheme, symbolically represented as $\mu_{art}{}^{RHS}$ in equation (4.2).

Because an iterative solver is used at each Newton iteration to solve the ill-conditioned linear system coming from the N-S equations, it has also been found highly beneficial for the convergence of the iterative scheme to introduce a similar dissipation in the Jacobian matrix itself. This is symbolically represented as $\mu_{art}{}^{LHS}$ in equation (4.2). Equation (4.2), after the introduction of these artificial viscosity terms, can be re-expressed in the form:

$$\left[K(\lambda,\mu_{art})\right]\begin{Bmatrix}\Delta\rho\vec{V}\\ \Delta p\end{Bmatrix} = -\begin{Bmatrix}R_{\vec{V}}(\mu_{art})\\ R_p(\lambda)\end{Bmatrix} \tag{4.9}$$

The momentum residual, $R_{\rho\vec{V}}$ is also unloaded during the outer iteration, reaching the smallest possible value of dissipation parameters, for which the outer Newton iteration converges. Normally, the dissipation for the left hand side, representing the iterative scheme, is left at a higher level than the right-hand-side, representing the problem's physics. This is equivalent to setting up the iteration to be at a lower Reynolds number.

4.5 Steady Flow (Time-Marching) and Unsteady Flow (Time-Accurate) Algorithms

There are two algorithms in *NS3D*, one solves the steady-flow equations by a time-marching procedure (here called steady-flow algorithm, SFA, see flow chart presented in figure (4.2a)) and the second solves the unsteady flow equations by a time-accurate procedure (here called unsteady-flow algorithm, UFA, see flow chart presented in figure (4.2b)). In both algorithms, the discretized time terms affect the system matrix, K, improving its condition number (by increasing diagonal dominance) and hence provide a mechanism to ensure the convergence of the linear system, in the steady-flow case, by dynamically choosing the time step size, as necessitated by the problem.

Steady Flow Algorithm: SFA

In the Steady Flow algorithm, also called the "hybrid artificial viscosity algorithm", assuming the initial values of $\rho\vec{V}$ and p being given, $||R_V,R_p||_o$ can be computed, and the iterations are carried as follows:

For each unloading step,

1. Compute λ^{RHS}, λ^{LHS}, $\mu_{art}{}^{RHS}$ and $\mu_{art}{}^{LHS}$
2. Solve the turbulence equations every K_{int} Newton iterations and the energy equation every E_{int} Newton iterations

Newton Iteration:

3. Solve $\Delta\rho\vec{V}_i$ and Δp_i with PCGS at each Newton iteration,

$$\left[K(\lambda^{LHS},\mu_{art}^{LHS})\right]\begin{Bmatrix}\Delta\rho\vec{V}\\ \Delta p\end{Bmatrix} = -\begin{Bmatrix}R_{\vec{V}}(\mu_{art}^{RHS})\\ R_p(\lambda^{RHS})\end{Bmatrix} \tag{4.10}$$

4. Update $\rho\vec{V}$ and p:

$$\begin{Bmatrix}\rho\vec{V}_{i+1}\\ p_{i+1}\end{Bmatrix} = \begin{Bmatrix}\rho\vec{V}_i\\ p_i\end{Bmatrix} + \begin{Bmatrix}\Delta\rho\vec{V}_i\\ \Delta p_i\end{Bmatrix} \tag{4.11}$$

till $||R_V,R_p||_{i+1} \,/\, ||R_V,R_p||_o <$ TOL, repeat from 1.

The hybrid artificial viscosity scheme is a key feature in allowing large time steps, making the use of iterative methods viable for steady-state problems.

Unsteady Flow Algorithm: UFA

In the Unsteady Flow algorithm, which can also be used for steady-state problems, the values of $\rho\vec{V}$ and p are assumed to be given at an initial time t, hence $||R_V, R_p||_o$ can be computed. At each time step, the solution is as follows:

1. Solve the turbulence equations every K_{int} Newton iterations and the energy equation every E_{int} Newton iterations

Newton Iteration:

2. Solve the $\Delta\rho\vec{V}_i$ and Δp_i at each Newton iteration:

$$\left[K(\lambda^{LHS},\mu_{art}^{LHS})\right]\begin{Bmatrix}\Delta\rho\vec{V}\\ \Delta p\end{Bmatrix} = -\begin{Bmatrix}R_{\vec{V}}(\mu_{art}^{RHS})\\ R_p(\lambda^{RHS})\end{Bmatrix} \tag{4.12}$$

3. Update $\rho\vec{V}$ and p:

$$\begin{Bmatrix}\rho\vec{V}_{i+1}\\ p_{i+1}\end{Bmatrix} = \begin{Bmatrix}\rho\vec{V}_i\\ p_i\end{Bmatrix} + \begin{Bmatrix}\Delta\rho\vec{V}_i\\ \Delta p_i\end{Bmatrix}$$

till $||R_V, R_p||_{i+1} / ||R_V, R_p||_o < \text{TOL}$.

4. Advance solution in time, repeat from 1.

5. Results

5.1 Test Cases

The time-accurate implementation of the Navier-Stokes equations described in Chapter 3 has been validated against two test cases for which accurate experimental and reliable computational results exist: that of a laminar incompressible flow past a circular cylinder at Reynolds numbers, **Re**, between 35 and 100, and that of a turbulent incompressible flow over a triangular flame holder at **Re**=45,000. For practical considerations, the validation cases are kept two-dimensional, although the unsteady implementation is embedded in a three-dimensional code, *NS3D*. To simulate such flows in two-dimensions, two symmetry planes are assumed in the third direction as described in Chapter 3. Finally, incompressibility is simulated through this compressible code by using a Mach number of 0.05, inducing a density change of less than 0.25%.

5.2 Flow over a circular cylinder: Re=100

Figure (5.1) shows the computational domain and the boundary conditions for the flow over a circular cylinder, while the mesh is shown in figure (5.2) and contains 4050 nodes and 1806 elements. It was found that, if the spatial mesh is coarse, instabilities develop and continue to grow indefinitely.

First, a no artificial viscosity, steady-state calculation, at **Re**=100 was carried out using the steady flow algorithm, SFA. The convergence history of the L_2 residual of the Navier-Stokes equations is shown in figure (5.3). About 240

Newton iterations were needed to reduce it by two orders of magnitude. The fact that the flow at **Re**=100 is physically unsteady is the cause of the dramatic performance deterioration of the steady-state code. The behavior of the residual, plotted in figure (5.3), indicates that the solution is periodic and hence a time-accurate computation is a necessity for capturing the actual flow physics. Figure (5.4) shows the velocity vectors-and the vorticity contours behind the cylinder. It is clear from this figure that the flow is symmetric, with a region of recirculation behind the cylinder.

The time-accurate calculation was started from the steady-state one obtained by the SFA. The boundary conditions used are summarized in figure (5.1). The second-order Gear method with a non dimensional time step $\Delta t = 0.23$ was used, corresponding to approximately 25 time steps per shedding cycle. At each time step, 5 Newton iterations are sufficient to reduce the residuals of the Navier-Stokes equations by 4 orders of magnitude. The convergence history of the unsteady Navier-Stokes equations for the laminar flow past a circular cylinder at **Re**=100 is shown in figure (5.5), with the peaks corresponding to the beginning of a time step and the valleys corresponding to its end.

Figures (5.6) and (5.7) show the vorticity contours and velocity vectors of vortex shedding behind the cylinder during a period of 6.0 (about 1.05 cycle). The global flow field was saved at 5 equally spaced time levels, covering one cycle of vortex shedding. The flow is periodic with a period of T=5.75, as can be seen in figures (5.8-5.10), where the evolution of the horizontal velocity u and transverse velocity v are plotted versus time at $x/D = 0.65$, $x/D = 5$, and $x/D = 8$, downstream from the cylinder along the symmetry line $y = 0$. The

Strouhal number (vortex shedding frequency), $\mathbf{Sr}=f\,D/V_\infty$, is computed by measuring the vortex shedding period based on the transverse velocity v from figure (5.8) and found to be within 5% of the experimental one given in [29]. It was also found from figure (5.8) that the horizontal velocity oscillates at twice the shedding frequency.

The variations of the drag and lift coefficients with respect to time at $\mathbf{Re}=100$ are shown in figures (5.11) and (5.12), respectively. These coefficients have a contribution from the pressure and the viscous force, and are calculated as follows:

$$C_d = -2\int_S \left\{ \left[p + \frac{2}{3}\frac{\mu_{eff}}{\mathbf{Re}}(v_y + w_z) - \frac{1}{3}\frac{\mu_{eff}}{\mathbf{Re}}u_x \right] n_x + \left[-\frac{\mu_{eff}}{\mathbf{Re}} v_x \right] n_y \right.$$
$$\left. + \left[-\frac{\mu_{eff}}{\mathbf{Re}} w_x \right] n_z - \frac{\mu_{eff}}{\mathbf{Re}} u_n \right\} dS \tag{5.1}$$

$$C_l = -2\int_S \left\{ \left[-\frac{\mu_{eff}}{\mathbf{Re}} u_y \right] n_x + \left[p + \frac{2}{3}\frac{\mu_{eff}}{\mathbf{Re}}(u_x + w_z) - \frac{1}{3}\frac{\mu_{eff}}{\mathbf{Re}} v_y \right] n_y \right.$$
$$\left. + \left[\frac{\mu_{eff}}{\mathbf{Re}} w_y \right] n_z - \frac{\mu_{eff}}{\mathbf{Re}} v_n \right\} dS \tag{5.2}$$

The evolution of viscous and pressure coefficients for the drag and the lift with respect to time are also given in figures (5.11) and (5.12).

Comparison of the principal parameters of the flow over the cylinder at $\mathbf{Re}=100$ are presented in table (5.1). The Strouhal number $\mathbf{Sr}$, the maximum transverse velocity v_{max} at the points, $x/D = 0.65$ and $x/D = 5.0$, on the centerline behind the cylinder, the average and peak-to-peak drag coefficients, and the peak-to-peak lift coefficient obtained from the present work are in general in good agreement with the numerical results in [2,13] and the experimental measurements in [29].

	Sr	v_{max} $\frac{x}{D}=0.65$	v_{max} $\frac{x}{D}=5.0$	C_d avg.	C_d pk-pk.	C_l pk-pk.	Grid size	Method
Present work	0.174	0.24	0.65	1.682	0.02	0.75	4050	FEM
Li et al. [2]	0.163	0.25	0.86	1.330	0.05	0.72	826	FEM
Gresho [13]	0.180	------	0.62	1.760	0.07	1.48	1852	FEM
Exp. [29]	0.166	------	------	1.470	------	------	------	------

Table 5.1 Comparison of principal parameters for the flow over the circular cylinder at Re=100

Several tests were carried out for **Re** between 30 and 100 to establish a relation between the Strouhal number, **Sr**, and the Reynolds number, **Re**. It was found that vortex shedding could only be sustained above a certain value of **Re** between 36 and 48.

5.3 Flow Over a Triangular Flame Holder at Re=45,000

Figure (5.13) shows the computational domain and the boundary conditions for a mesh of 2600 nodes (see figure (5.14)). First, a steady-state calculation at **Re**=45,000 was carried out using the steady flow algorithm, SFA. Note that artificial viscosity was needed in this test case. The convergence history of the L_2 residual of the Navier-Stokes equations is shown in figures (5.15-5.16). About 210 Newton iterations were needed to reduce the residual by 5 orders of magnitude. The resulting vorticity and velocity fields behind the flame holder are given in figure (5.17).

Unsteady flow calculations were then started from the above mentioned steady-state solution. The boundary conditions for the continuity and momentum equations are summarized in figure (5.13). In addition, the boundary conditions for the turbulence equations are [30]:

$$\text{Inlet} \qquad \kappa_{in} = (0.05\ V_\infty)^2 \qquad \varepsilon_{in} = \frac{0.16\ \kappa_{in}^{1.5}}{0.2\ l}$$

$$\text{Exit} \qquad \frac{\partial \kappa}{\partial n} = 0 \qquad \frac{\partial \varepsilon}{\partial n} = 0$$

where $l = 3H$ denotes the channel height.

The second-order Gear method with time step $\Delta t = 0.12$ was used, corresponding to approximately 32 time steps per shedding cycle. It was found that 5 Newton iterations per time step, and 15 iterations on the (κ,ε) turbulence model, were sufficient to reduce the residual of all governing equations by 3 orders of magnitude. The convergence history of the unsteady Navier-Stokes equations for the turbulent flow past a triangular cylinder (flame holder) at **Re** =45,000 is shown in figures (5.18, 5.19), with the peaks corresponding to the beginning of a time step and the valleys corresponding to its end.

Figures (5.20) and (5.21) show the vorticity contours and velocity vectors of vortex shedding behind the flame holder during a period of 3.85. The global flow field was saved at 6 equally spaced time levels, covering one cycle of vortex shedding. The flow is periodic with a period of T=3.85, as can be seen in figure (5.22), where the evolution of the horizontal velocity u and transverse velocity v are plotted versus time at x/H= 0.76, downstream from the flame holder along the symmetry line $y = 0$. At the same location in space, as can be seen in figure (5.23), the variations of the effective viscosity μ, the rate of energy dissipation ε, and the turbulent kinetic energy κ, with respect to time are also plotted.

The Strouhal number (vortex shedding frequency), $\mathbf{Sr} = fH/V_\infty$, is computed by measuring the vortex shedding period based on the transverse velocity v from figure (5.22) and found to be within 4% of the experimental one given in [31]. Comparison of the principal parameters of the flow over the flame holder at **Re**=45,000 is presented in table (5.2).

	T period	**Sr**	v_{max} $\frac{x}{H} = 0.76$	Grid size nodes	Method
Present work	3.850	0.260	1.00	2600	FEM
Johansson [30]	3.703	0.270	------	18000	FVM
Exp. [31]	4.000	0.250	------	-------	-------

Table 5.2 Comparison of principal parameters for the flow over the flame holder at Re=45,000

6. Conclusions and Recommendations

6.1 Conclusions

The conservative formulation of the steady Navier-Stokes equations in [3] has been extended to the time-accurate analysis of unsteady flows. The governing equations are discretized in space by the Galerkin method, in time by a second-order Gear method and the overall system linearized by a Newton method. The resulting set of algebraic equations, at each time step, is implicitly solved for the velocity and pressure by an iterative solver. The temperature is updated, in a segregated manner, by solving a simplified algebraic form of the energy equation. The κ-ε equations are solved in a segregated manner by an iterative solver.

The performance of the Gear method has been evaluated through the solution of the unsteady nonlinear Burgers equation and shown to be superior to the performance of the Crank-Nicolson method. The Gear method provided higher ranges of stability and accuracy as was illustrated in Chapter 2.

This time accurate implementation of the Navier-Stokes equations has been embedded into a Concordia-Pratt & Whitney Canada three-dimensional, turbulent, steady Navier-Stokes code, *NS3D*. The code has been validated, for the purpose of the Thesis, against two well-known 2-D test cases. The first case is that of a laminar flow past a circular cylinder at Reynolds numbers between 35 and 100, and the second is that of a turbulent flow over a triangular shaped flame holder at **Re**=45,000. The von Karman vortex street shedding, observed experimentally, is well captured in both cases and its computed shedding frequency is shown to be within 5% of the experimental one.

6.2 Recommendations

The present formulation is capable of analyzing the unsteady flow over a geometry consisting of a number of objects that are stationary relative to one another. The formulation could be extended in the future to analyze the unsteady flow in situations consisting of a number of objects moving relative to one another.

In the context of turbomachinery, the work of this Thesis can be used to analyze the flow in the passage of one blade row (rotor or stator), if the inlet and exit boundary conditions are presumed known. In the general case where unsteady flow phenomena such as wake/rotor interaction and potential stator/rotor interaction need to be captured, one needs to carry out a multistage analysis in which the boundary conditions are specified only at the inlet of the upstream stage and at the exit of the downstream stage. For all other intermediate components or stages unsteady boundary conditions need to be defined iteratively. The work described here is therefore being extended in *NS3D* to the analysis of the flow within the passage of a blade row embedded in a multistage environment. Four, increasingly more complex, options are available:

a- Through-Flow Approach

It assumes that the flow in the vicinity of every blade row is time invariant. This means that there should be an axisymmetric surface of revolution somewhere between every two blade rows. The scheme is an interaction between separate 3-D solution domains for individual blade rows and an axisymmetric 2-D (through-flow) domain covering the whole machine. For the through-flow, the effect of three dimensionality is introduced by circumferencial averaging of the 3-D equations [32,33].

Although every blade row flow is supposed to be linked to an axisymmetric average model, the axisymmetric model for one turbomachine should be unique. For a multi-row machine, the solution of the through-flow is used to get the necessary boundary conditions for individual blade row 3-D solutions while the 3-D solutions are used to incorporate loss modeling and blockage effects into the through-flow. Although the scheme is feasible as far as computing time is concerned, it smears the transport of flow features between blade rows and lacks the complete effect of multistage environment representation while solving for one blade row.

b- Mixing Plane Approach

As an improvement to the previous approach, while retaining the steady flow assumption, the mixing plane between blade rows allows the coupled solution of 3-D domains while averaging only the quantities necessary for conservation laws at the inter-row mixing plane and passing these quantities axisymmetrically to the adjacent blade row.

The multistage effect can be carried out either by coupling a through-flow domain covering other blade rows to the 3-D domain for the target blade row, or by solving the 3-D domains simultaneously.

The added advantage is the ability to represent multistage environment while solving for an individual blade row and the fact that inter-row boundary values are calculated rather than imposed. However, the scheme still has the smearing disadvantage of its predecessor [34].

c- Average-Passage Flow Approach

This model represents a time-averaged flow field, over a time interval which ensures temporal periodicity, as seen by an observer whose frame of reference is fixed with respect to a given blade row [35].

Relative to an individual blade row's frame of reference, a 3-D solution is defined which represents the domain of the whole turbomachine. the effect of unsteadiness due to other blade rows is accounted for using time and space averaging. A gate function controls the averaging procedure and excludes all moments when the point is contained within a blade thickness (no flow). If the point is within a relative moving row, the gate function can be formed by a group of step functions rotating with the blade row and having zero value inside blade thickness and unity elsewhere. Outside blade rows, the function value is identically unity. Because the existence of rigid bodies (other blade rows) is accounted for, the resulting time and space-averaged quantities cover the whole machine domain and the blade rows will be represented by an axisymmetric blockage, correlation and body force-like terms. Since Euler or Navier-Stokes equations are nonlinear, the new time-averaging will include new correlations between time-varying flow variables. These correlations represent the effect of unsteadiness on the time-averaged solution and constitute, with the previously mentioned body forces, energy sources and the space-averaging correlation, the closure requirements for the average-passage equations. Since the machine should have one axisymmetric component of the flow field, the closeness of the axisymmetric parts of the ensuing solutions is taken as a measure of convergence.

The advantage of the average-passage scheme is that temporally and spatially averaged equations are solved on a steady basis and the solution is supposed to represent the total effect of all other blade rows. The disadvantage is the complexity and rising cost for multistage cases as well as the uncertainty concerning the correlation models.

d- Reynolds-Averaged Unsteady Navier-Stokes Equations

In this approach the Reynolds-averaged unsteady Navier-Stokes equations are solved throughout the computational domain, comprising rotors and stators, with no averaging of flow properties at the interface between any two blade rows. The time-accurate flow properties are communicated by introducing a time-inclined computational plane at the interface between a rotor and stator. The advantage of such an approach is that no closure requirements are involved. However, it is expensive in terms of both computing time and memory [1].

Approach (d), the most complete and complex is extremely demanding in terms of computing time and resources. It is not currently in the realm of turbomachinery industrial design settings. It is intended, therefore, to march in complexity through the (a) and (b) approaches, and ultimately when computer resources permit, implement approach (d).

References

1. M. B. Giles, "Calculation of Unsteady Wake Rotor Interaction", *AIAA Journal of Propulsion and Power,* Vol. 4, pp. 356-362, August 1988.

2. J. Li, A. Chambarel, M. Donneaud, R. Martin, "Numerical Study of Laminar Flow Past One and Two Circular Cylinders", *Computers & Fluids,* Vol. 19, pp. 155-170, 1991.

3. M. F. Peeters, W. G. Habashi, B. Q. Nguyen and P. L. Kotiuga, "Finite Element Solutions of the Navier-Stokes Equations for Compressible Internal Flows", *AIAA Journal of Propulsion and Power,* Vol. 8, No. 1, pp. 192-198, January 1992.

4. R. Peyret, T. D. Taylor, "Computational Methods for Fluid Flow", *Spinger Physics in Computational Physics,* Vol. 15, pp. 371-376, 1972.

5. A. Jameson, W. Schmidt, E. Turkel, "Numerical Simulation of the Euler Equations by Finite Volume Methods Using Range-Kutta Time Stepping Schemes", *AIAA Paper 81-1259 - AIAA 5th Computational Fluid Dynamics Conference,* 1981.

6. R. M. Beam, R. F. Warming, "An Implicit Factored Scheme For the Compressible Navier-Stokes Equations", *AIAA Journal,* Vol. 16, pp. 393-402, 1978.

7. S. K. Jordan, J. E. Fromm, "Oscillatory Drag, Lift, and Torque on a Circular Cylinder in a Uniform Flow", *Phys. Fluids*, New York, 1983.

8. M. Braza, P. Chassaing, H. Ha. Minh, "A Numerical Study of the Dynamic of Different Scale Structures in the Near Wake of a Circular Cylinder in Laminar to Turbulent Transition", *J. Fluid Mechanics*, Vol. 165, p. 79, 1986.

9. R. V. Chima, P. W. Giel, R. J. Boyle, "An Algebraic Model for Three-Dimensional Viscous Flows", *NASA TM 105931*, 1993.

10. San-Yih Lin, Yan-Shin Chin, "Discontinuous Galerkin Finite Element Method for Euler and Navier-Stokes Equations", *AIAA Journal*, Vol. 31, No. 11, November, 1993.

11. M. O. Bristeau, R. Glowinski, B. Mantel, J. Periaux, P. Perrier, "Numerical Methods for the Time-Dependent Compressible Navier-Stokes Equations", *Computing Methods in Applied Science and Engineering*, 1984.

12. B. E. Launder, M. Kato, "Modelling Flow-Induced Oscillations in Turbulent Flow Around a Square Cylinder", *ASME Paper*, Vol. 157, February, 1993.

13. P. M. Gresho, S. T. Chan, R. L. Lee, C. D. Upson, "A Modified Finite Element Method for Solving the Time-Dependent, Incompressible Navier-Stokes Equations. Part 2: Applications", *International Journal for Numerical Methods in Fluids,* Vol. 4, 619-640, 1984.

14. F. N. Von De Vosse, A. Segal, A. A. Van Steenhoven, J. D. Janssen, "A Finite Element Approximation of the Unsteady Two-Dimensional Navier-Stokes Equations", *International Journal for Numerical Methods in Fluids,* Vol. 6, pp. 427-443, 1986.

15. J. D. Hoffman, *Numerical Methods for Engineers and Scientists,* McGraw-Hill, pp. 214-305, 1992.

16. W.S. Ghaly, "Energy Equation implementation in *NS3D*: A Status Report", *P&WC memo,* December 1992.

17. H. Schlichting, *Boundary Layer Theory,* McGraw-Hill, 7th Edition, p. 280, 1967.

18. F. M. White, *Viscous Fluid Flow,* McGraw-Hill, 1974.

19. R. Peyret and H. Viviand, "Computation of Viscous Compressible Flows Based on the Navier-Stokes Equations", *R. Peyret and H. Viviand,* AGARDograph No. 212, 1975.

20. B. E. Launder and D. B. Spalding, "The Numerical Computation of Turbulent Flows", *Computer Methods in Applied Mechanics and Engineering*, Vol. 3, pp. 269-289, 1974.

21. G. S. Baruzzi, W. G. Habashi, M. M. Hafez, "An Improved Finite Element Method for the Solution of the Compressible Euler and Navier-Stokes Equations", Proceedings of the First European CFD Conference, Brussels, Belgium, Vol. II, pp. 643-650, September 1992.

22. W. S. Ghaly, M. Sleiman, "*NS3D* Time-Accurate Simulation and Validation on Stationary Meshes", *P&WC memo*, File # S-10350, Code # 600-14-33, April 7, 1994.

23. H. Manouzi and M. Fortin, "A Treatment of Wall Boundaries For Turbulent Flows by the Use of a Transmission Finite Element Method", *International Journal for Numerical Methods in Engineering*, Vol. 31, 1991, pp. 113-126.

24. V. Haroutunian and M. Engelman, "On Modeling Wall-Bound Turbulent Flows Using Specialized Near-Wall Finite Elements and the Standard k-ε Turbulence Model", *Advances in Numerical Simulation of Turbulent Flows*, pp. 97-105, ASME Conference, 1991.

25. V. N. Nguyen, W. G. Habashi and M. V. Bhat, "Vector-Parallel Gauss Elimination Solver for Large-Scale Finite Element Computational Fluid Dynamics", *Proceedings of the Supercomputing Symposium 1990*, Montreal, pp. 363-369, June 1990.

26. W. G. Habashi, V. N. Nguyen and M. V. Bhat, "Efficient Direct Solvers for Large-Scale Computational Fluid Dynamics Problems", *Computer Methods in Applied Mechanics and Engineering,* Vol. 87, pp. 253-265, 1991.

27. W. G. Habashi, M. Fortin, J. W. H. Liu, M. P. Robichaud, J. S. Strigberger, V. N. Nguyen and W. S. Ghaly, "Large-Scale Computational Fluid Dynamics by the Finite Element Method", *AIAA Paper 91-0120, AIAA 29th Aerospace Sciences Conference,* Reno, January 1991.

28. L. C. Dutto, W. G. Habashi, M. Fortin and M. P. Robichaud, "Parallelizable Block Diagonal Preconditioners for the Compressible Navier-Stokes Equations", *9th International Conference on Finite Element Methods in Flow Problems,* Barcelona, Spain, July 1993.

29. M. Hammache and M. Gharib, "An experimental study of the parallel and oblique vortex shedding from circular cylinders", *Journal of Fluid Mechanics,* Vol. 232, p. 567, 1991.

30. S. H. Johansson, L. Davidson, E. Olsson, "Numerical Simulation of Vortex Shedding Past Triangular Cylinders at High Reynolds Number Using a κ-ε Turbulence Model", *International Journal for Numerical Methods in Fluids,* Vol. 16, 859-878, 1993.

31. H. E. Hartensson, L. E. Eriksson, "Large Eddy Simulation of Turbulent Wake Flow", *Volvo Flygmotor AB Internal Report,* S-461-81, Trollhattan, Sweden, 1992.

32. W. N. Dawes, "Towards Improved Throughflow Capacity: The Use of 3D Viscous Flow Solvers in a Multistage Environment", *Trans ASME Journal of Engineering for Power,* 90-GT-18, 1990.

33. W. N. Dawes, "The Use of 3D Viscous Flow Solvers in a Multistage Environment", *Trans ASME Journal of Engineering for Power,* 90-GT-18, 1990.

34. R. H. Ni, J. Bogoian, "Prediction of 3D Multi-Stage Turbine Flow Field Using a Multi-Grid Euler Solver", *AIAA Paper,* 8900091, 1989

35. J. Adamczyk, "Model Equation for Simulating Flows in Multistage Turbomachinery" *ASME Paper,* 85-GT-226, March 1985.

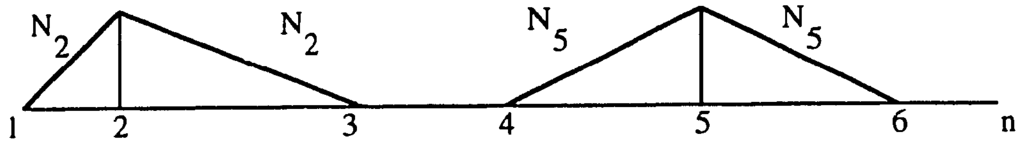

Figure 2.1 Interpolation functions for a 1-D linear element.

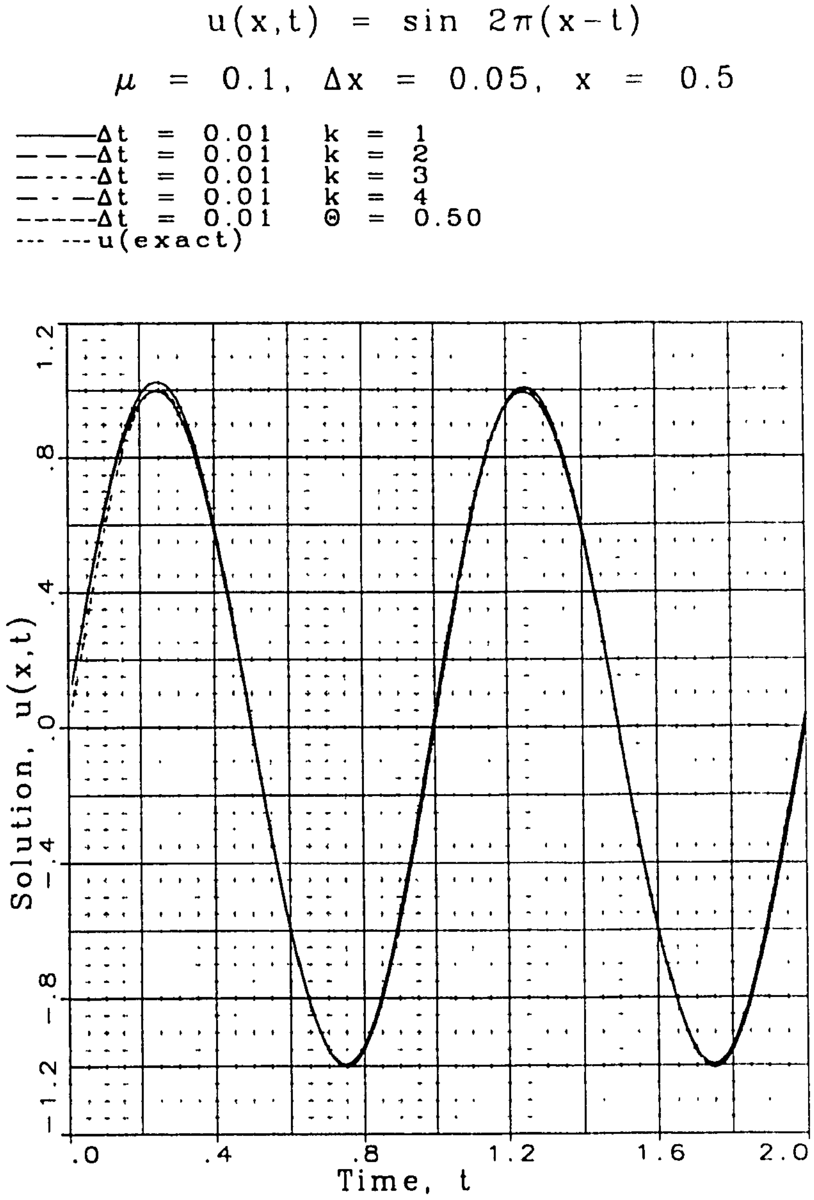

Figure 2.2 Finite element solution of the Burgers equation by the Gear method and the Crank-Nicolson method, for Δt=0.01 and μ=0.1.

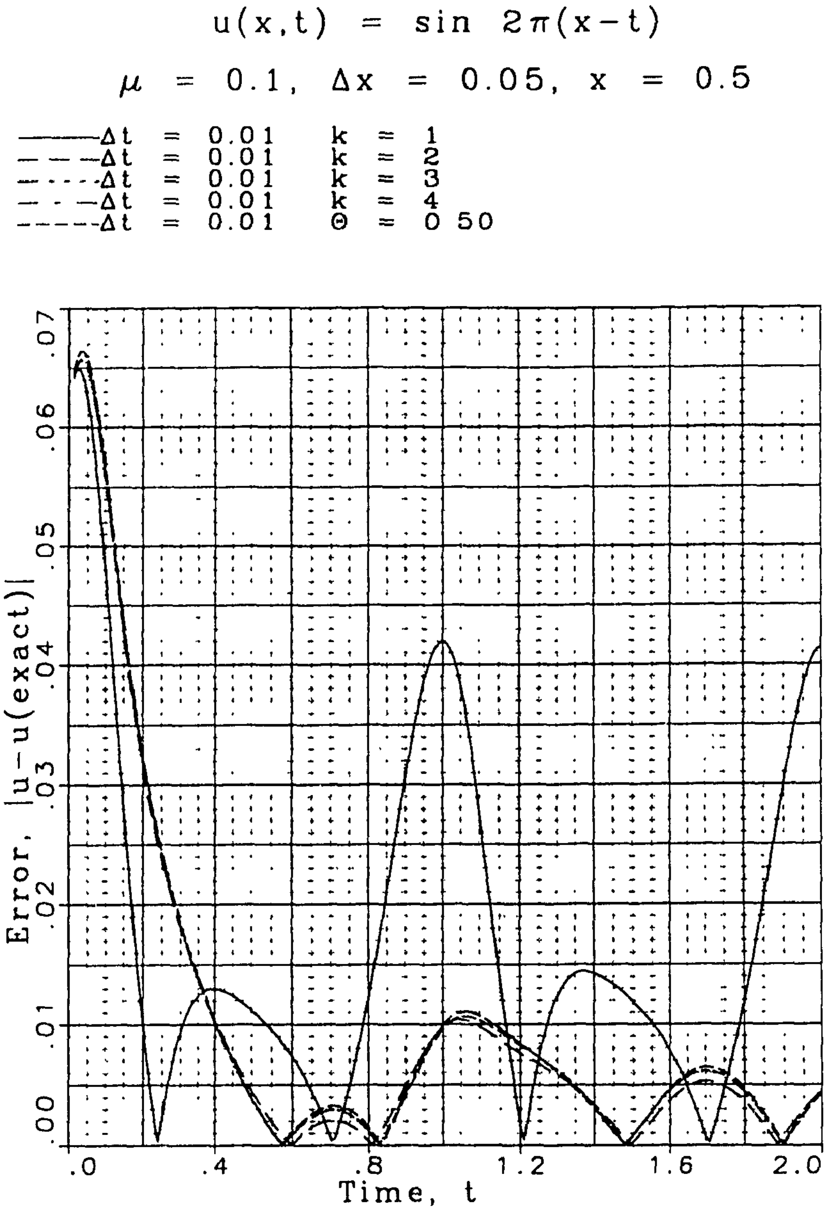

Figure 2.3 Error in the solution by the Gear method and the Crank-Nicolson method, for Δt=0.01 and μ=0.1.

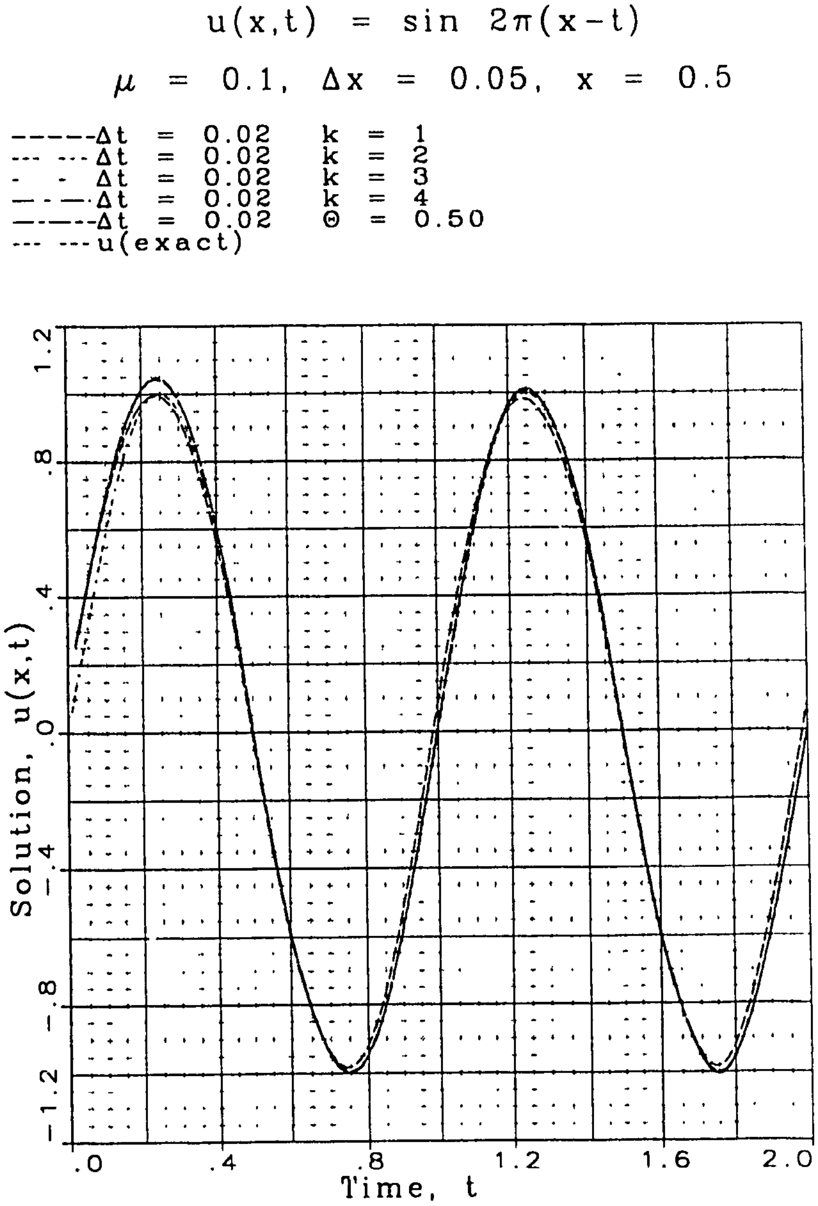

Figure 2.4 Finite element solution of the Burgers equation by the Gear method and the Crank-Nicolson method, for Δt=0.02 and μ=0.1.

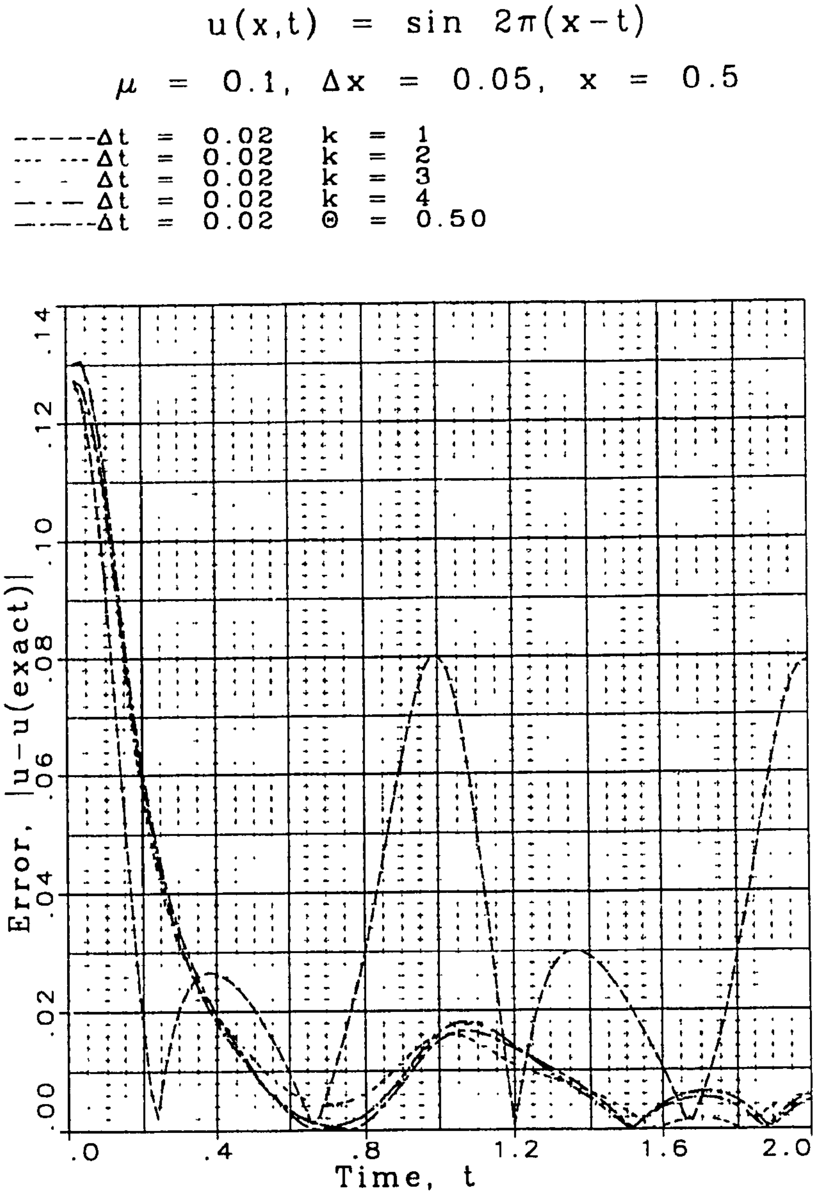

Figure 2.5 Error in the solution by the Gear method and the Crank-Nicolson method, for Δt=0.02 and μ=0.1.

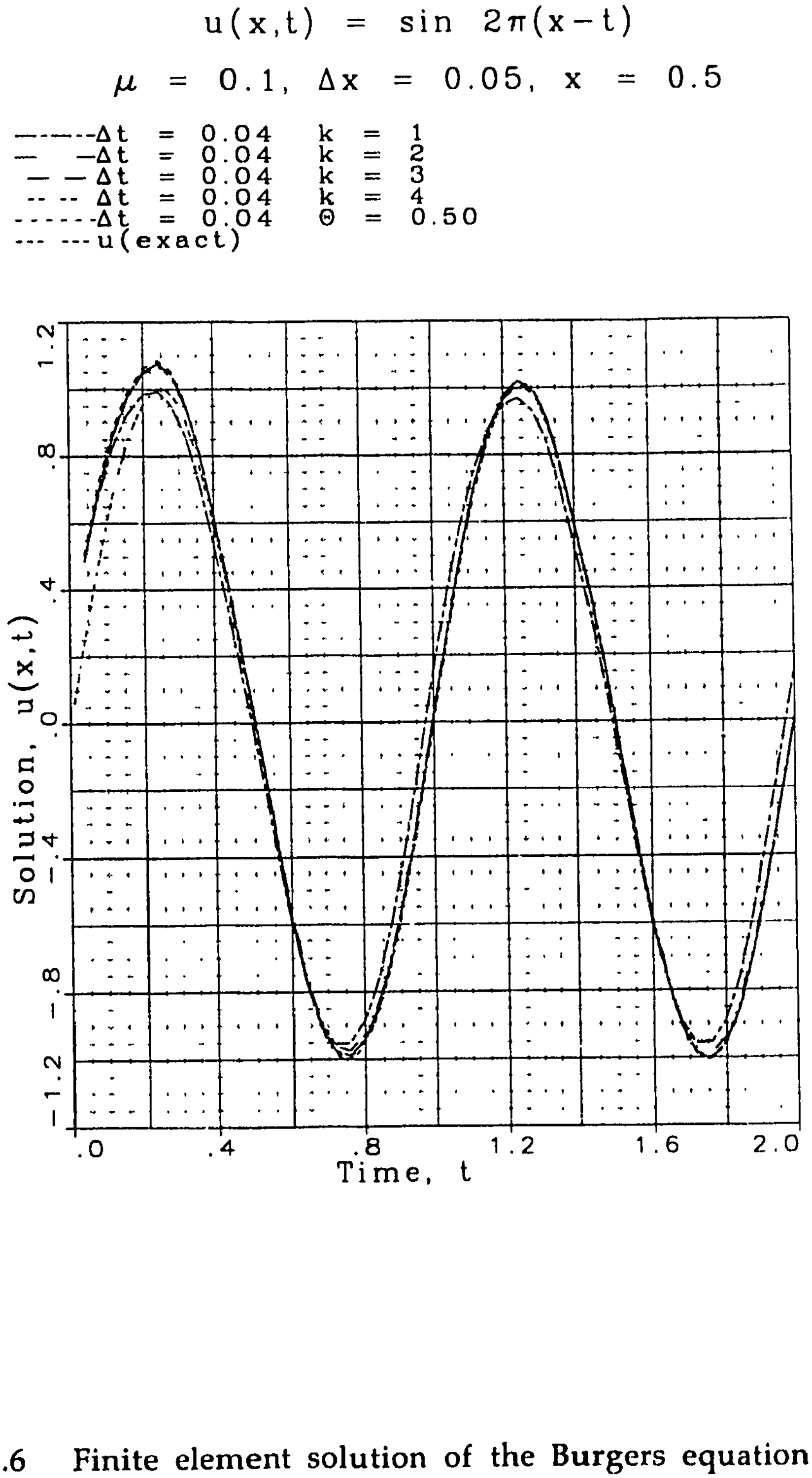

Figure 2.6 Finite element solution of the Burgers equation by the Gear method and the Crank-Nicolson method, for Δt=0.04 and μ=0.1.

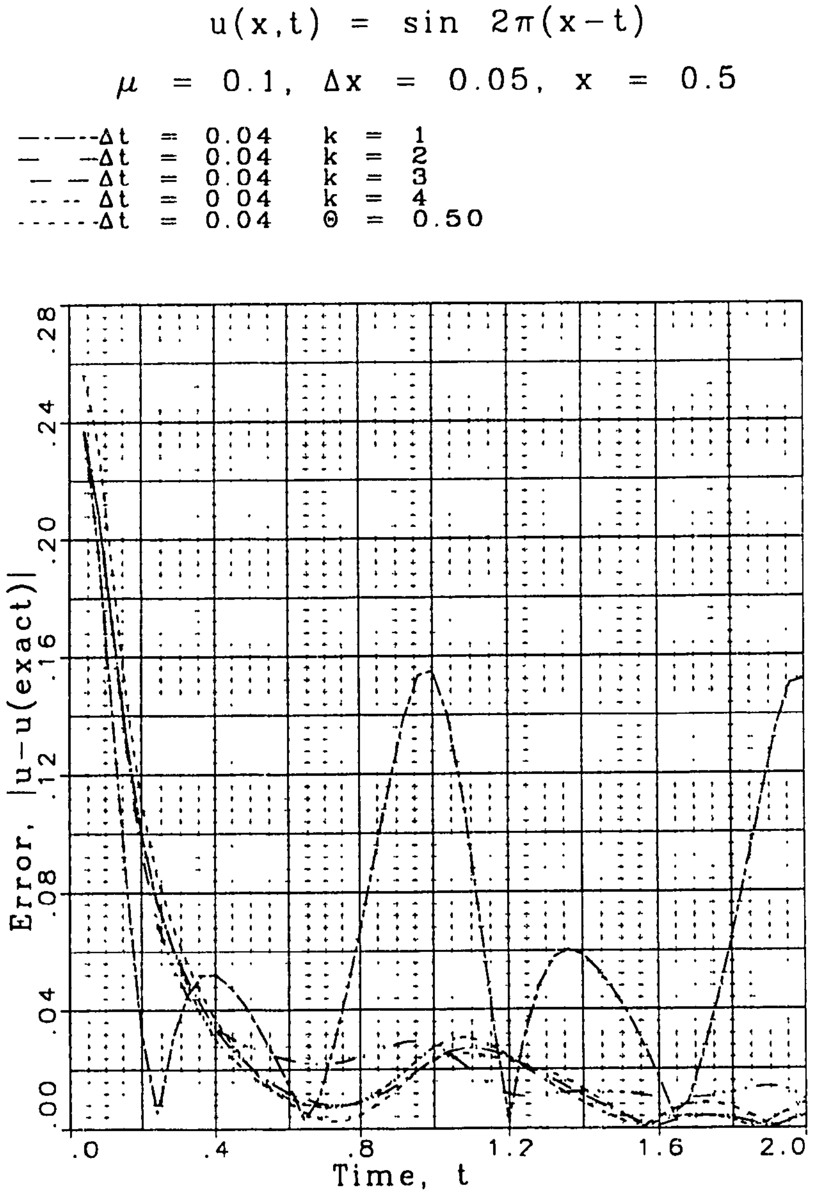

Figure 2.7 Error in the solution by the Gear method and the Crank-Nicolson method, for Δt=0.04 and μ=0.1.

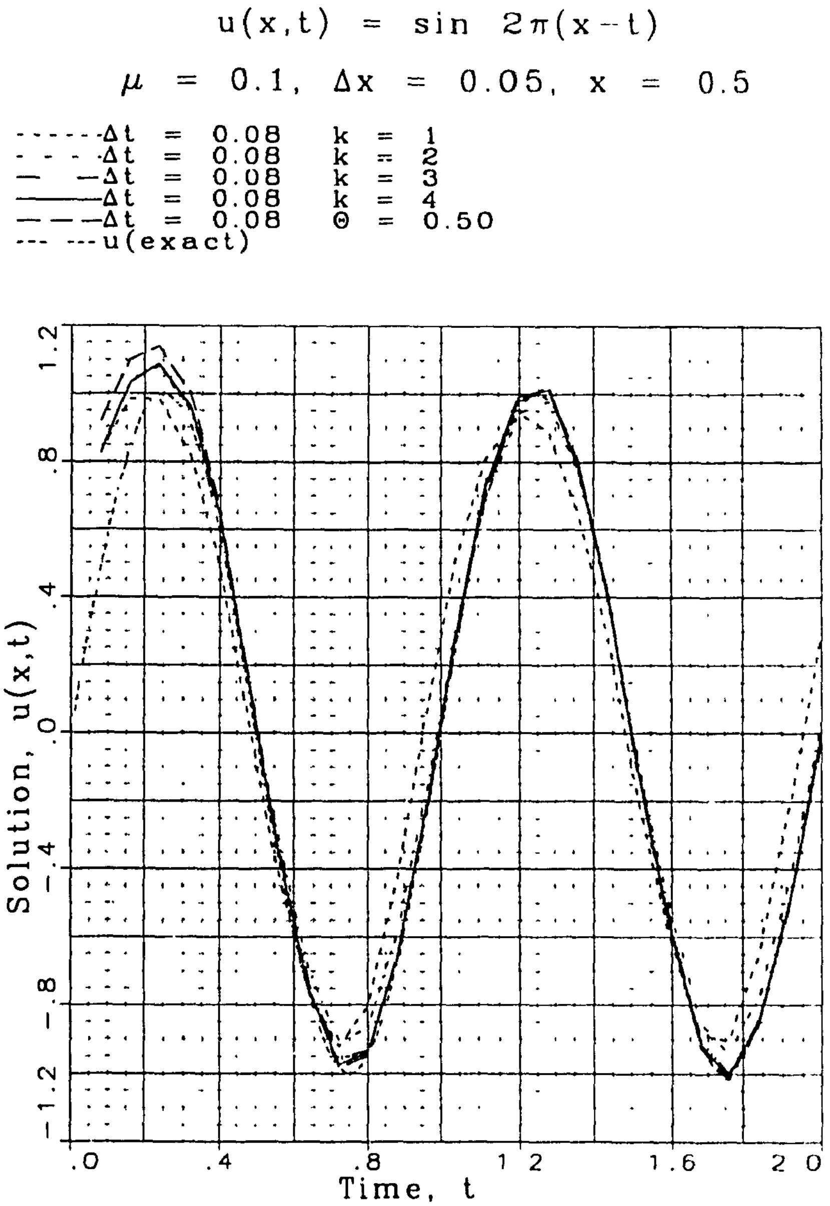

Figure 2.8 Finite element solution of the Burgers equation by the Gear method and the Crank-Nicolson method, for Δt=0.08 and μ=0.1.

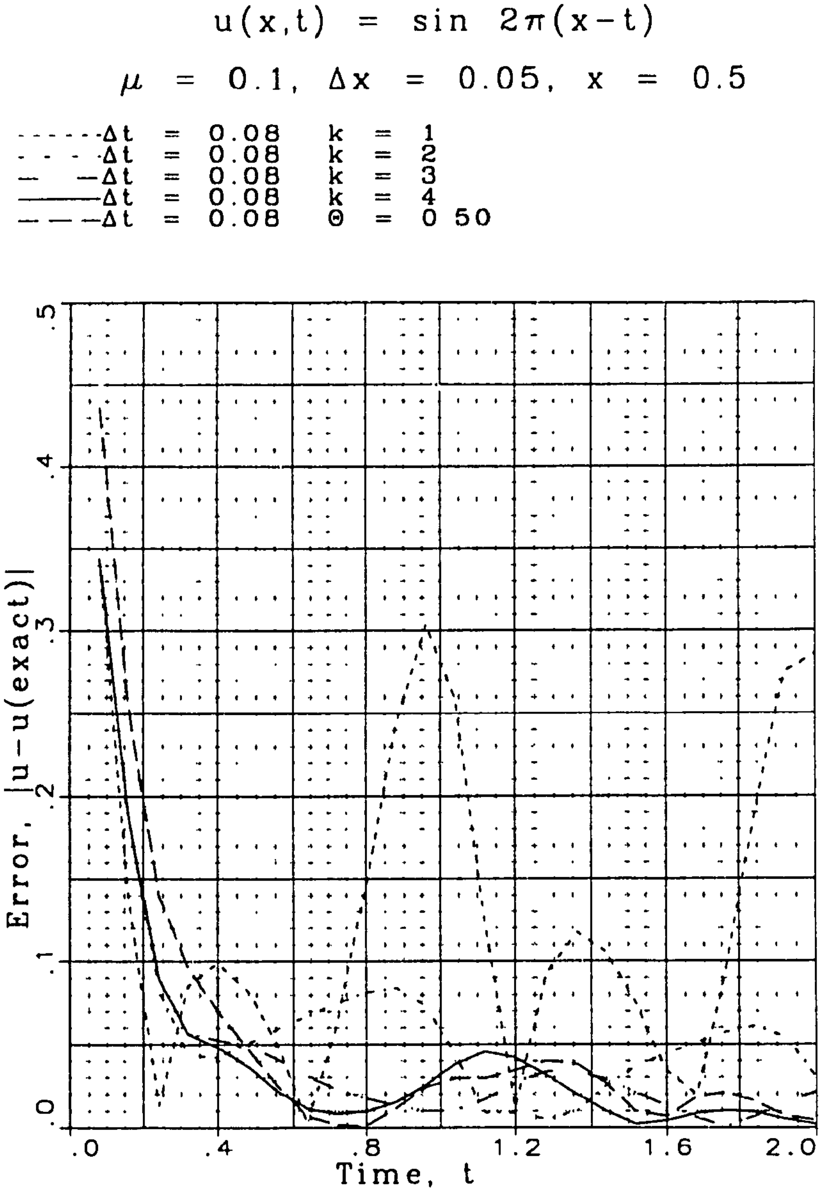

Figure 2.9 Error in the solution by the Gear method and the Crank-Nicolson method, for Δt=0.08 and μ=0.1.

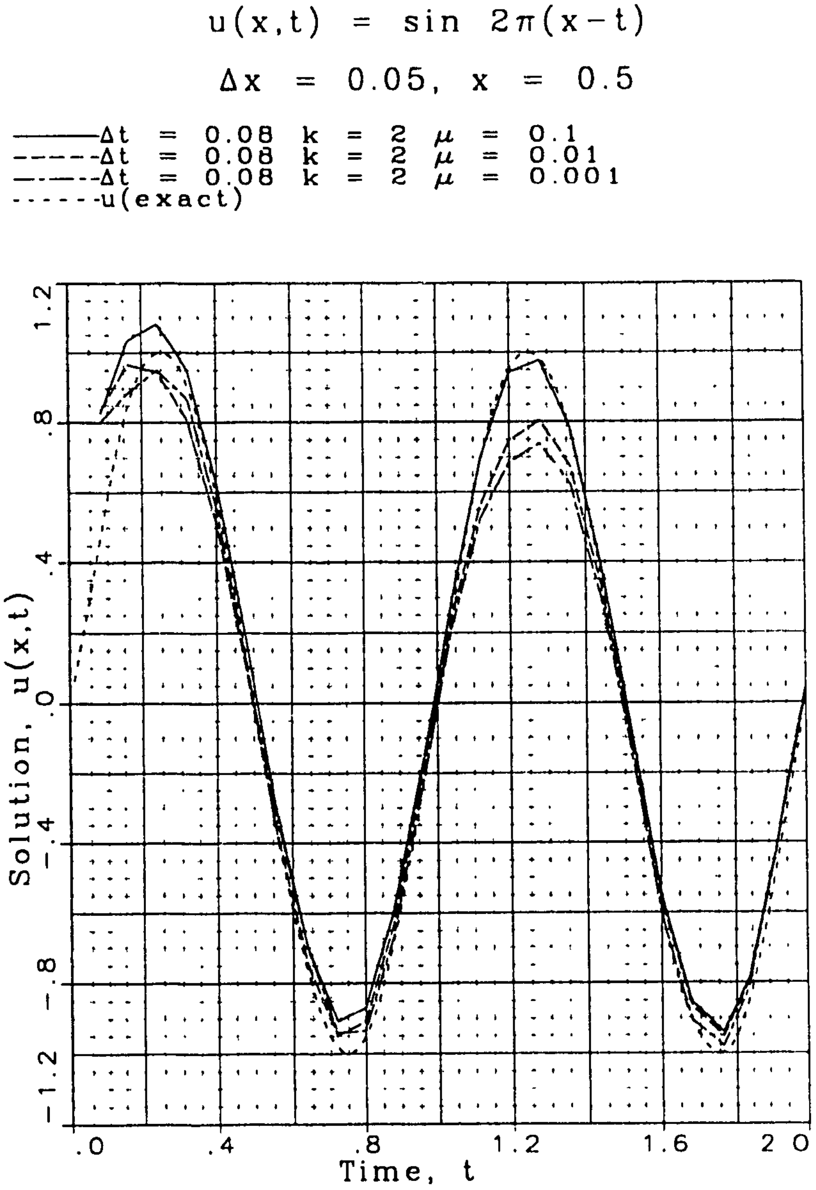

Figure 2.10 Finite element solution of the Burgers equation by the second-order Gear method and the Crank-Nicolson method, for Δt=0.08 and μ=0.1, 0.01, 0.001.

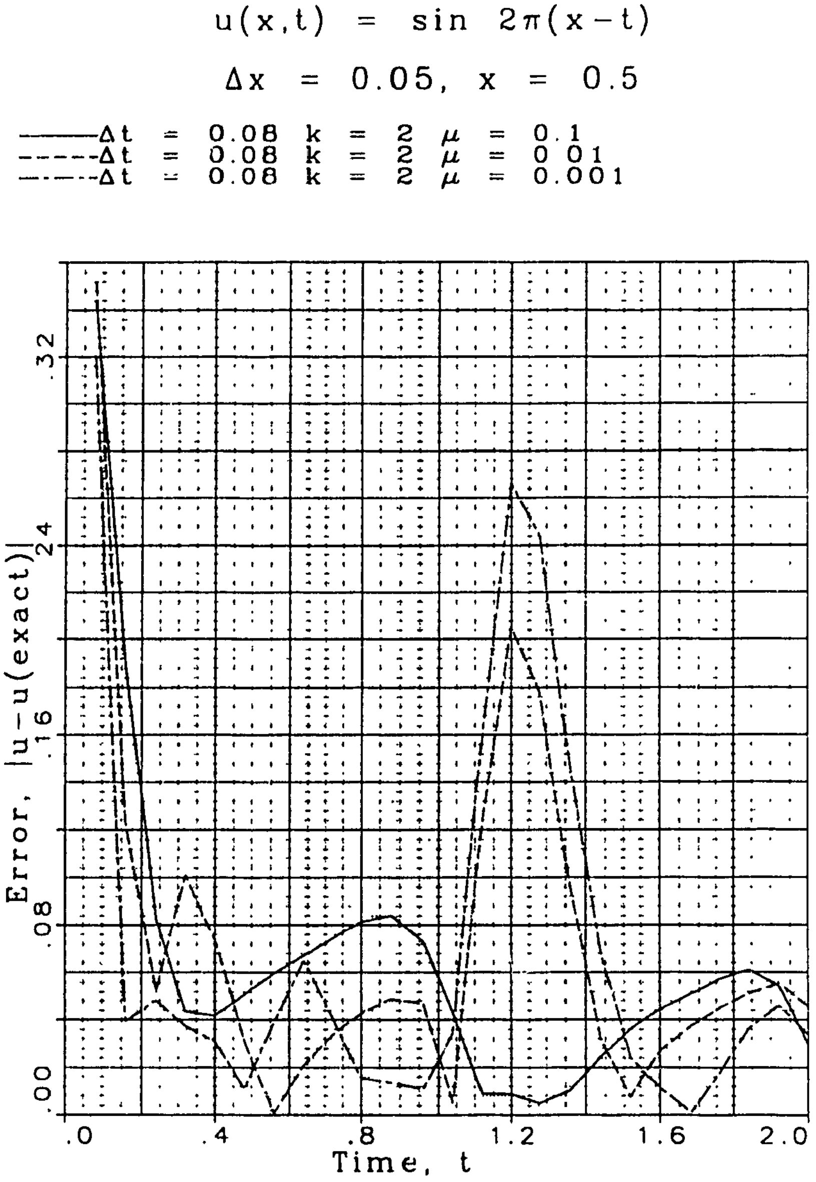

Figure 2.11 Error in the solution by the second-order Gear method and the Crank-Nicolson method, for Δt=0.08 and μ=0.1, 0.01, 0.001.

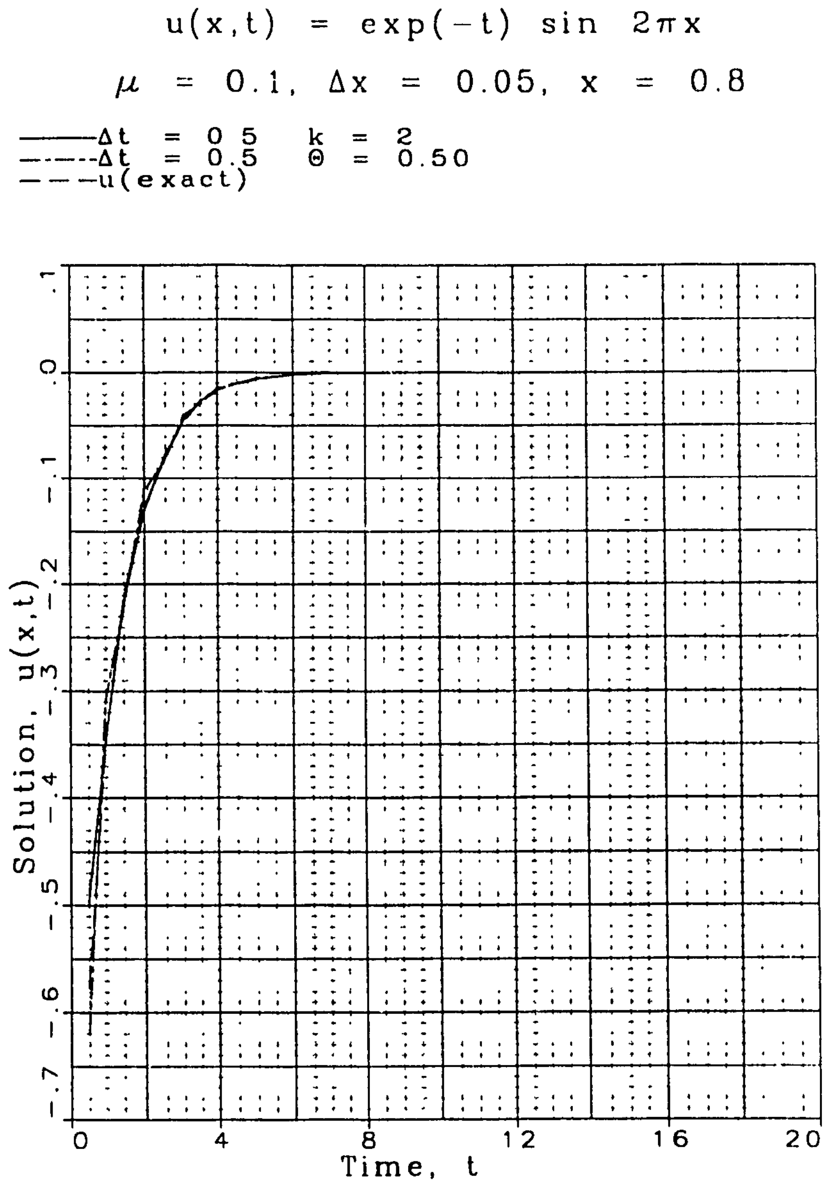

Figure 2.12 Finite element solution of the Burgers equation by the second-order Gear method and the Crank-Nicolson method, for Δt=0.5 and μ=0.1

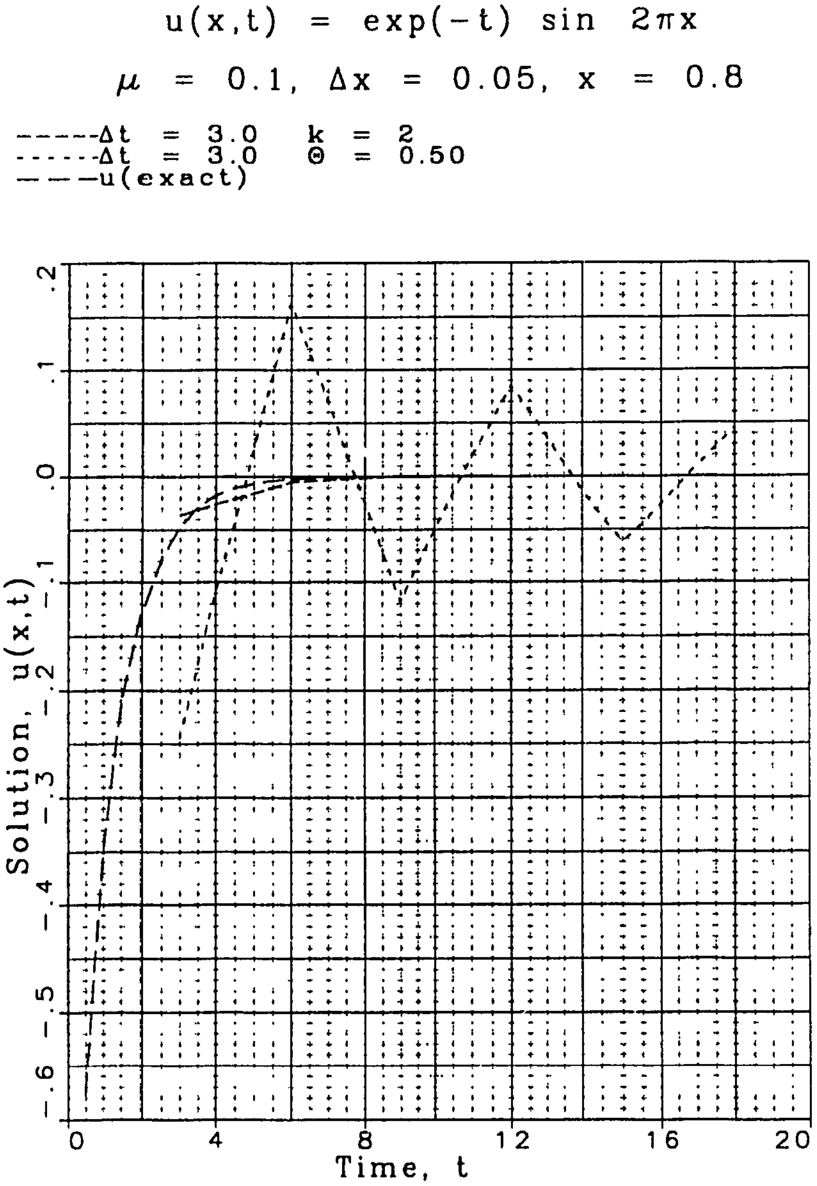

Figure 2.13 Finite element solution of the Burgers equation by the second-order Gear method and the Crank-Nicolson method, for Δt=3.0 and μ=0.1

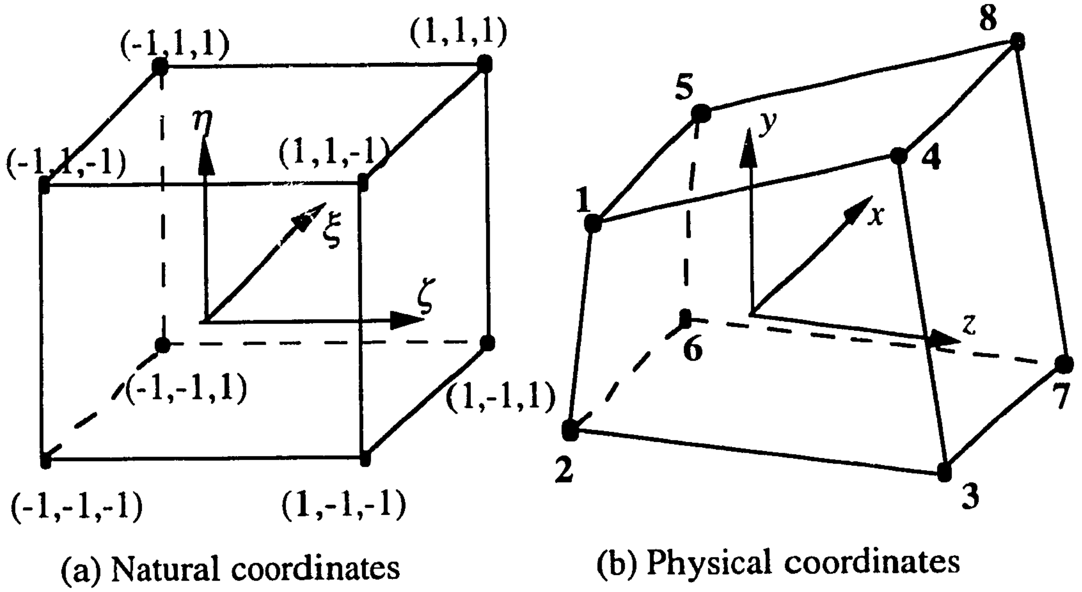

Figure 3.1 Isoparametric trilinear finite element.

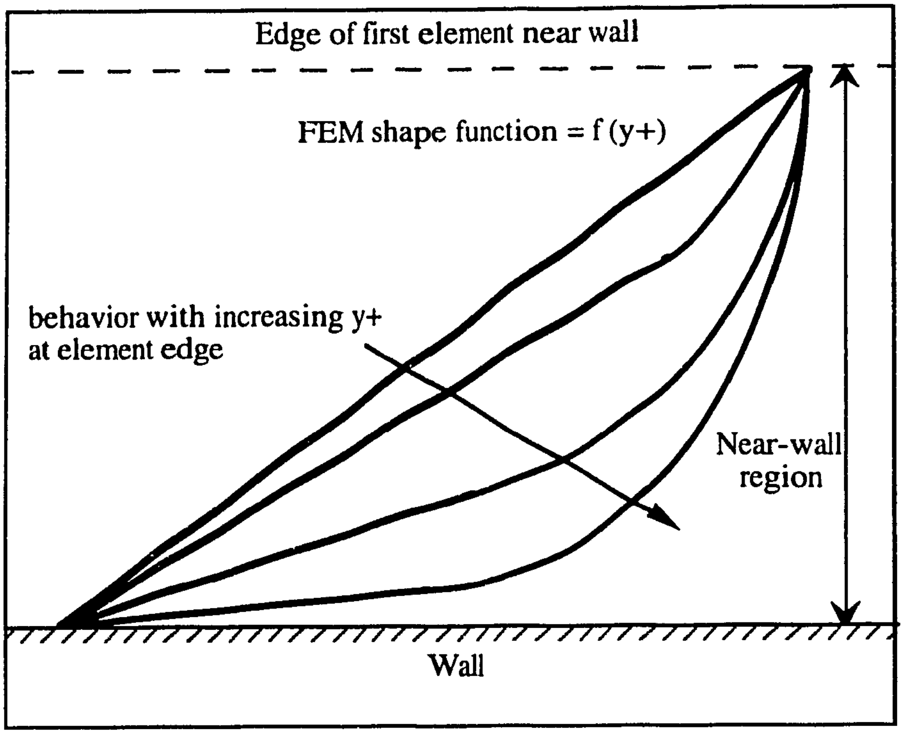

Figure 4.1 Wall-integration logarithmic shape function.

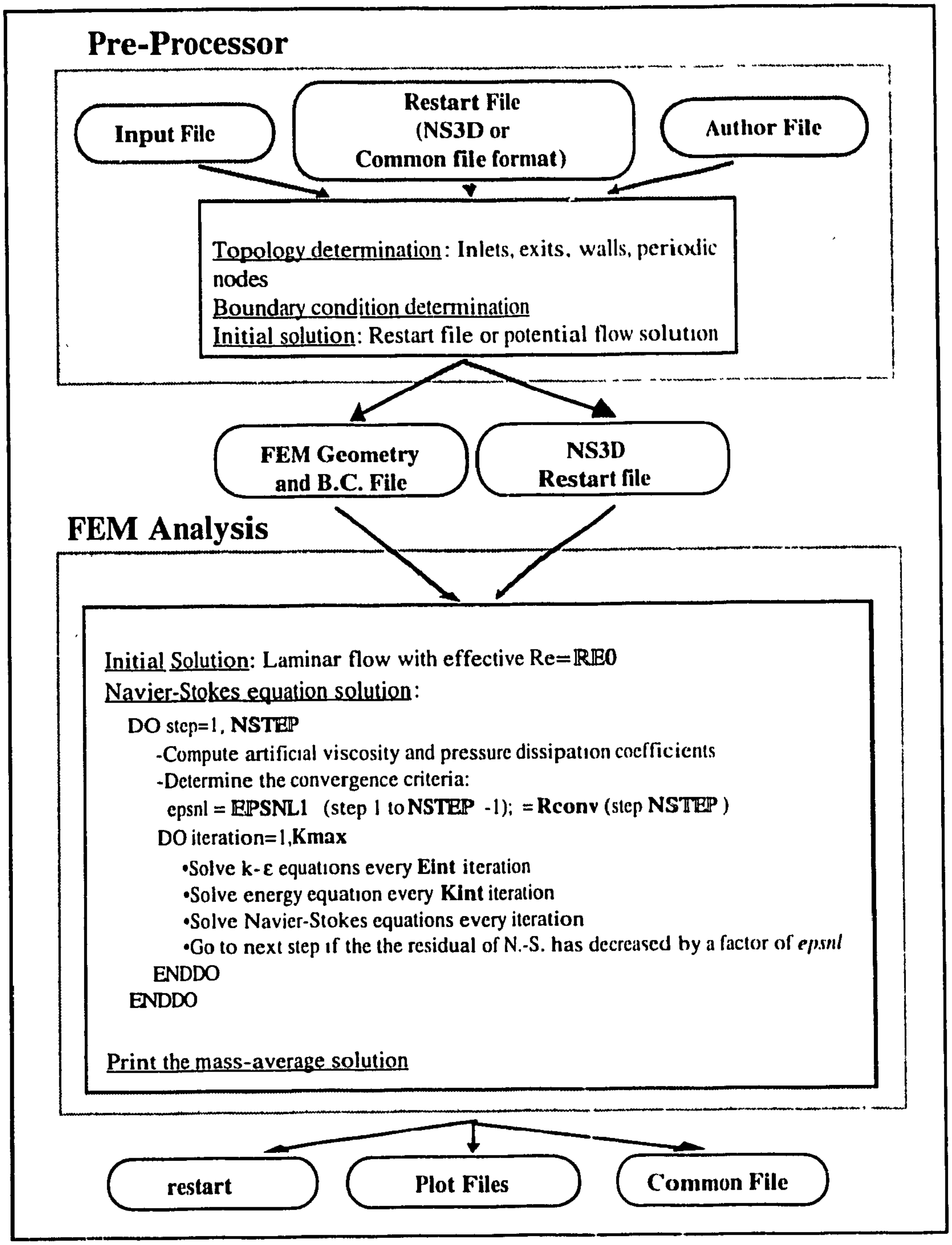

Topology determination: Inlets, exits, walls, periodic nodes
Boundary condition determination
Initial solution: Restart file or potential flow solution

```
Initial Solution: Laminar flow with effective Re=RE0
Navier-Stokes equation solution:
  DO step=1, NSTEP
     -Compute artificial viscosity and pressure dissipation coefficients
     -Determine the convergence criteria:
      epsnl = EPSNL1  (step 1 to NSTEP -1);  =Rconv (step NSTEP )
     DO iteration=1,Kmax
        •Solve k-ε equations every Eint iteration
        •Solve energy equation every Kint iteration
        •Solve Navier-Stokes equations every iteration
        •Go to next step if the the residual of N.-S. has decreased by a factor of epsnl
     ENDDO
  ENDDO

Print the mass-average solution
```

Figure 4.2a Algorithm flowchart for the steady flow scheme.

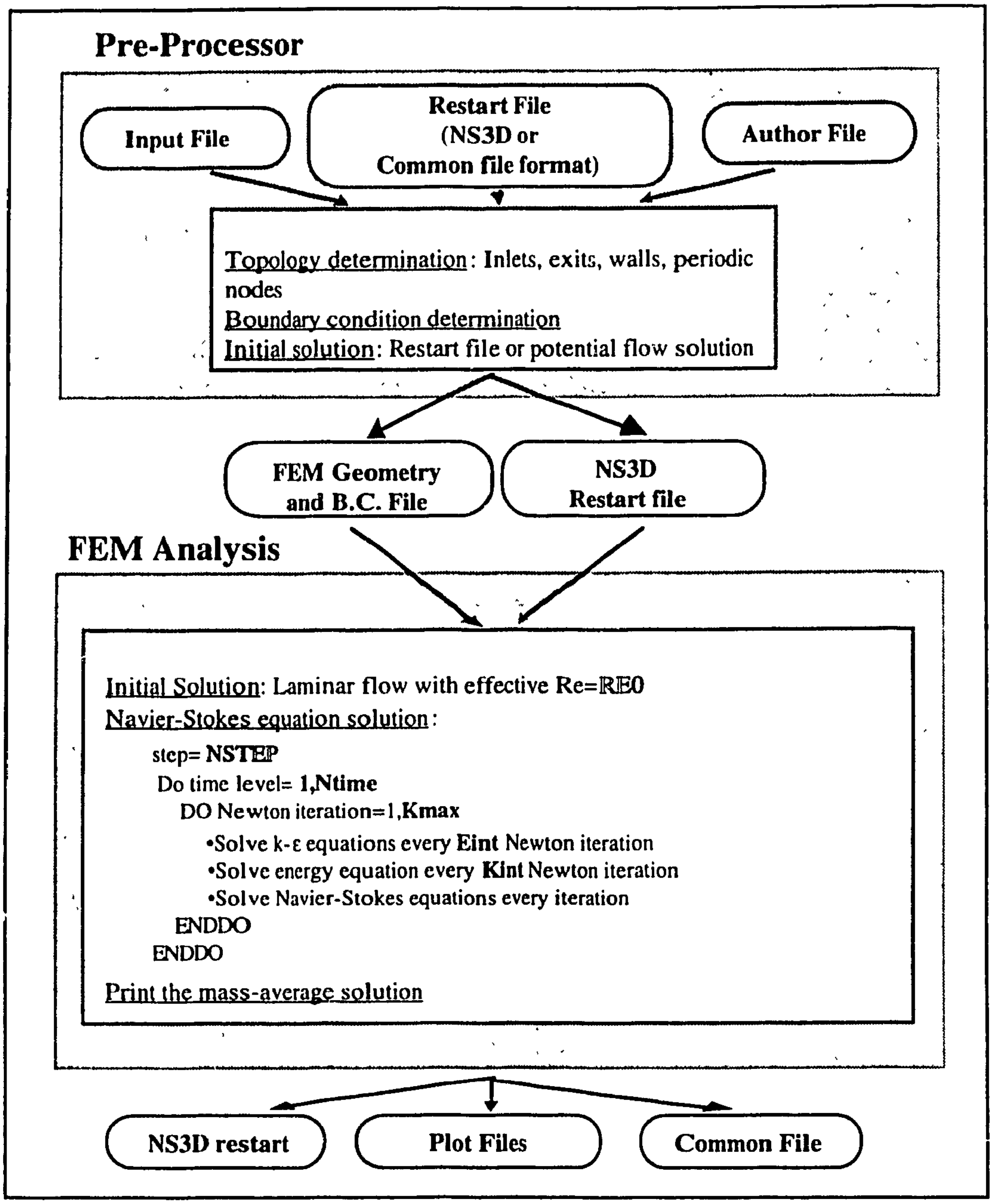

```
Initial Solution: Laminar flow with effective Re=RE0
Navier-Stokes equation solution:
    step= NSTEP
     Do time level= 1,Ntime
        DO Newton iteration=1,Kmax
            •Solve k-ε equations every Eint Newton iteration
            •Solve energy equation every Kint Newton iteration
            •Solve Navier-Stokes equations every iteration
        ENDDO
     ENDDO
Print the mass-average solution
```

Figure 4.2b Algorithm flowchart for the unsteady flow scheme.

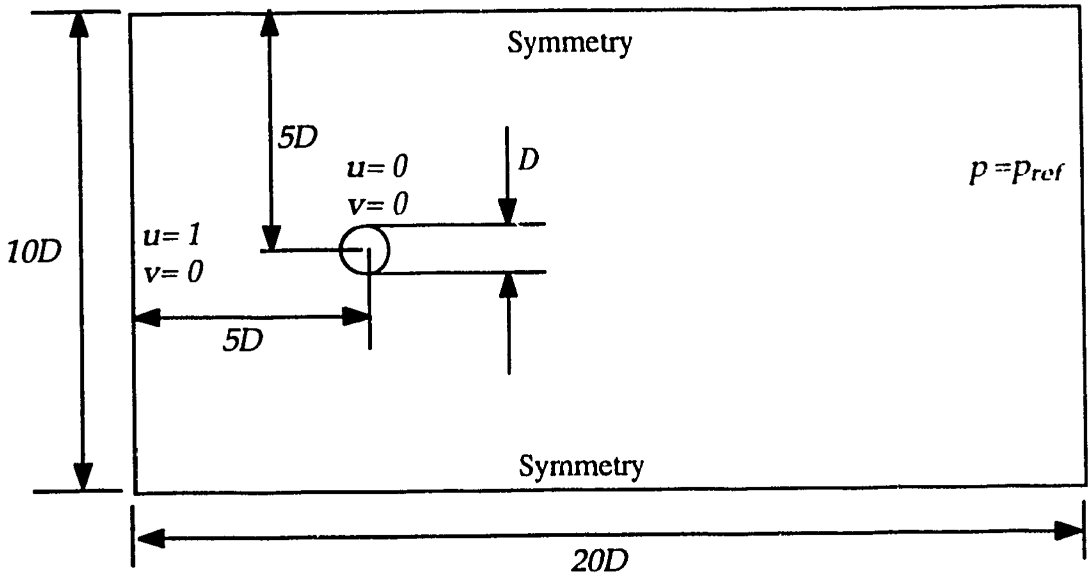

Figure 5.1 Computational domain and boundary conditions for the flow around a circular cylinder.

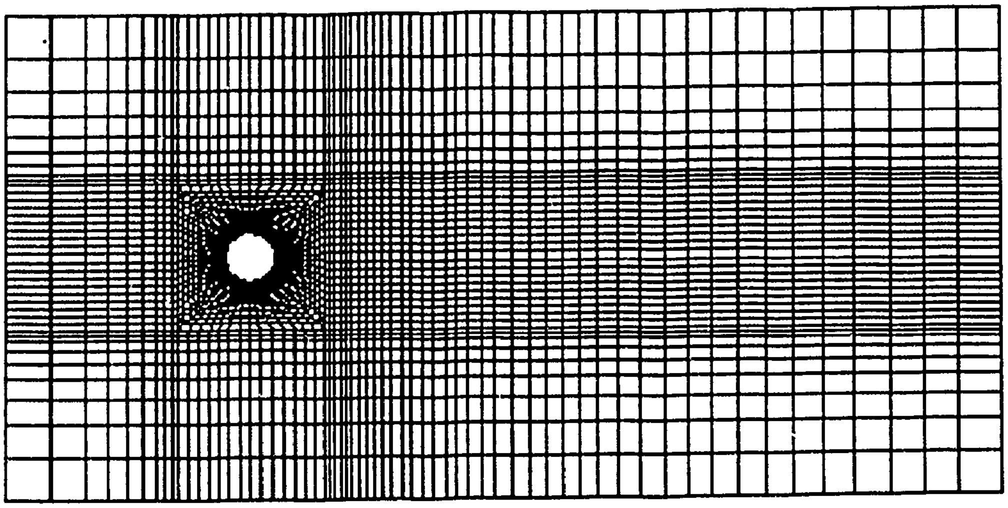

(a) Finite element mesh

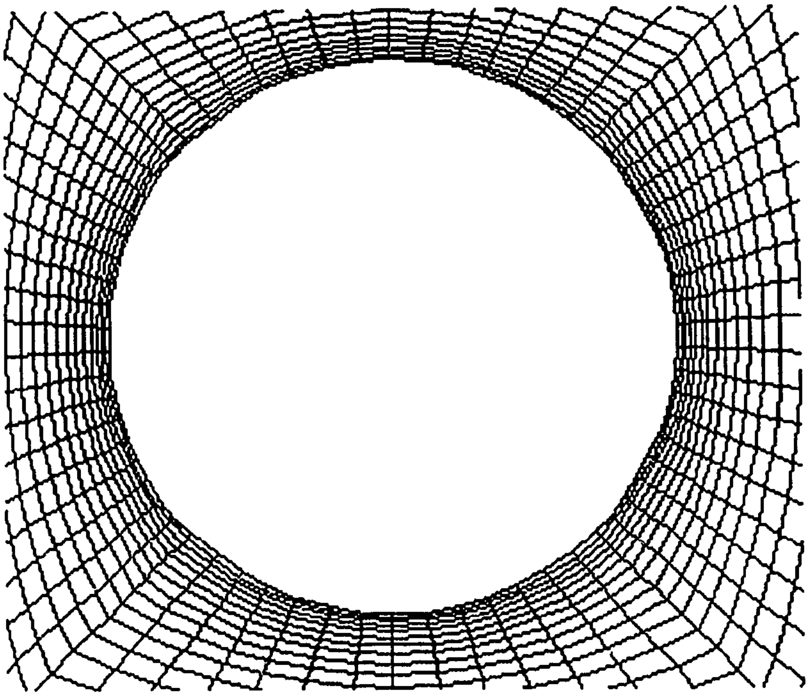

(b) Mesh details near cylinder

Figure 5.2 Finite element mesh for flow over a circular cylinder.

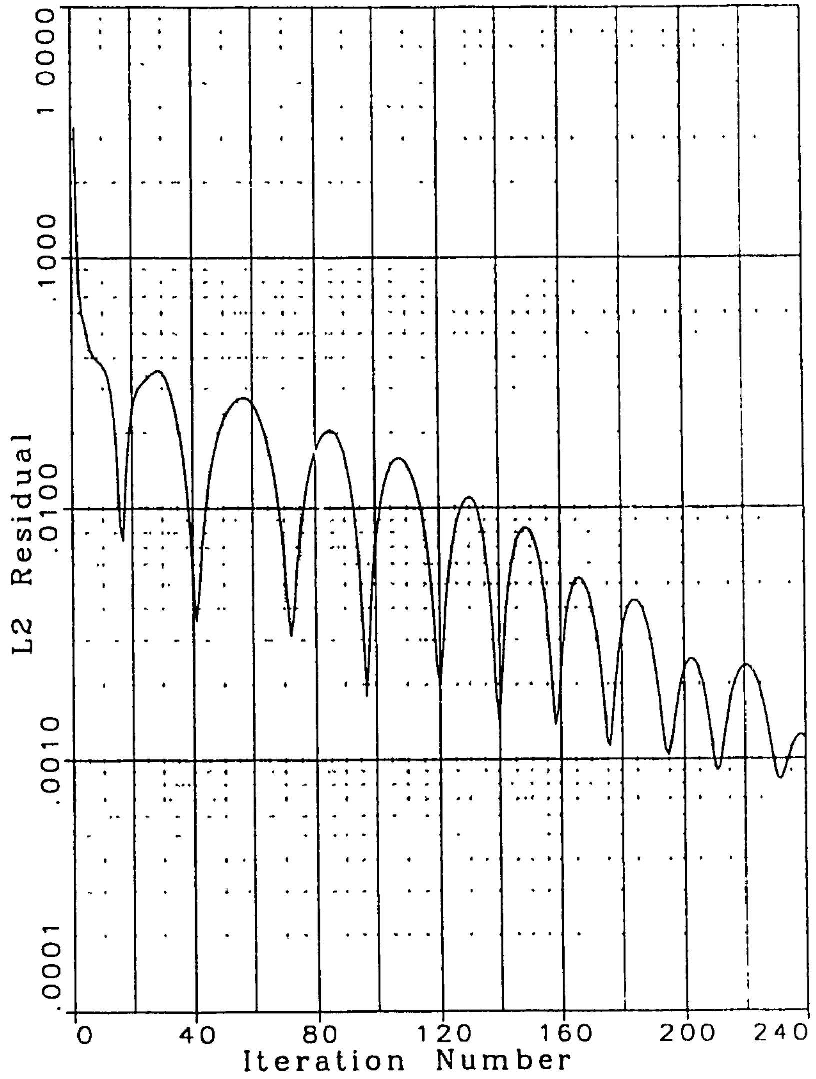

Figure 5.3 Convergence history of the steady Navier-Stokes equations for the laminar flow past a circular cylinder at Re=100.

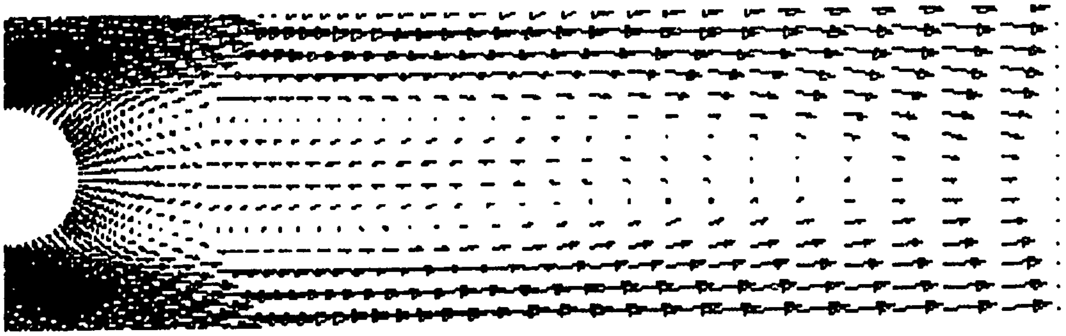

(a) Velocity field

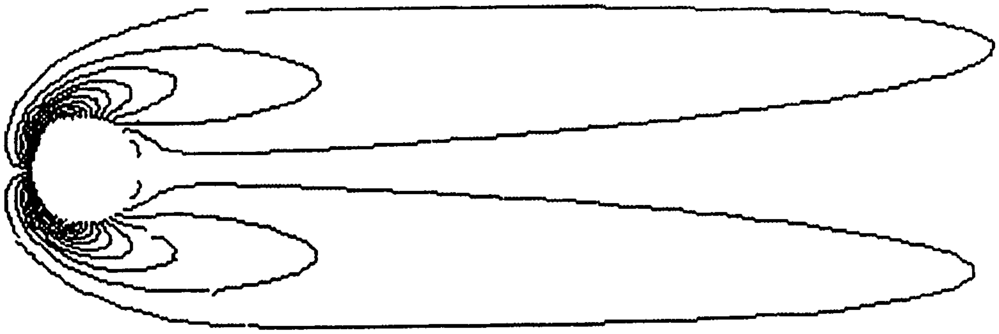

(b) Vorticity contours

Figure 5.4 Velocity and vorticity fields for the flow past a circular cylinder at t=0 and Re=100.

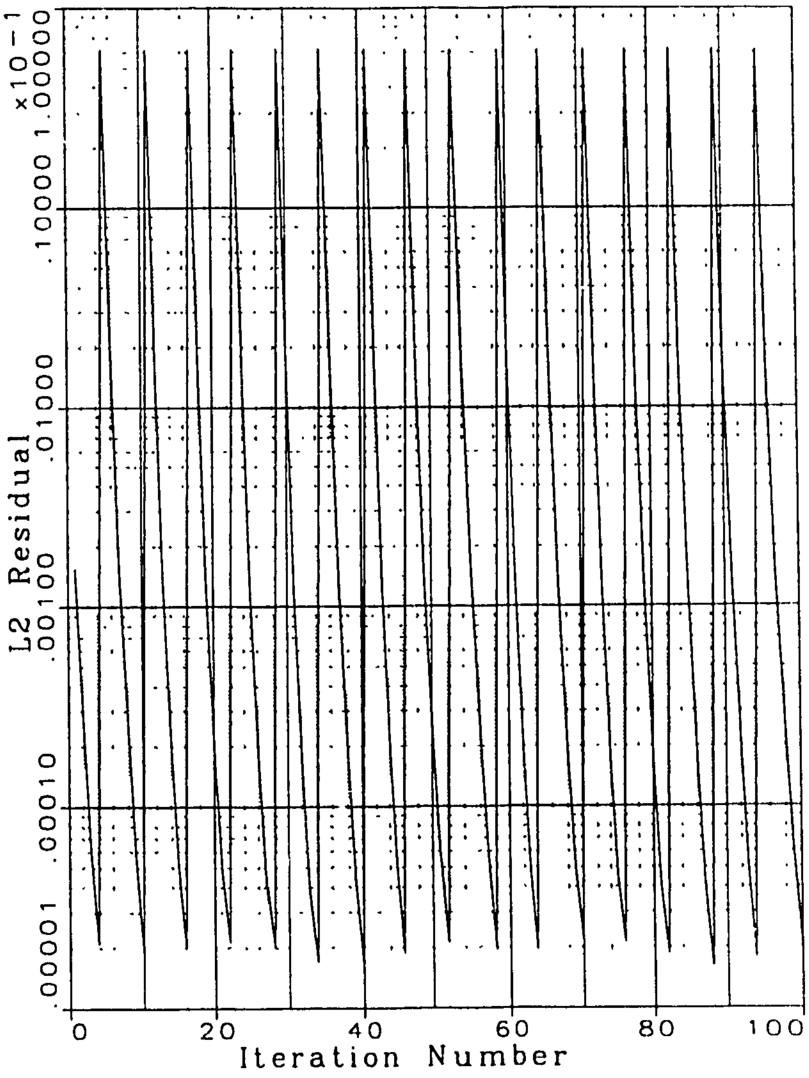

Figure 5.5 Convergence history of the unsteady Navier-Stokes equations for the laminar flow past a circular cylinder at Re=100.

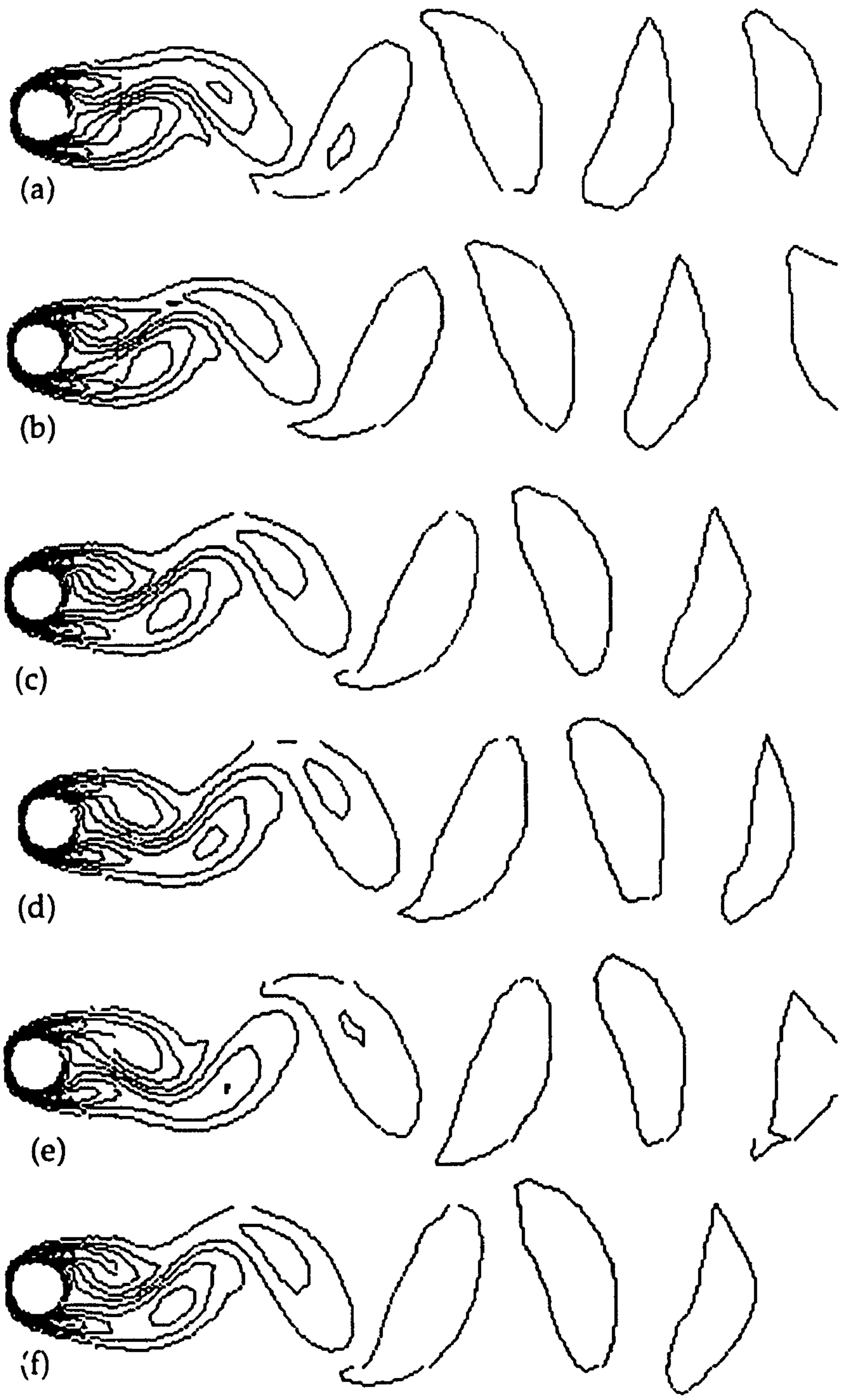

Figure 5.6 Predicted vorticity contours behind the cylinder over one cycle at times; (a) 0, (b) 0.23*T*, (c) 0.46*T*, (b) 0.69*T*, and (e) 0.92*T*. Laminar flow, Re=100, *T*=5.75, Sr=0.174.

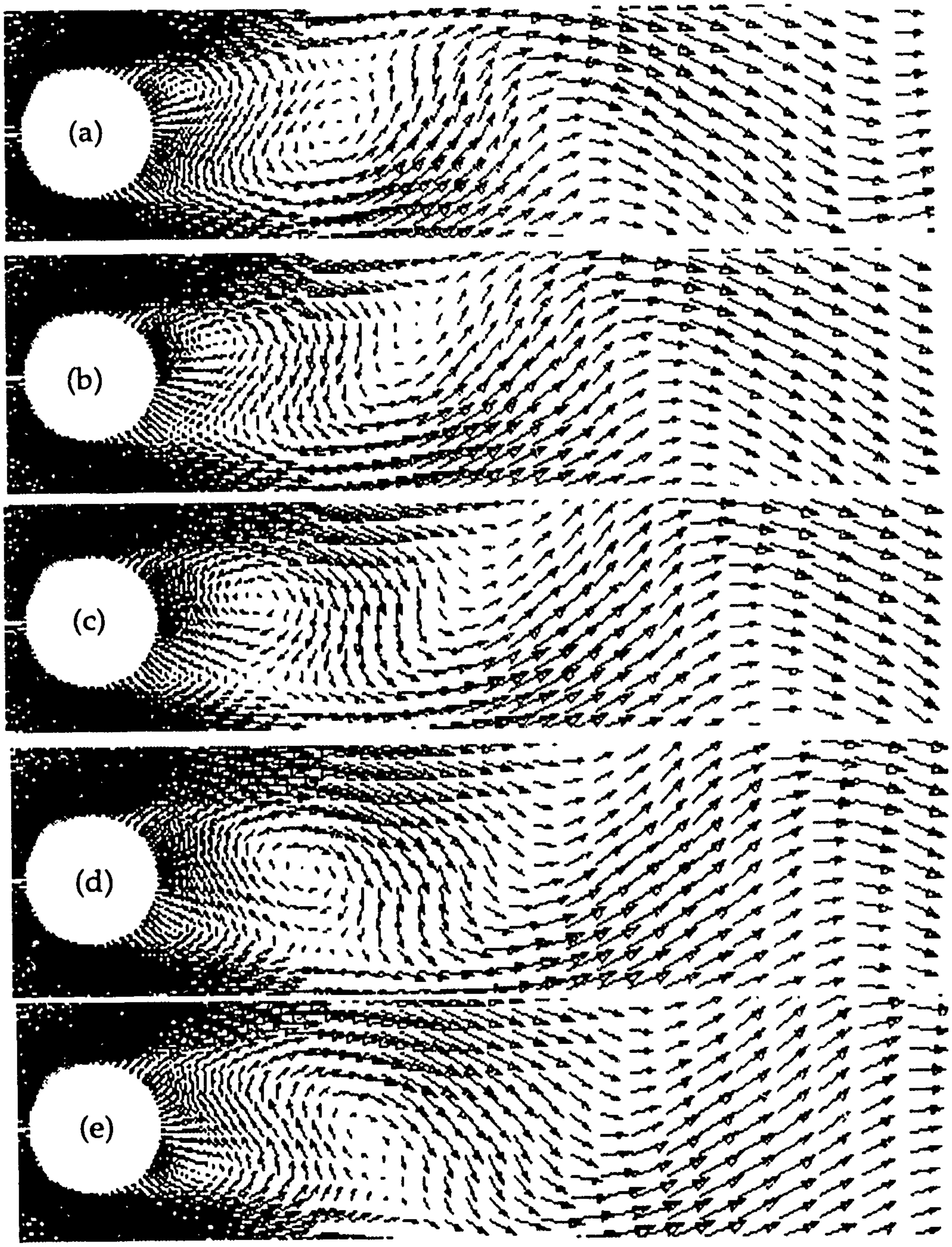

Figure 5.7 Predicted velocity vectors behind the cylinder over one cycle at times; (a) 0, (b) 0.23*T*, (c) 0.46*T*, (b) 0.69*T*, and (e) 0.92*T*. Laminar flow, Re=100, *T*=5.75, Sr=0.174.

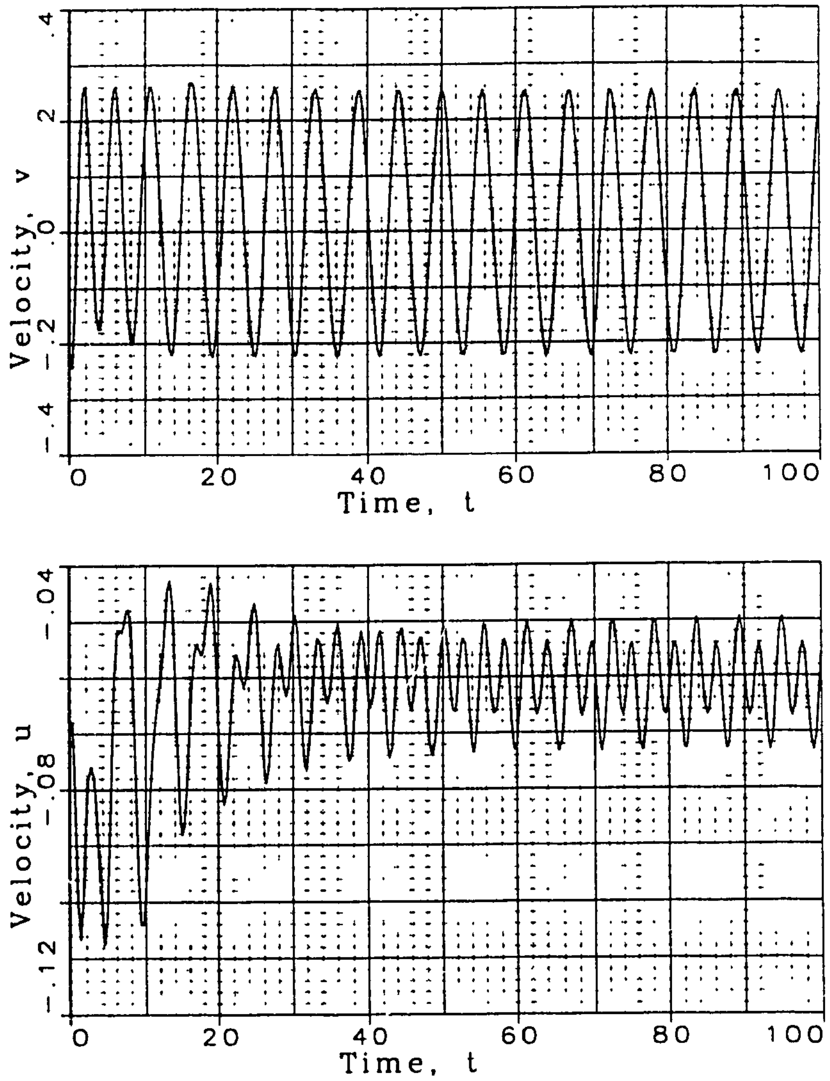

Figure 5.8 Predicted evolution of the x-component of velocity, u, and the y-component of velocity, v, with respect to time. Solution at a point (x/D=0.65, y=0) on the centerline behind the cylinder; Re=100, Δt=0.23, T=5.75, Sr=0.174.

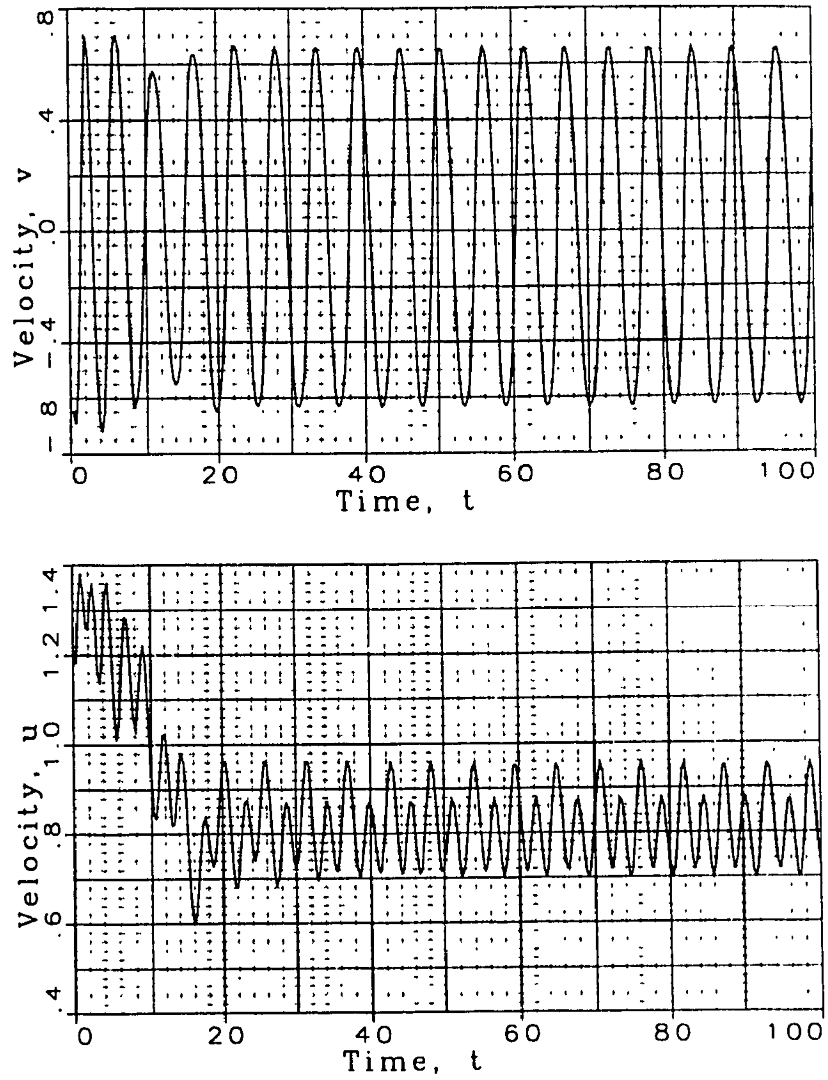

Figure 5.9 Predicted evolution of the *x*-component of velocity, *u*, and the *y*-component of velocity, *v*, with respect to time. Solution at a point (x/D=5.0, y=0) on the centerline behind the cylinder; Re=100, Δt=0.23, T=5.75, Sr=0.174.

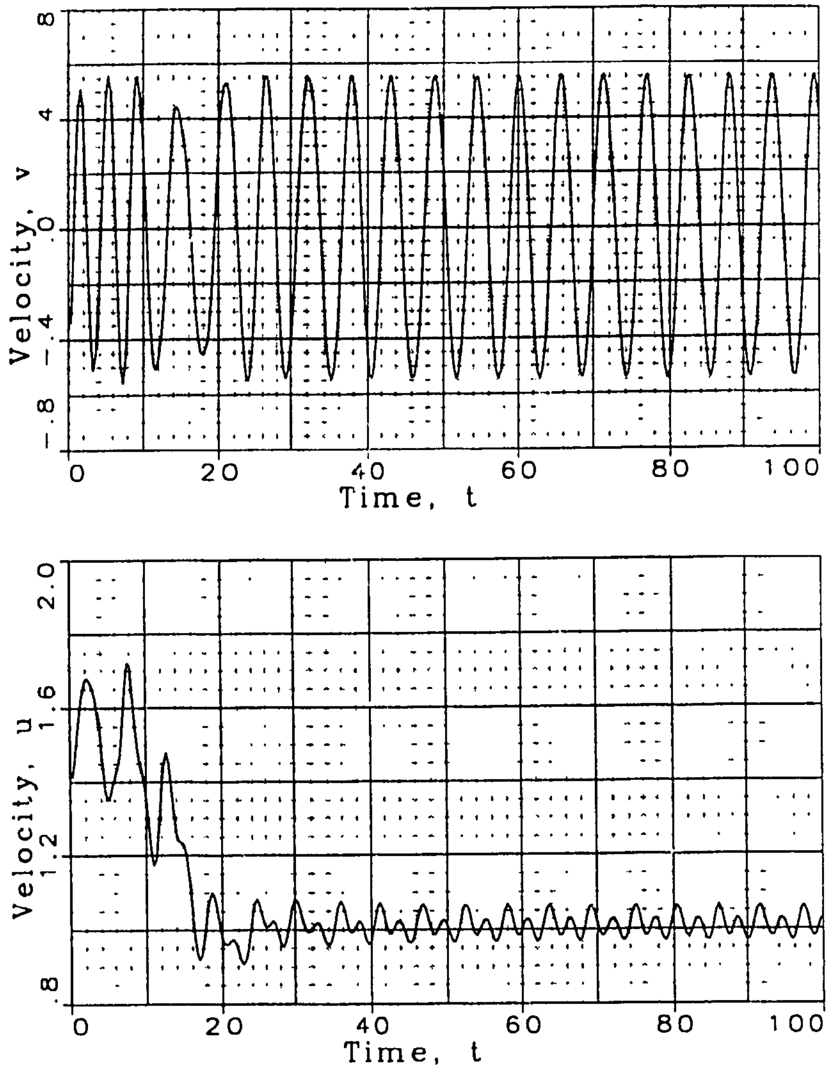

Figure 5.10 Predicted evolution of the *x*-component of velocity, *u*, and the *y*-component of velocity, *v*, with respect to time. Solution at point (x/D=8.0, y=0) on the centerline behind the cylinder; Re=100, Δt=0.23, T=5.75, Sr=0.174.

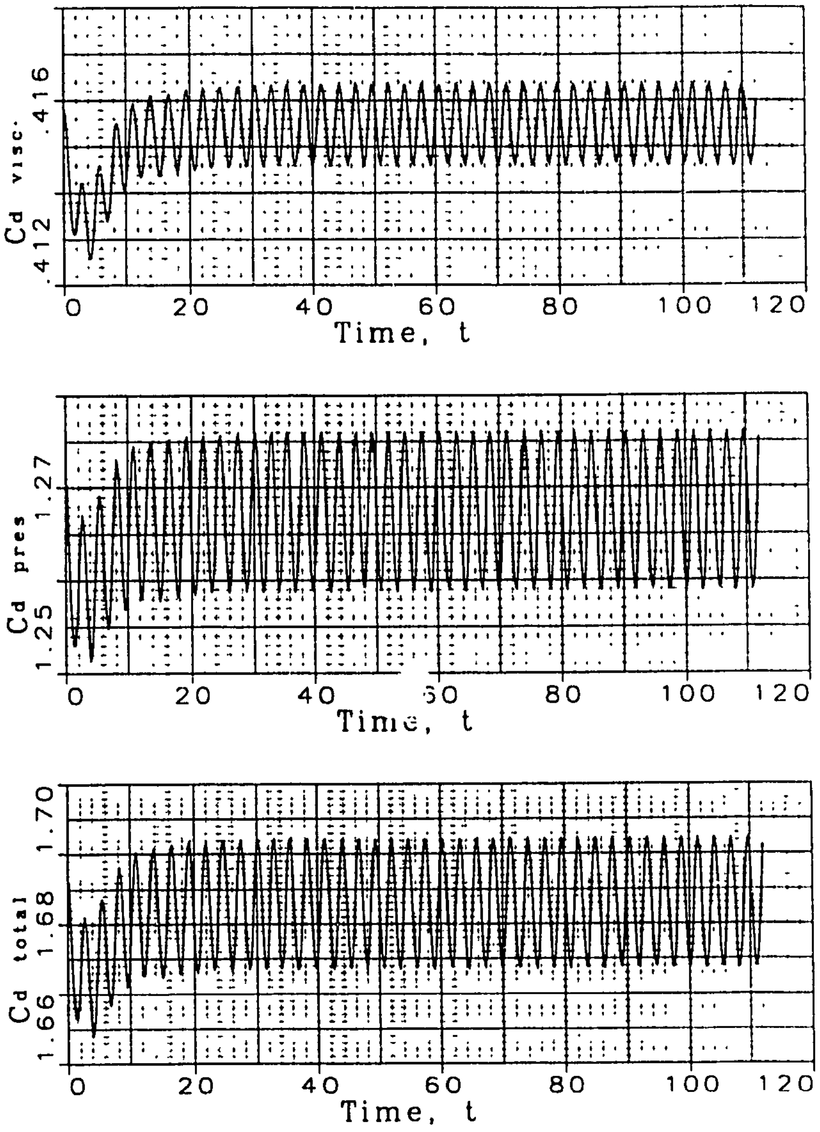

Figure 5.11 Predicted viscous and pressure drag coefficients with respect to time at Re=100.

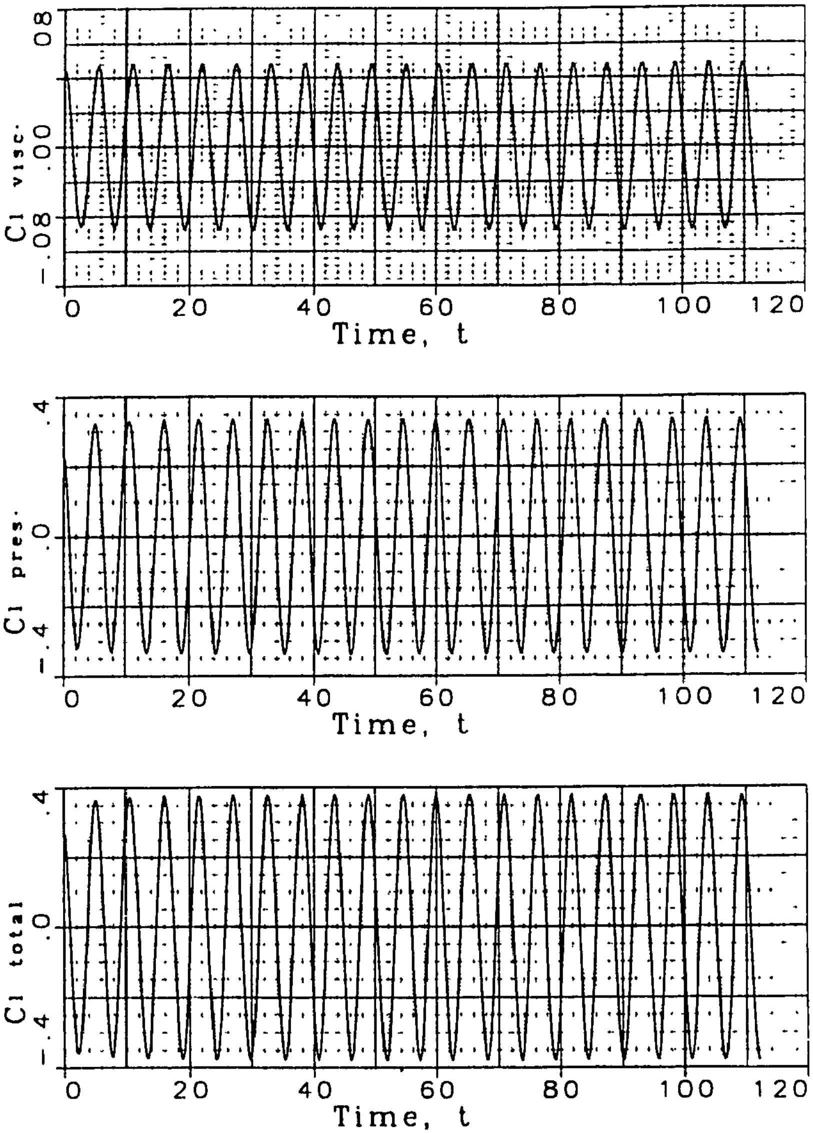

Figure 5.12 Predicted viscous and pressure lift coefficients with respect to time at Re=100.

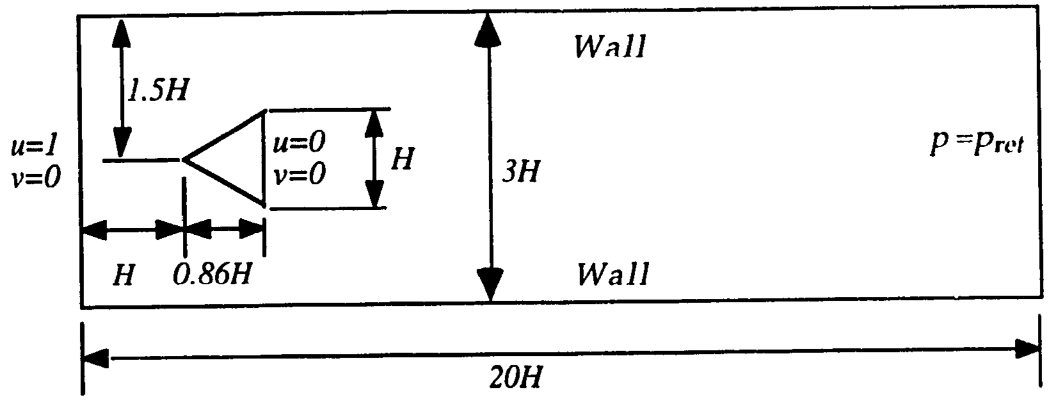

Figure 5.13 Computational domain and boundary conditions for the flow behind a flame holder.

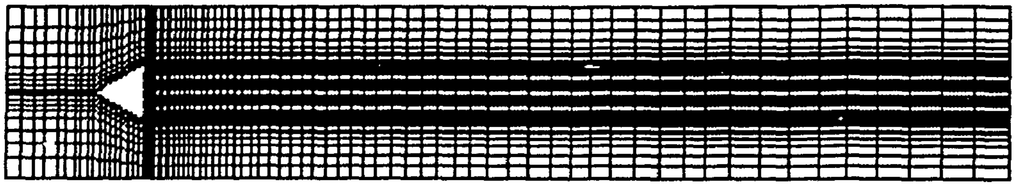

(a) Finite element mesh

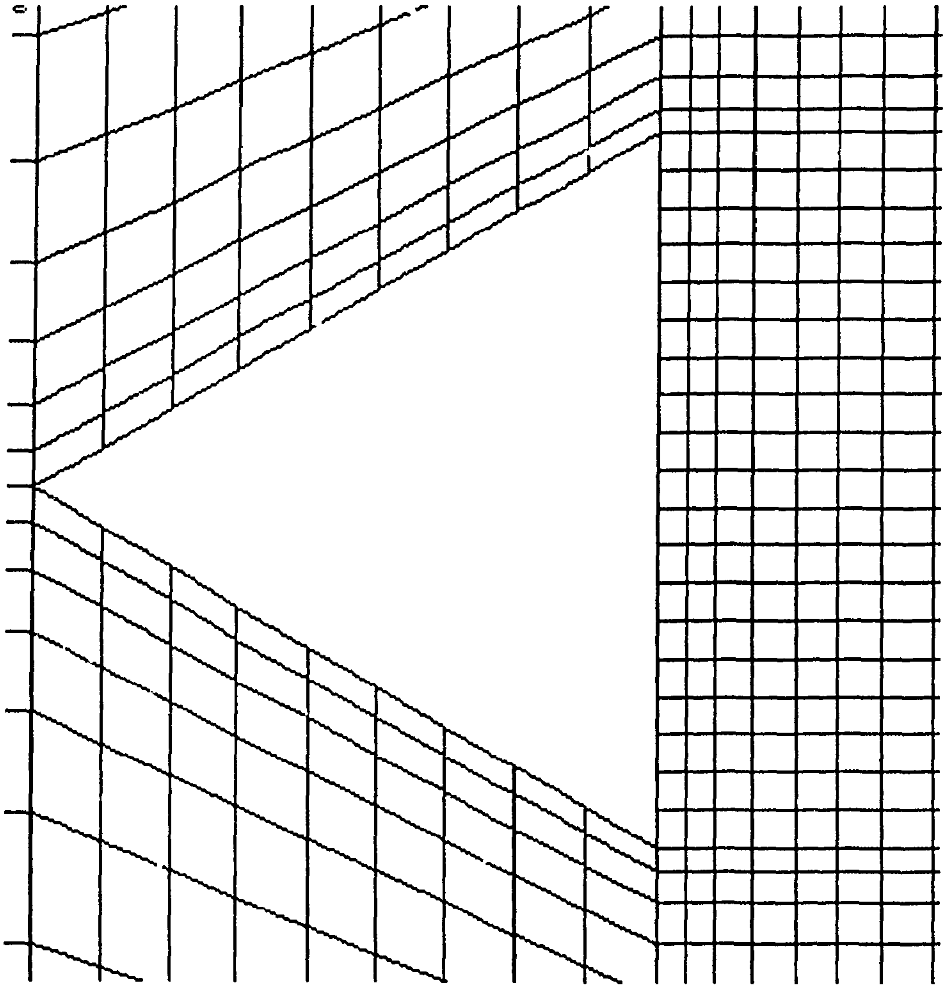

(b) Mesh details near flame holder

Figure 5.14 Finite element mesh for flow over a triangular shaped flame holder.

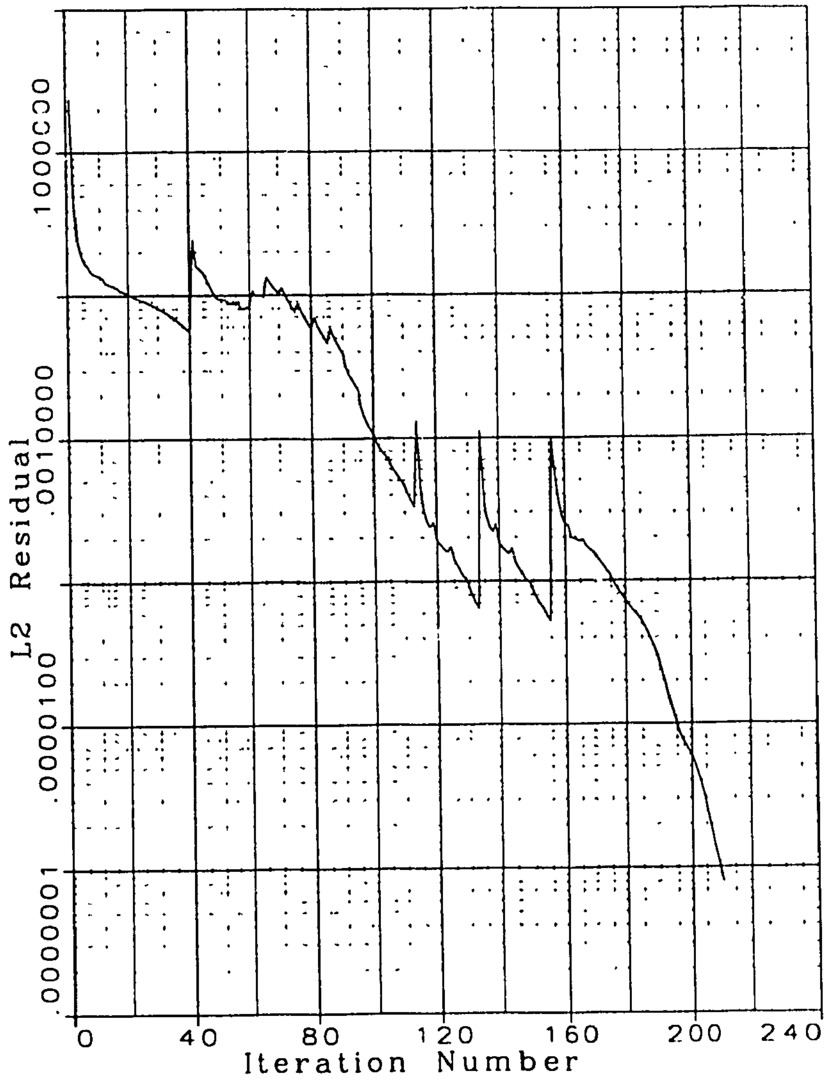

Figure 5.15 Convergence history of the steady Navier-Stokes equations for the turbulent flow over a triangular shaped flame holder at Re=45,000.

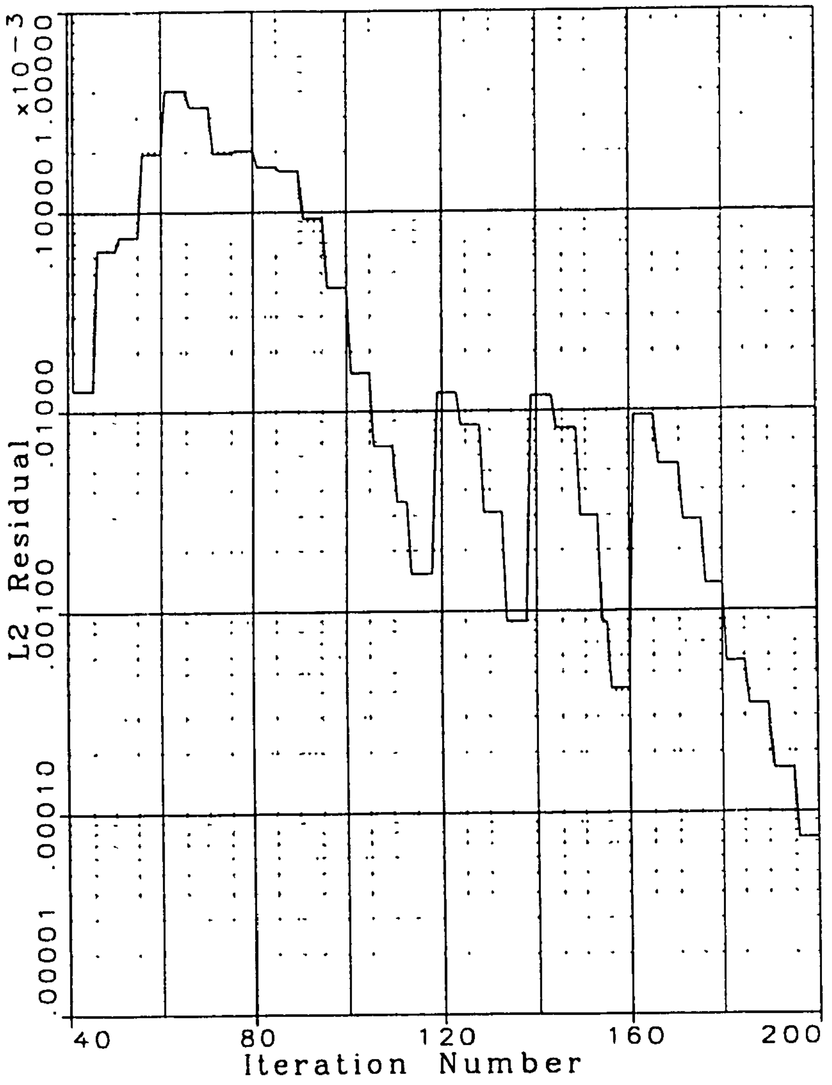

Figure 5.16 Convergence history of the steady ε-equation for the turbulent flow over a triangular shaped flame holder at Re=45,000.

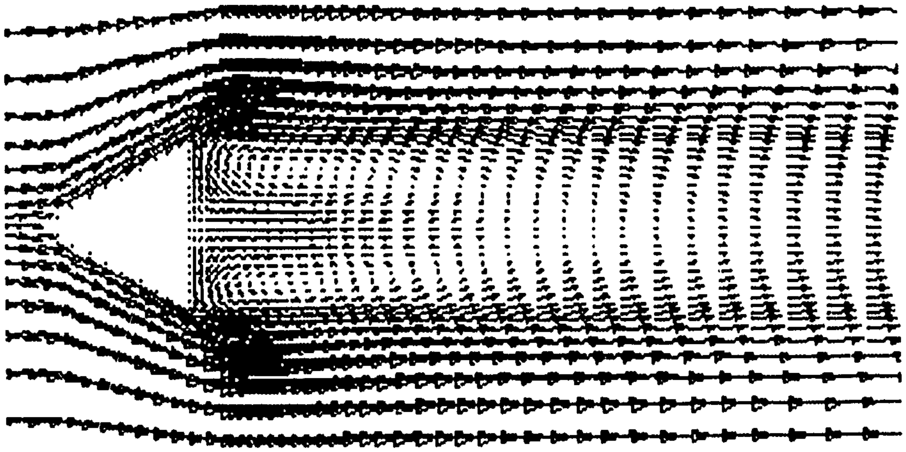

(a) Velocity field

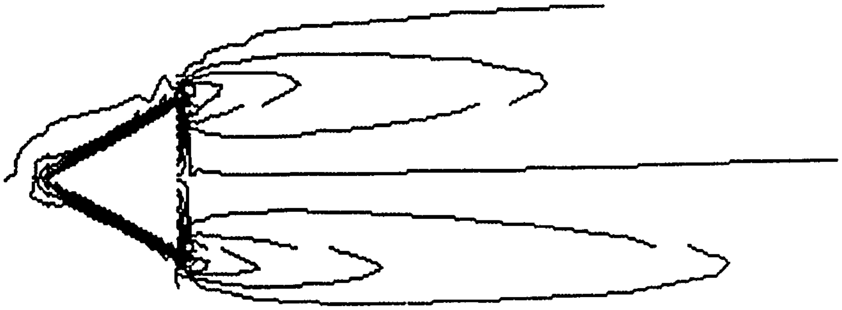

(b) Vorticity contours

Figure 5.17 Velocity and vorticity field for the flow past a triangular shaped flame holder at t=0 and Re=45,000.

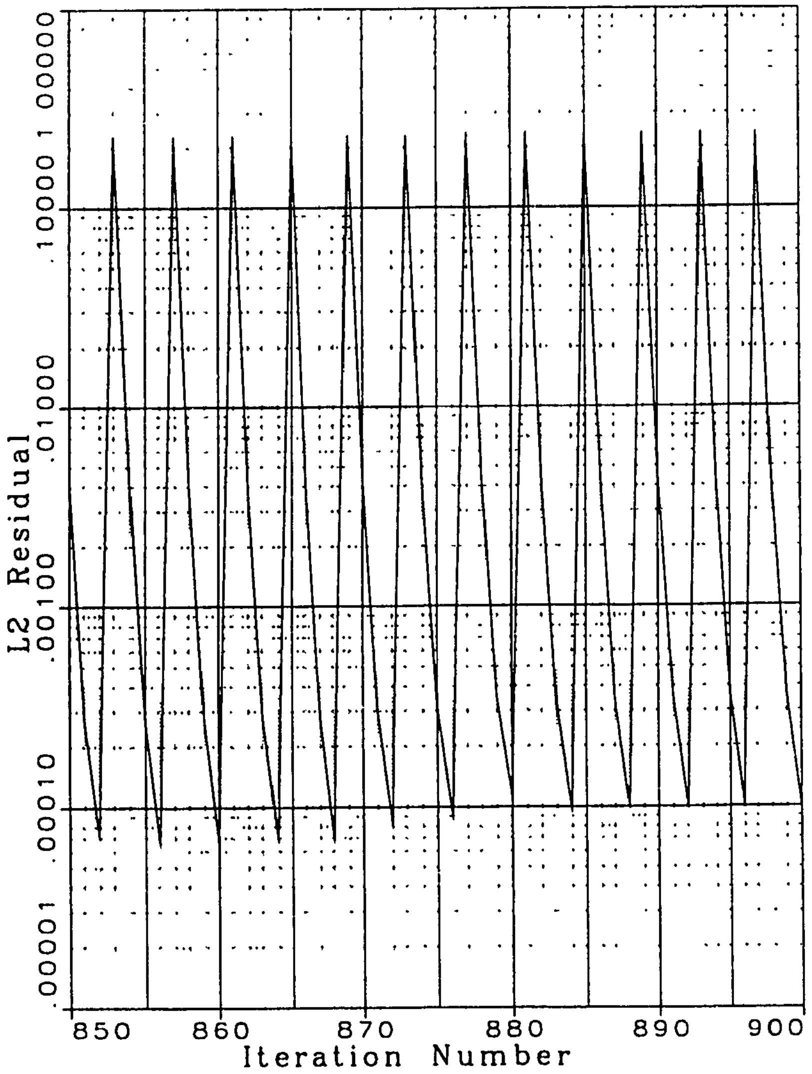

Figure 5.18 Convergence history of the unsteady Navier-Stokes equations for the turbulent flow over a triangular shaped flame holder at Re=45,000.

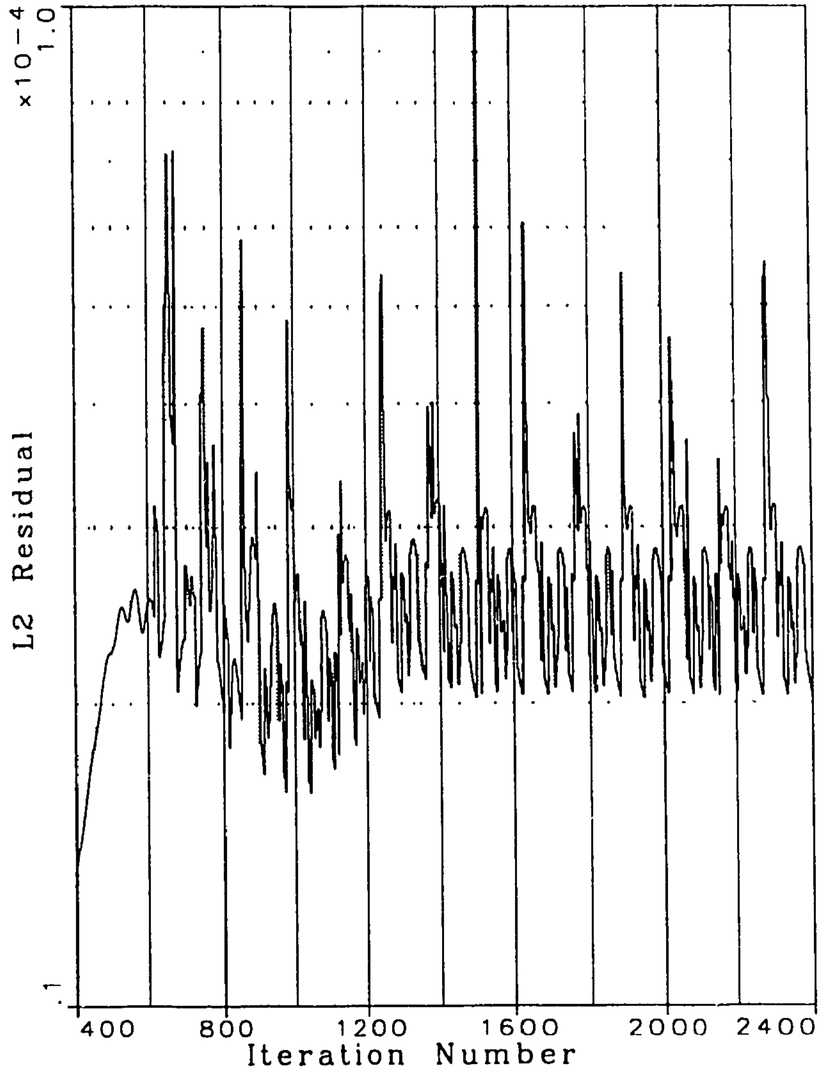

Figure 5.19 Convergence history of the unsteady ε-equation for the turbulent flow over a triangular shaped flame holder at Re=45,000.

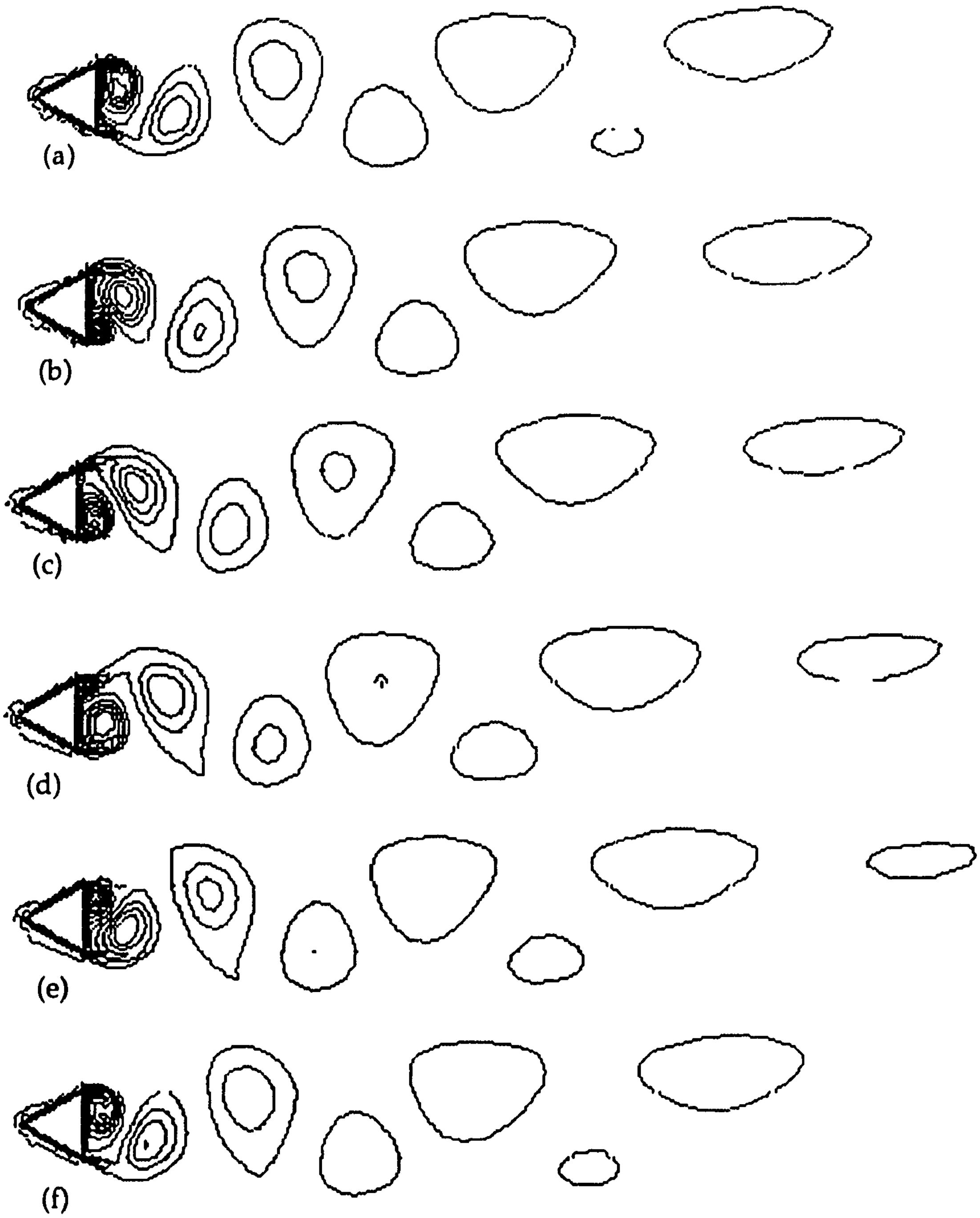

Figure 5.20 Predicted vorticity contours over one cycle at times; (a) 0, (b) $0.18T$, (c) $0.36T$, (d) $0.54T$, (e) $0.72T$, and (f) $0.9T$. Turbulent flow past a triangular cylinder; Re=45,000, Δt=0.12, T=3.85, Sr=0.26.

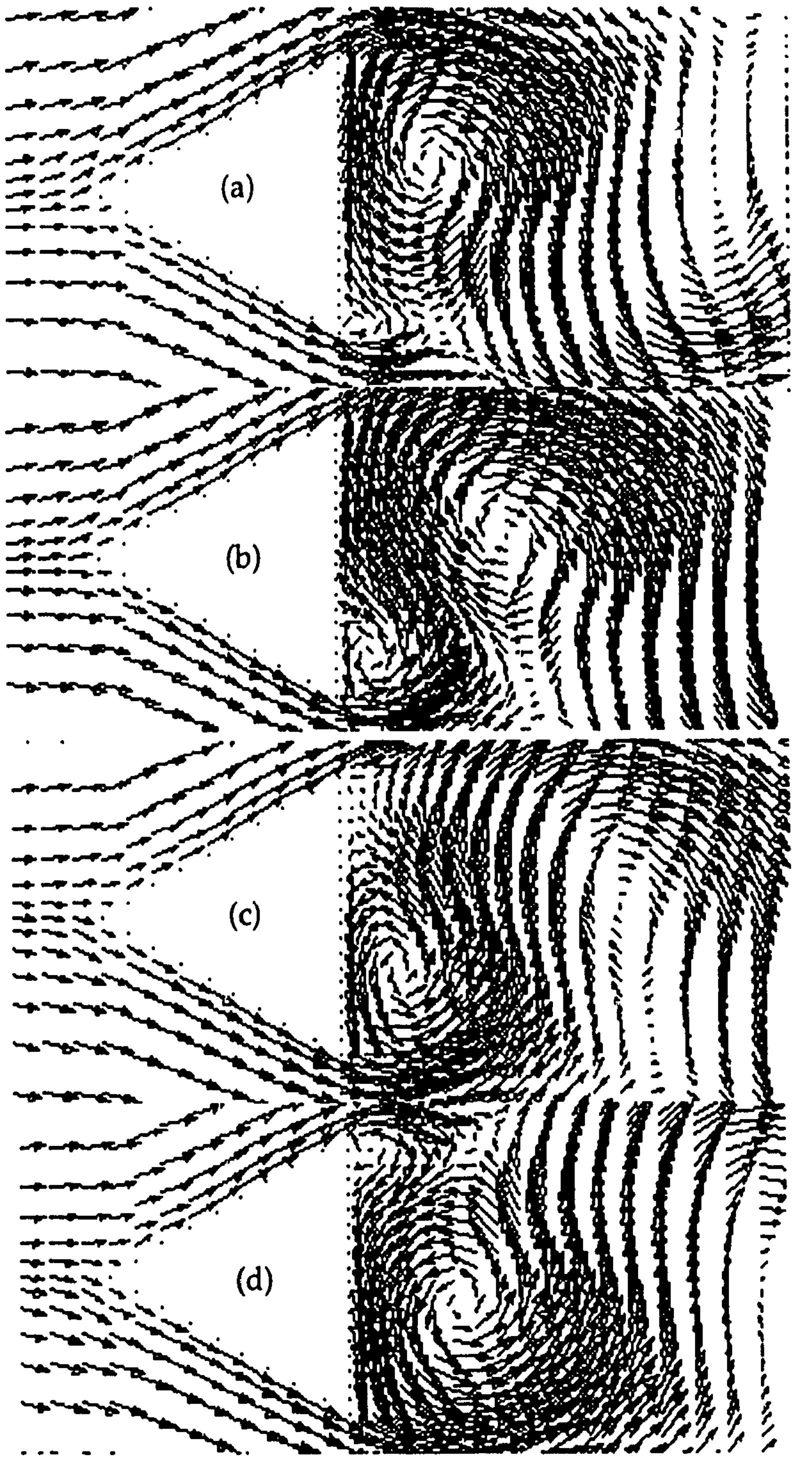

Figure 5.21 Predicted velocity vectors over one cycle at times; (a) 0, (b) 0.18T, (c) 0.36T, (d) 0.54T, (e) 0.72T, and (f) 0.9T. Turbulent flow past a triangular cylinder; Re=45,000, Δt=0.12, T=3.85, Sr=0.26.

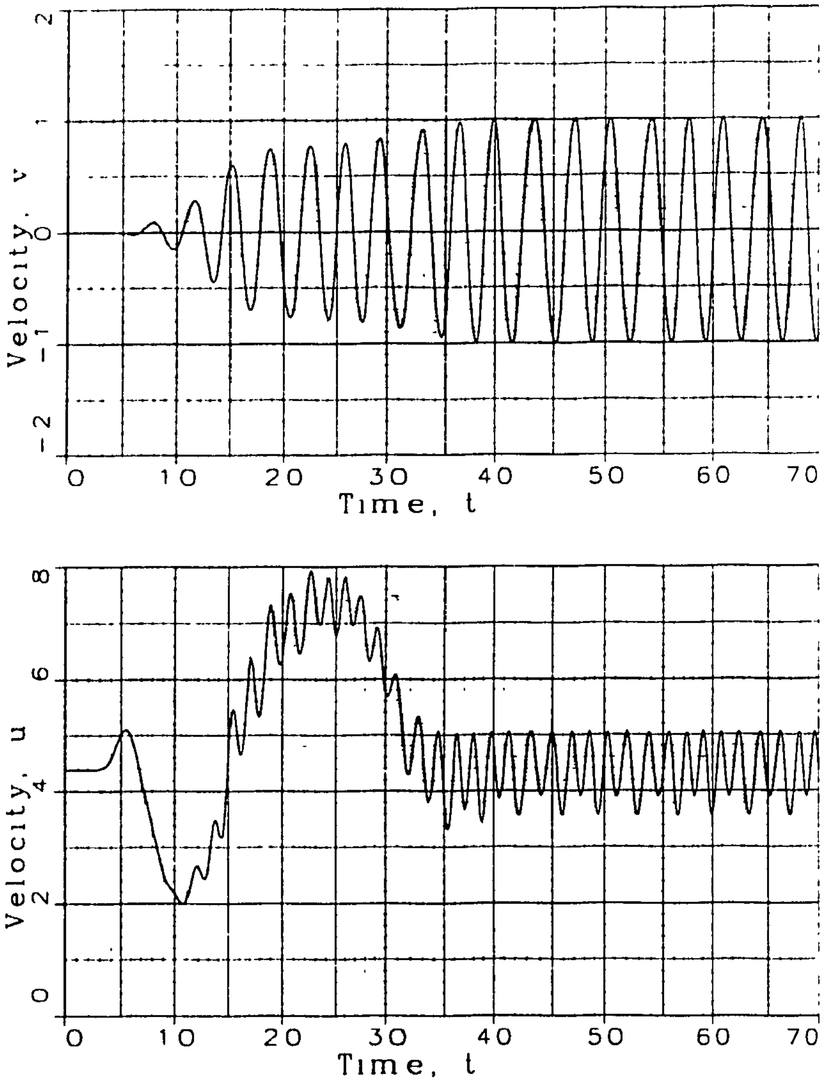

Figure 5.22 Predicted evolution of the x-component of velocity, u, and the y-component of velocity, v, with respect to time. Solution at a point (x/H=7.6, y/H=0) on the centerline behind the flame holder; Re=45,000, Δt=0.12, T=3.85, Sr=0.26.

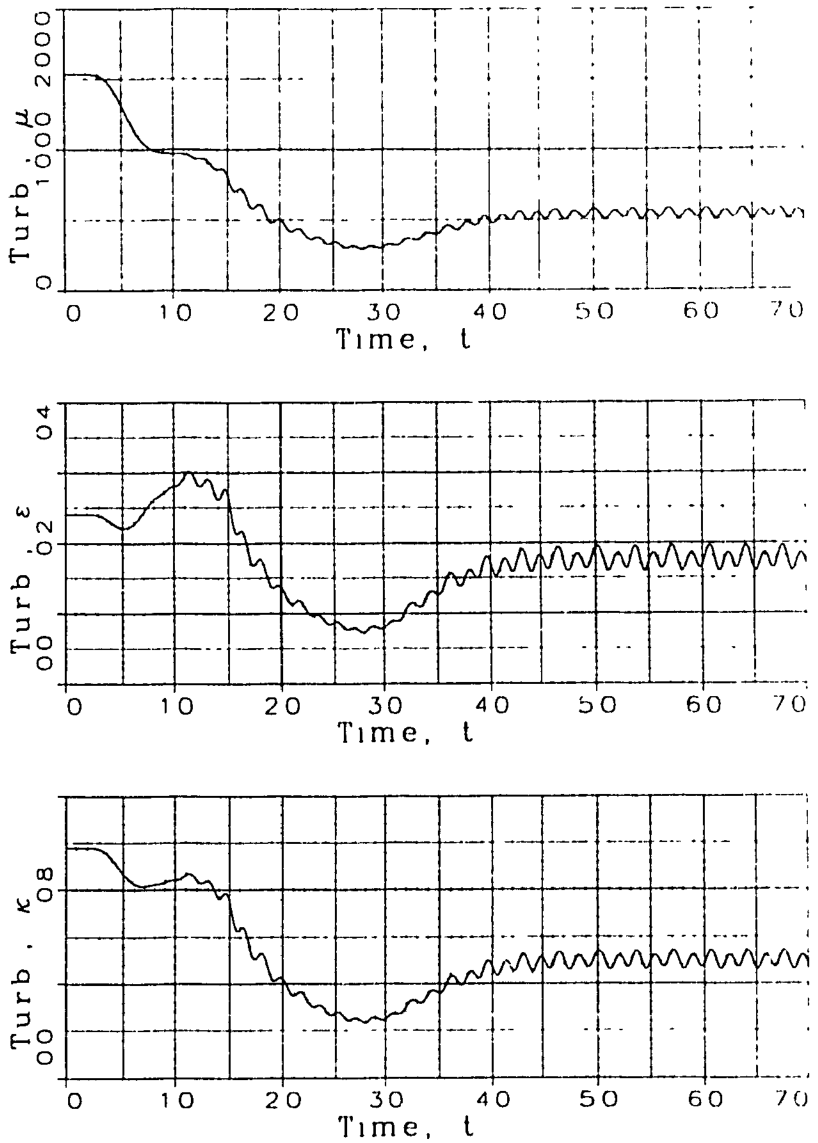

Figure 5.23 Predicted evolution of turbulent kinetic energy, *κ*, rate of energy dissipation, ε, and turbulent viscosity, *μ*, with respect to time. Solution at a point (*x/H*=7.6, *y/H*=0) on the centerline behind the flame holder; Re=45,000, *Δt*=0.12, *T*=3.85, Sr=0.26.